Diverse priming outcomes under conditions of very rare precursor B cells

Patrick J. Madden[1,2], Ester Marina-Zárate[1,2^], Kristen A. Rodrigues[3^], Jon M. Steichen[2,4^], Monolina Shil[1,2], Kaiyuan Ni[3], Katarzyna Kaczmarek Michaels[3], Laura Maiorino[3], Amit A. Upadhyay[5,6], Swati Saha[7], Arpan Pradhan[5], Oleksandr Kalyuzhiny[2,4,8], Alessia Liguori[2,4,8], Paul G. Lopez[1,2], Ivy Phung[1,2], Nicole Phelps[2,4], Erik Georgeson[2,4], Nushin Alavi[2,4], Michael Kubitz[2,4], Danny Lu[2,4], Saman Eskandarzadeh[2,4], Amanda Metz[5,6], Oscar L. Rodriguez[7], Kaitlyn Shields[7], Steven Schultze[7], Melissa L. Smith[7], Brandon S. Healy[5], Deuk Lim[5], Vanessa R. Lewis[5], Elana Ben-Akiva[3], William Pinney III[3,10], Justin Gregory[3], Shuhao Xiao[3], Diane G. Carnathan[5], Sudhir Pai Kasturi[5], Corey T. Watson[7], Steven E. Bosinger[5,6], Guido Silvestri[5], William R. Schief[2,4,8,9], Darrell J Irvine[2,3,10,11]*, Shane Crotty[1,2,12]*

[1]Center for Vaccine Innovation, La Jolla Institute for Immunology, La Jolla, CA, USA
[2]Consortium for HIV/AIDS Vaccine Development (CHAVD), The Scripps Research Institute, La Jolla, CA, USA
[3]Koch Institute for Integrative Cancer Research, Massachusetts Institute of Technology, Cambridge, MA, USA
[4]Department of Immunology and Microbiology, The Scripps Research Institute, La Jolla, CA, USA
[5]Emory National Primate Research Center and Emory Vaccine Center, Emory University School of Medicine, Atlanta, GA, USA
[6]Department of Pathology and Laboratory Medicine, Emory School of Medicine, Atlanta, GA, USA
[7]Department of Biochemistry and Molecular Genetics, University of Louisville School of Medicine, Louisville, KY, USA
[8]IAVI Neutralizing Antibody Center, The Scripps Research Institute, La Jolla, CA, USA
[9]Moderna, Inc., Cambridge, MA, USA
[10]Department of Biological Engineering, Massachusetts Institute of Technology, Cambridge MA USA
[11]Howard Hughes Medical Institute, Chevy Chase, MD, USA
[12]Department of Medicine, Division of Infectious Diseases and Global Public Health, University of California, San Diego (UCSD), La Jolla, CA, USA

^ These authors contributed equally.
*Co-Senior authors. Email: shane@lji.org (SC), djirvine@mit.edu (DJI)

SUMMARY

Rare B cells can have special pathogen-recognition features giving them the potential to make outsized contributions to protective immunity. However, rare naive B cells infrequently participate in immune responses. We investigated how germline-targeting vaccine antigen delivery and adjuvant selection affect priming of exceptionally rare BG18-like HIV broadly neutralizing antibody-precursor B cells (~1 in 50 million) in non-human primates. Only escalating dose (ED) priming immunization using the saponin adjuvant SMNP elicited detectable BG18-like cells in germinal centers (GCs). All groups had strong GC responses, but only ED+SMNP and bolus+SMNP induced BG18-like memory B cells in >50% of animals. One group had vaccine-specific GC responses equivalent to ED+SMNP, but BG18-like memory B cells were rarely detected. Following homologous boosting, BG18-like memory B cells were more frequent in a bolus priming group, but had lower somatic hypermutation and affinities. This outcome was inversely associated with post-prime antibody titers, suggesting antibody feedback can significantly influence rare precursor B cell responses.

INTRODUCTION

The aim of many vaccines against viruses is to induce neutralizing antibodies that protect against infection[1–3]. The B cell precursors that give rise to these types of neutralizing responses can be extremely rare in the naïve B cell repertoire and infrequently participate in immune responses[4–12]. Germline-targeting vaccine design is one approach to prime these rare B cell specificities by designing immunogens that have affinity for the precursors of choice[13–16]. HIV broadly neutralizing antibody (bnAb) precursors have been a main focus of germline-targeting immunogen design[5,8,12,17–28]. This approach relies on the concept that immunogens that can be recognized with high affinity by rare bnAb-precursor B cells can overcome their inherent rarity and allow for sufficient B cell activation and recruitment into germinal center (GC) reactions[12,19,29]. Using adoptive transfer experiments in mice to model human precursor frequencies, rare bnAb-precursor B cells can be successfully primed if the immunogen has sufficient affinity for the target naïve B cell receptors (BCRs)[4]. These outcomes have been tested and validated in a first-in-humans germline-targeting vaccine clinical trial wherein rare VRC01-class bnAb precursors were primed in 97% of vaccine recipients[26].

It was recently shown that a novel HIV germline-targeting immunogen, N322-GT5, designed to target and prime rare precursors similar to the HIV bnAb BG18, successfully primed BG18-class responses in 8 out of 8 rhesus macaques (RMs) [12,19,25]. In humans, N332-GT5 reactive BG18-class precursors were found at a frequency of 1 in 53 million in the naïve B cell repertoire[12], and are estimated to be 8-fold rarer in RM[25]. In addition to being an important advance in HIV candidate vaccine development in the germline-targeting vaccine field, the success of N332-GT5 in NHPs provides a new opportunity for a model system to study rare B cell priming (defined as precursor frequencies < 1 in 1 million naive B cells) in outbred, non-transgenic animals. It is particularly advantageous to be able to do so in a primate species, given the much more similar immunoglobulin gene repertoire features and heavy chain complementarity determining region 3 (H-CDR3) lengths between non-human primates and humans compared to rodents[30,31].

It is yet to be elucidated how adjuvants and antigen delivery strategies affect the recruitment of rare B cells into GCs, despite much activity in adjuvant development and new vaccine technologies[32–36]. To build on the success of germline targeting immunogen design and explore the immunology of rare B cell recruitment, here we investigated the impact of various delivery strategies and adjuvants on the priming of BG18-class precursor B cells in RMs. The results reveal key features about successful versus failed priming and maturation of rare naive B cells in different contexts.

RESULTS

Adjuvant/delivery strategies and vaccine study design

To assess whether different immunization strategies affect recruitment of rare bnAb-precursor B cells in the context of a germline-targeting priming immunization, 36 RMs were split into six groups (n = 6/group) and immunized with the recombinant HIV Env-based germline-targeting immunogen N332-GT5 (**Fig. 1**). ED immunization is a slow antigen delivery immunization technique[37,38]. Saponin and monophosphoryl lipid A (MPLA)-containing nanoparticle (SMNP) is a potent adjuvant[25,39] being developed for clinical use[40]. ED immunization adjuvanted with other immune stimulating complexes (ISCOMs) has been previously shown to recruit a more diverse set of naïve B cells to participate in GCs[38], including rare neutralizing antibody precursor B cells, when compared to traditional bolus immunization[37]. ED immunization adjuvanted with SMNP (ED + SMNP) successfully primed BG18-class B cells in NHPs[25].

We hypothesized that the extended-antigen availability afforded by ED immunization may lead to better recruitment and priming of BG18-class B cells[25,41]. An additional method to extend antigen availability is via adsorption of phosphoserine-tagged immunogens on aluminum hydroxide (alum)

(pSer:alum)[42]. Tethering immunogens to alum particles in this way slows antigen clearance while simultaneously increasing the potential avidity of the immunogen[42–44]. Previously, we have shown that pSer:alum delivery of a native-like HIV Env trimer in RMs enhanced responses compared to unmodified antigen with alum, and adjuvanting the pSer:alum complexes with SMNP led to even better responses[45]. The bnAb BG18 targets the V3/glycan site on HIV Env, which includes the N322 glycan. By orienting the N332-GT5 Env trimer on alum, it may promote responses to the V3/glycan bnAb epitopes and reduce off-target Env base-binding responses[42,43,45]. We thus synthesized N332-GT5 trimers with an optimized C-terminal Cys linker[43], and coupled a peptide containing 4 phosphoserines to the base of each protomer to enable pSer-mediated anchoring to alum (**Supp. Fig. 1A**). pSer-modified N332-GT5 showed stable binding to alum in the presence of serum and exhibited high binding of HIV bnAbs (particularly inferred-germline BG18) and low binding of trimer base-specific Abs, as expected (**Supp. Fig. 1B-D**).

Alum is a suspension of aluminum hydroxide nanocrystals that aggregate to form particles of varying sizes[42,46,47]. Stable dispersions of sub-micron sized aluminum hydroxide particles, termed nano-alum, have been shown to elicit stronger antibody responses against multiple vaccines when compared to normal alum[48]. To test the potential of nano-alum in the setting of germline targeting, we generated nano-alum by dispersing Alhydrogel in the presence of a poly(ethylene glycol) (PEG) phospholipid. The PEG-lipid bound to the alum through its phosphate group, allowing individual needle-like aluminum hydroxide crystals to be stably dispersed in buffer (**Supp. Fig. 2A**). Nano-alum had a particle size under 100 nm diam. as assessed by dynamic light scattering and individual rod-like nanocrystals observed in TEM, which were smaller than the microscale aggregates of alum particles in unmodified Alhydrogel (**Supp. Fig. 2B-C**). While unmodified alum slowly sediments in water, nano-alum formed a stable opalescent solution (**Supp. Fig. 2D**). When mixed with pSer-trimer, many Env trimers could be observed decorating the length of individual nano-alum crystals by TEM (**Supp. Fig. 2E**). In preliminary immunization studies in mice, nano-alum loaded with pSer-modified Env trimers elicited substantial increases in antigen-specific GC B cells and serum IgG titers compared to traditional alum loaded with pSer-trimer (**Supp. Fig. 2F-H**).

Toll-like receptor (TLR) agonists are also being widely studied as vaccine adjuvants[33,34,36,39], and this study also evaluated multiple TLR agonist formulations for their potential to recruit rare B cell precursors. The MPLA in SMNP is a TLR-4 agonist. CpG is a TLR9 agonist that can be further enhanced by the addition of an albumin-binding lipid tail (Amph-CpG, **Supp. Fig. 3**)[49]. Amph-CpG takes advantage of the fact that large proteins, such as albumin, cannot efficiently pass from tissue to blood and therefore must enter lymphatics[49]. This leads to increased uptake of the amph-CpG in draining lymph nodes (LNs) by bypassing systemic distribution in blood[49]. Amph-CpG has been shown to be a potent adjuvant in RMs immunized with a SARS-CoV-2 protein vaccine[50].

The six study groups comprised different combinations of three delivery strategies (bolus, ED, and pSer) and four adjuvants (SMNP, alum, nano-alum, Amph-CpG) and are detailed in **Fig. 1**. Each of these adjuvants have distinct properties and have been highly successful in different contexts, but they have not been tested in the context of rare precursor B cell recruitment. All immunizations were administered subcutaneously in each thigh (50μg protein/side, 100μg total) at weeks 0 and 10 (**Fig. 1A**). The week 10 boosting immunizations were all bolus, using the same immunogen plus adjuvant combination and dose used at the priming timepoint by group. To date, only ED SMNP delivery of N332-GT5 has been tested and shown to prime BG18 type I precursor cells. A primary objective of this study was to thus determine the immunology of rare bnAb-precursor B cell priming under a range of conditions. Two secondary objectives were also explored to determine whether the pSer:alum based immunizations were superior to traditional bolus immunization, and to assess how pSer:alum behaved when delivered in an ED immunization with different adjuvants. Statistical tests presented here were designed to reflect these specific objectives and are detailed in the methods.

142 **Escalating dose immunizations and SMNP prime larger GC responses**
143 GC responses were measured by flow cytometry from lymph node fine needle aspirates (LN FNAs) at
144 multiple timepoints throughout the study. ED immunizations led to significantly larger total GC B cell (B_{GC},
145 $CD38^{-}CD71^{+}$) and GC-T_{FH} (PD-$1^{Hi}CXCR5^{+}$) responses post-prime (weeks 3-9) when compared to bolus
146 groups using the same adjuvant combinations (G1 vs G2, and G4 vs G5, **Fig. 2A-F**). G3 had lower B_{GC} and
147 GC-T_{FH} responses throughout the study compared to G1 and G4, indicating that SMNP was more effective
148 in driving GC responses than Amph-CpG in the setting of escalating-dose immunization (**Fig. 2B, E**).
149 B_{GC} cells were also stained with fluorophore-labeled N332-GT5 probes to detect antigen-specific
150 (two colors of N332-GT5 probes; N332-$GT5^{++}$) and epitope-specific (N332-$GT5^{++}$N332-GT5KO^{-}) B_{GC} cells
151 (**Fig. 2G-L**). All groups had detectable antigen- and epitope-specific B_{GC} cells starting at week 3, but the
152 kinetics of GC priming differed (**Fig. 2G-L**). G1 and G4 had the largest post-prime antigen- and epitope-
153 specific B_{GC} frequencies. At week 3, bolus SMNP vaccination (G2) elicited a frequency of antigen-specific
154 B_{GC} cells barely above the limit of detection (LOD, baseline determined pre-immunization), followed by a
155 sharp rise at week 6, which was mirrored by the expansion of epitope-specific B_{GC} cells (**Fig. 2H, K**).
156 Interestingly, all of the groups employing SMNP in an extended-delivery regimen (either ED or pSer)
157 expanded antigen-specific B_{GC} cells 10-fold or more by week 3 (**Fig. 2H**). This was most pronounced in
158 G1, where by week 3 both antigen- and epitope-specific B_{GC} cells were rapidly increased 30-40-fold above
159 baseline. Despite the rise at week 6, G2 still had a ~10-fold lower frequency of epitope-specific B_{GC} cells
160 at weeks 6 and 9 compared to G1 (**Fig. 2K**, $p = 0.002$ week 6 and 0.002 week 9, Mann-Whitney). When
161 looking at total post-prime responses, G1 had significantly higher AUC values for both antigen- and
162 epitope-specific B_{GC} cells compared to all groups except G4 and G6 (**Fig. 2I, L**). These data suggest that
163 ED SMNP generated robust GCs faster than other groups and recruited epitope-specific cells to GCs to a
164 greater extent than all but G4 and G6.
165 We also examined the antigen- and epitope-specific non-B_{GC} cells at weeks 3 and 9 to determine
166 if certain groups drove a more extrafollicular or memory response in lymph nodes. The hierarchy of the
167 non-B_{GC} cell responses for the animal groups mirrored that seen for the B_{GC} for both antigen- and epitope-
168 specific cells (**Supp. Fig 4B-C**).
169 Unexpectedly, the slow-delivery behavior of pSer:alum combined with SMNP immunization did
170 not enhance total GC or antigen-specific B_{GC} cell responses over SMNP alone in either bolus or ED
171 administration. However, pSer-conjugated trimer delivered on nano-alum led to significantly more
172 epitope-specific B_{GC} cells out to week 10 compared to traditional alum (G6 vs G5) and was the only bolus-
173 administered formulation to increase GC responses approaching ED dosing (**Fig. 2I, L**), suggesting that
174 pSer:nano-alum has a unique mechanism of action.
175 Overall, these data from 36 animals over a 10-week time course indicate that the two ED SMNP
176 containing immunizations primed the most robust total and antigen-specific GC responses, with notably
177 accelerated B_{GC} expansion compared to bolus vaccination. Enhanced frequencies of epitope-specific B_{GC}
178 suggested that ED immunization with SMNP can better recruit diverse B cells after priming compared to
179 bolus or non-SMNP adjuvanted immunizations.
180
181 **Escalating dose adjuvanted with SMNP leads to a larger and more diverse BCR response**
182 Epitope-specific B_{GC} cells were FACS sorted and single cell BCR sequencing was completed at week 3
183 post-immunization to assess the ability of different delivery and adjuvant combinations to recruit and prime
184 rare BG18 type I precursor cells. A total of 26,207 epitope-specific paired BCRs from week 3 LN FNAs
185 were sequenced across all groups. BG18 type I BCRs are defined based on immunoglobulin heavy chain
186 (HC) sequence features and H-CDR3 length (**Supp. Fig. 5A**). BG18 type I BCRs were detected in 3/6
187 animals from G1 but no animals in any other group (**Fig. 3A, Supp.Table 1**). The results from G1 were
188 consistent with the original N332-GT5 RM study, in which 5/8 ED SMNP animals had BG18 type I B_{GC} cells

189 at week 3 (ref. [25]). G4 and G6 had similar total post-prime antigen- and epitope-specific B_{GC} cells compared
190 to G1 (**Fig. 2H, K**), thus it was surprising that no BG18 type I BCRs were found in these groups. If BG18
191 type I precursor priming was equivalent in all groups, BG18 type I BCRs were expected in all groups except
192 the non-SMNP group (G3) based on total sequencing per group (**Fig. 3A**). These data indicate that only
193 ED SMNP immunization possessed properties necessary for successful recruitment and expansion of very
194 rare BG18 type I precursor cells above a limit of detection of ~1 in 3,000 B_{GC} by 3-weeks post-vaccination.
195 As an additional measure of rare B cells, we searched for two other populations of cells; cells
196 similar to BG18 type I cells but with shorter H-CDR3 length, and potential BG18 type III cells. The original
197 definition used for BG18 type I cells in RMs includes H-CDR3s of at least 22 amino acids with additional
198 specific H-CDR3 sequence features[12], but we observed BCRs that otherwise meet the criteria for being
199 BG18 type I but have H-CDR3s of 20 or 21 AAs ("$BG18_{20\text{-}21AA}$" **Supp. Fig. 5A-B**). When quantified, $BG18_{20\text{-}21AA}$
200 cells were found in the same three animals from G1 where the traditional BG18 type I cells were found
201 but at a slightly lower frequency (**Supp. Fig. 5B**). We also observed a single $BG18_{20\text{-}21AA}$ BCR in one animal
202 each from G2 and G3 despite no traditional BG18s being found. BG18 type III BCRs, defined as those
203 having H-CDR3 lengths ≥20 AAs and a binding angle of approach and footprint similar to BG18 type I but
204 lacking other sequence features of BG18 type I or type II, were previously identified from RMs immunized
205 with N332-GT5 using B cell sorting, Fab production, and cryoEM studies[25]. We searched the BCRs for
206 sequences that used the same IGHD gene and contained the important contact residues from the cryoEM
207 structures as potential type III cells. These cells were found at similar frequencies to the traditional and
208 $BG18_{20\text{-}21AA}$ responses but were identified in two additional animals (**Supp. Fig. 5C**). These results further
209 corroborate that rare potential bnAb-precursor B cells are recruited and expanded after ED SMNP
210 immunization better than other immunization strategies.
211 To further understand the composition of the B_{GC} response at the population level, clonal richness
212 (Chao1) and diversity (Simpson index) were calculated of the epitope-specific B_{GC}. ED SMNP elicited a
213 larger and more diverse population of B_{GC} cells compared to all others groups except G6 (**Fig. 3B,**
214 **Supp.Fig. 5D**). There were no significant differences between pSer:alum groups G2, G4, and G5 in either
215 clonal richness or diversity, indicating that pSer:alum delivery, by bolus or ED, offered no clear advantage
216 over bolus immunization for increasing on-target B cell diversity (**Fig. 3B, Supp.Fig. 5D**). In contrast, G6
217 (nano-alum) had clonal richness comparable to G1 and significantly increased clonal richness compared to
218 G5 (**Fig. 3B**), indicating that pSer:nano-alum changed the overall B cell composition of the GC responses
219 compared to pSer:alum.
220 Clonal abundance curves were plotted for each group (**Fig. 3C**), and the cumulative abundance
221 of the top 5 clones was calculated for each animal (**Fig. 3D**). For G1, the top 5 clones accounted for ~30%
222 of the total B_{GC} response (median per group), while for G2 the median was significantly higher at ~80%
223 (**Fig. 3D**). Together, these parameters show that ED SMNP recruited large numbers of clones with
224 moderated immunodominance, whereas bolus SMNP immunization recruited fewer total B cell clones and
225 a small number of those clones dominated the GC response.
226 Ig isotype was determined for each sequenced BCR (**Fig. 3E**). All ED groups had a higher
227 frequency of class-switched isotypes (IgG1-4, IgA) than bolus immunization. For G2, over 50% of the
228 epitope specific B_{GC} cells at week 3 were IgM. This was in contrast to 90% of the epitope-specific B_{GC} cells
229 being IgG class-switched in G1 (**Fig. 3E**). When interpreted with the GC kinetics data (**Fig. 2H, K**), the class
230 switch frequency differences suggest that the GC responses were delayed after bolus immunization
231 compared to ED SMNP (**Fig. 3E**). Despite the increased size and diversity of the GC response for G6
232 compared to G5, both groups had similar isotype distributions, indicating that GC kinetics may be similar
233 in both groups, and the differential mechanism of nano-alum may lie more in the total number of different
234 B cells recruited to GCs.

Overall, the antigen-specific BCR sequencing data showed that in GCs 3-weeks post-prime, only ED SMNP recruited detectable BG18 type I cells, which correlated with a distinctly clonally rich, diverse, and rapid B_{GC} cell response compared to other groups. Regarding kinetics of the GCs, antigen- and epitope-specific B_{GC} frequencies showed that many groups still had low vaccine-specific GC responses at the 3-week time point, which subsequently peaked at 6 weeks post-prime, or even 10 weeks post-prime (**Fig 2H, K**). It therefore remained possible that the clonal composition of those more slowly amplifying B cell responses may evolve after week 3.

Vaccine-specific T cell responses

Germinal center responses require CD4 T cell help, specifically T_{FH} cells[51]. N332-GT5 specific T cell responses were measured by activation-induced marker (AIM) and intracellular cytokine staining (ICS) assays at 2-weeks post-immunization for multiparametric enumeration and functional analysis of the CD4 T cell response (**Fig. 4A**). N332-GT5–specific (AIM$^+$, CD40L$^+$OX40$^+$) CD4$^+$ T cell responses were detected in all six groups above the pre-immunization levels (**Fig. 4B**). The three pSer:alum groups had the lowest T cell responses (G4-G6, **Fig. 4B**). Similar trends between groups were seen with other AIM parameters, and by ICS for IFNγ, granzyme B, IL2, and TNF (**Supp.Fig. 6B-F**). Antigen-specific circulating T_{FH} (cT_{FH}) cells were measured (**Fig. 4C**). G1 had a significantly higher frequency of antigen-specific (AIM$^+$CD40L$^+$OX40$^+$) cT_{FH} cells compared to all other groups (**Fig. 4D, Supp.Fig. 6G**). The remaining groups had similar frequencies of cT_{FH} cells, despite clear differences in GC-T_{FH} frequencies between groups. For G4 and G6, both had ~3-fold higher frequencies of GC-T_{FH} compared to other groups but similar levels of cT_{FH} (**Fig. 4D, 2E-F,** week 3).

IL-21 ICS was performed to assess whether the vaccine-specific cells were able to produce IL-21, which is an important cytokine for B_{GC} and plasma cells (B_{PC}) (AIM+ICS, CD40L$^+$IL21$^+$, **Fig. 4E**). Detectable IL21$^+$ antigen-specific CD4 T cells were identified in some animals, with only G1 (4/6) and G3 (3/6) having significantly higher responses compared to pre-immunization ($p = 0.001$ (G1) and 0.013 (G3), **Fig. 4F**).

CD8$^+$ T cell responses were examined by AIM+ICS to determine whether these protein immunizations primed antigen-specific CD8$^+$ T cells (AIM+ICS, CD69$^+$IFNγ$^+$). All groups had at least 3 animals with detectable IFNγ-secreting CD8$^+$ T cells, with all but G5 and G6 significantly higher than background (**Fig. 4G-H**).

Altogether, these T cell data show that all immunization strategies primed antigen-specific CD4$^+$ T cells. cT_{FH} cell and IL-21 responses were particularly robust after ED SMNP immunization, consistent with the larger early GC responses seen in G1, which may have contributed to the strongest early recruitment of very rare BG18 Type 1 precursors in G1.

Escalating dose with SMNP led to rapid induction of antigen-specific serum IgG

To further dissect the response to each delivery strategy and adjuvant combination, serum IgG titers were measured over time by ELISA, and AUC values were calculated (**Fig. 4I-L** and **Supp.Fig. 7A-B**). G1 had rapid induction of high titers of N332-GT5 specific serum IgG at week 2, which peaked at week 6 and remained high at the time of boosting (**Fig. 4I**). In contrast, G2 had low levels of serum IgG that remained stagnant after seroconversion at week 2 (**Fig. 4I**). Antigen-specific serum IgG peaked at week 6 in G3, G4, and G6, with declines at week 10. G1 maintained significantly higher titers at week 10 than all other groups (**Fig. 4I-J**). IgG AUC values for G1 were 5 times higher than G2 at week 10, demonstrating a significant enhancement in the ability of ED immunizations to induce high titers of antigen-specific IgG after priming compared to bolus immunization. Epitope-specific IgG AUC values in G1 were 6 times higher at week 10 compared to G2, further emphasizing the stark difference in the serum IgG response between ED and bolus priming (**Fig. 4K-L.** Median log10 endpoint titers G1 vs G2, 1.81 vs 0.39; **Supp.Fig. 7B**). G6 (nano-alum) exhibited the lowest IgG titers post-prime (**Fig. 4K-L**), contrasting with the relatively strong GC

282 responses measured (**Fig. 2**). When post-prime antigen- and epitope-specific B_{GC} responses were graphed
283 together with IgG AUC values at week 10, G6 is a clear outlier (**Supp.Fig. 7C-D**); exclusion of G6 increases
284 the Pearson correlation values and significance of the B_{GC} cell to serum IgG association for both antigen-
285 and epitope-specific responses (**Supp.Fig. 7C-D**). This suggests that although for most groups there is a
286 strong association between GC and serum antibody responses, nano-alum immunization generates
287 unusually divergent B_{GC} and B_{PC} responses. In total, the serum IgG data showed that early priming
288 responses were much stronger after ED SMNP immunization compared to all other groups, with sustained
289 high titers of antigen- and epitope-specific IgG in G1.
290

291 **Escalating dose primed larger B_{mem} responses but bolus immunization led to better memory recall**
292 **responses post-boost**

293 To evaluate the immune memory elicited by the different adjuvants and vaccine delivery mechanisms,
294 antigen- and epitope-specific IgD^- memory B (B_{mem}) cells were interrogated longitudinally by flow
295 cytometry (**Fig. 5A, C**). G1 had the highest B_{mem} frequencies for both total antigen-specific and epitope-
296 specific cells at week 6 (**Fig. 5B, D**). Most groups had modest measurable antigen- and epitope-specific
297 B_{mem} cells at week 6 or 10 post-prime (**Fig. 5B, D, E, G**). At week 10, G1 had a significantly higher frequency
298 of epitope-specific B_{mem} cells compared to all other groups and was 10-fold higher than G2 (**Fig. 5G**).
299 Despite antigen-specific GC responses similar to G1 (**Fig. 2I**), G4 and G6 had significantly lower levels of
300 antigen-specific B_{mem} at week 10 compared to G1 (**Fig. 5E, G**).
301 After boosting at week 10, an increase in antigen-specific B_{mem} frequencies were observed for all
302 groups. Unexpectedly, G2 exhibited a median antigen-specific B_{mem} frequency equal to G1 at week 12,
303 despite having the lowest pre-boost antigen-specific B_{mem} frequency (**Fig. 5E**). The median epitope-
304 specific B_{mem} frequency at week 12 was also equal between G2 and G1 (**Fig. 5G**). To explore this change
305 further, the week 10 to 12 B_{mem} fold change was calculated for each animal (**Fig. 5F, H**). G2 had a 100-fold
306 increase in B_{mem} (**Fig. 5F**), ~20 times greater than the increase observed for G1. Nano-alum G6 had the 2nd
307 lowest B_{mem} frequency post-prime, and exhibited a 30-fold increase at week 12 (**Fig. 5F**). Similar results
308 were observed with epitope-specific B_{mem} (**Fig. 5H**). Despite major shifts in B_{mem} frequencies, the LN FNA
309 antigen- and epitope-specific B_{GC} frequencies were mostly unchanged from week 10 to 12 (**Fig. 2E, H**).
310 Notably, the G2 B_{GC} frequencies at week 12 were still 5- and 20-fold lower than G1 for antigen- and
311 epitope-specific B_{GC} cells respectively, despite similar B_{mem} frequencies (**Fig. 2E, H**). In sum, ED
312 immunizations formulated with SMNP led to the highest frequencies of antigen- and epitope-specific B_{mem}
313 cells post-prime; however, booster immunization drastically increased the frequency of B_{mem} in response
314 to bolus SMNP or nano-alum combined with SMNP, suggesting a substantial shift in the parameters
315 regulating immunogenicity between the prime and the booster immunization.
316

317 **Bolus SMNP induced a high frequency of BG18 type I B_{mem} cells post-boost**

318 Epitope-specific B_{mem} were sorted and sequenced from PBMCs at week 12. BG18 type I B_{mem} sequences
319 were found in 5 of 6 animals in G1 (**Fig. 5I, Supp.Table 2**), consistent with the GC data (**Fig. 3A**) and results
320 from the first study[25]. Unexpectedly, while no BG18 type I B_{GC} were detected in G2 at week 3, G2 had a
321 high frequency of BG18 type I B_{mem} at week 12 that was not significantly different from G1 (**Fig. 5I**). The
322 remaining study groups inconsistently developed BG18 type I B_{mem}, which were only detected in 2 of 24
323 animals (**Fig. 5I**). Of note, despite robust GC responses in G4 and G6, only one animal from G4 and two
324 from G6 had detectable BG18 type I B_{mem} (**Fig 5I**). The results observed for $BG18_{20\text{-}21AA}$ and potential type
325 III cells were similar to BG18 type I responses across the groups, with the caveat that G2 appeared to have
326 more sporadic responses (**Supp. Fig. 8B-C**).
327 The clonal diversity of B_{mem} in the immunized animals was examined by multiple metrics. B_{mem} were
328 more clonally rich and diverse across all groups compared to B_{GC}, likely due to the inherently less clonal

329 nature of circulating B_{mem} cells compared to B cells participating in a GC reaction in a single LN (**Fig 5J,**
330 **Supp.Fig. 8D** compared to **Fig 3B-E, Supp.Fig. 5D**). G1 still had the greatest B_{mem} clonal diversity across
331 multiple measures (**Fig 5J-L, Supp.Fig. 8D**). However, similar to B_{mem} frequencies above, G2 was much
332 more similar to G1, with only clonal richness showing a significant difference between G1 and G2 (**Fig 5J**).
333 Simpson diversity index and cumulative abundance curves showed similar trends (**Supp.Fig 8D, Fig 5K**).
334 Immunodominance in immune memory, as assessed by the dominance of the top 5 B_{mem} clones, was
335 lowest in G1, G2, and G6 (**Fig 5K-L**). Overall, the totality of the post-boost B_{mem} data showed that bolus
336 or ED immunizations adjuvanted with only SMNP could prime rare BG18 type I precursors after N332-GT5
337 immunization. All other combinations inconsistently led to priming of BG18 type I precursors. In addition,
338 the data indicated that, despite relatively low GC responses in G2 animals, a homologous booster
339 immunization could generate highly expanded BG18 type I B_{mem} cells and a more clonally rich and diverse
340 response than initially expected.
341
342 **IGHD3-41 Immunogenetics**
343 BG18-like type I BCRs utilize the RM D gene *IGHD3-41*[25]. In both humans and RMs, there is extensive
344 genetic diversity within the immunoglobulin (IG) gene loci, including coding and non-coding single
345 nucleotide variants, as well as large structural variants that can result in changes in IG gene copy number
346 [30,31,38,52–55]. To date, >800 IG alleles have been characterized in RMs, including multiple alleles at the IGHD
347 gene, *IGHD3-41*[30,38]. The coding sequence of IGH genes is known to be important for antigen binding and
348 development of specific responses to pathogens[56] and in the case of BG18, the D gene coding sequence
349 is an important part of the paratope[12,25]. To assess the genetic compatibility of animals in this study for
350 BG18 type I responses, we carried out long-read sequencing of the IGH locus in all 42 animals to genotype
351 *IGHD3-41* alleles. All animals carried *IGHD3-41* in their genome and were determined to be either
352 homozygous or heterozygous for the alleles *IGHD3-41*01* and *IGHD3-41*01_S8240* (**Supp.Table 3**). Both
353 of these alleles are capable of making BG18 type I responses using reading frame 1 or 3 (**Supp.Table 3**).
354 IG immunogenetic studies have shown that allelic variants can associate with differential gene
355 usage in the naïve B cell repertoire, which has the potential to skew the composition of B cell and antibody
356 responses[7,57–59]. For 35 animals, D gene usage in the IgM repertoire was examined using bulk adaptive
357 immune receptor repertoire sequencing (AIRR-seq). Animals that were **01/*01* homozygotes used *IGHD3-*
358 *41* at a higher frequency in naïve IgM^+ B cells than animals that were **01/*01_S8240* heterozygotes or
359 **01_S8240/*01_S8240* homozygotes (~1.5- and 2-fold higher, respectively. $p=7.94x10^{-7}$, **Fig. 5M**. The
360 three genotypes were relatively well distributed throughout the groups, with heterozygotes being the
361 dominant genotype represented (**Supp.Fig. 9A-B**). When testing for associations between genotype and
362 post-boost BG18 type I BCR frequencies, **01/*01* homozygotes had higher frequencies, but this
363 association did not reach significance when looking at all animals together (**Supp.Fig. 9B-C**). Despite the
364 relatively large number of total animals used in this study, it was still underpowered to detect differences
365 between genotypes due primarily to the scarcity of **01/*01* individuals. Nevertheless, all three genotypes
366 were capable of making BG18 type I responses after N332-GT5 vaccination (**Supp.Fig. 9B-C**), and the
367 three genotypes were randomly distributed between the groups (**Supp.Fig. 9A-B**). Thus, the *IGHD3-41*
368 genotypes influence on B cell precursor frequencies did not explain the majority of the inter-group BG18
369 type I B cell response differences observed.
370
371 **Serum IgG levels inversely predicted booster immunization outcomes**
372 Post-boost serum IgG titers were quantified (**Fig. 4I, K**). G2 antigen-specific IgG increased 5-fold from
373 week 10 to 12, while only a modest change was observed for G1 (**Fig. 6B, D**). At week 12, antigen- and
374 epitope-specific IgG AUC values for G2 were similar to G1 (**Fig. 4I, K. Fig. 6A, C**). A clear inverse
375 relationship was observed for all groups between pre- and post-boost IgG titers, whereby the higher the

week 10 IgG titers the smaller the fold increase after boosting (r = -0.96. P < 0.0001. **Fig. 6E**). A similar relationship was seen with epitope-specific IgG (r = -0.71. P < 0.0001. **Supp.Fig. 10A**). A significant inverse relationship was also seen between the B_{mem} fold changes (boost:pre-boost) and pre-boost serum IgG titers (week 10) across study groups (r=-0.52, p=0.001. **Fig. 6F**). These data indicate that very high levels of circulating N332-GT5 specific IgG at week 10 in G1 were associated with a blunted B cell recall response to homologous booster immunization, as observed in the modest increases in B_{mem} (**Fig. 5H**), BG18 type I BCRs (**Fig. 5I**), and serum IgG (**Fig. GD**). In contrast, the low levels of pre-boost IgG in G2 allowed for strong responses to the booster immunization, involving a dramatic 100-fold increase in antigen-specific B_{mem}, detectable BG18 type I B_{mem} in most animals, and large increases in serum IgG titers.

Bone marrow plasma cells

The durability of the humoral immune response for each group was assessed by quantifying N332-GT5 specific bone marrow (BM) B_{PC} (**Fig. 6G, Supp.Fig. 10B-C**). Only G1 developed substantial antigen-specific BM B_{PC} after priming (week 10, **Fig. 6G**), with levels ~40-fold greater than G2. All groups showed an increase in BM B_{PC} 6-weeks after the booster immunization (week 16, **Fig. 6G-H**). G2 had the most dramatic increases from week 10 to 16 (**Fig. 6H**), which correlated with the strength of the IgG and B_{mem} response post-boost. G2 had the second highest BM B_{PC} responses post-boost, although still 5-fold lower than G1 (**Fig. 6G**). However, the ELISA data (**Fig. 4I, K**) suggests that in G2 much of the post-boost response is short-lived, while both antigen- and epitope-specific responses appear to be more stable in G1, evident by the more rapid decline in titers from week 12 to 16 for G2. The BM B_{PC} data reinforced that SMNP adjuvanted bolus or ED immunizations led to the strongest outcomes across all measures of humoral immune responses.

BG18 type I BCRs had more SHM and higher affinity for boosting candidates

Similar levels of circulating BG18 type I B_{mem} cells were observed after booster immunization for both G1 and G2 (ED and bolus SMNP, **Fig. 5I**). BG18 type I B_{GC} cells were undetectable in G2 at week 3, and antigen-specific B_{GC} cells were 50-fold lower in G2 than G1 at week 3 (**Fig 3A and 2H**). Thus, the week 3 and week 12 BG18 type I cell outcomes were discordant. We therefore endeavored to better understand the underlying immunological processes resulting in these large changes. This topic was of particularly interest given the very rare precursor cells involved. Three plausible scenarios were considered. One possibility was that many fewer BG18 type I cells were primed in G2 compared to G1, but that post-boost those few BG18 type I clones in G2 massively expanded because of the high affinity interaction with N332-GT5 and the absence of competing circulating IgG. A second possible scenario was that BG18 type I cells were only primed in G2 after the second immunization, whereas BG18 type I cells were primed and expanded after the initial ED immunization of G1. A third possible scenario was that BG18 type I cells were primed in G2 after the first immunization, but at the 3-week time point G2 still had low vaccine-specific GC responses, which subsequently peaked 6-10 weeks post-prime (**Fig 2H, K**) resulting in the very rare BG18 type I cells being recruited into the GCs substantially later post-prime for G2 compared to G1, with a booster immunization required to expand the BG18 type I cells sufficiently to be detectable in G2. We resolved these three scenarios through a series of experiments, including assessment of clonality, quantitation of somatic hypermutation (SHM), and measurements of antibody affinities derived from G1 and G2 BG18 type I BCRs.

First, BCR sequence analysis revealed that responding B cells in both G1 and G2 had similar numbers of total BG18 type I clonal families (**Fig. 7A**). The clonal families had equally diverse usage of different IGHV genes (**Fig. 7B**). The clonal families also had equally diverse light chain usage in both groups (**Supp. Fig. 11A**). These data indicated scenario #1 was unlikely.

422 Scenario #2 (priming of BG18-like cells only after the G2 booster immunization) could be tested
423 by examination of SHM between G1 and G2. In that scenario, BG18 type I BCRs from G2 B_{mem} at week 12
424 would have low or no SHM, whereas BG18 type I BCRs from G1 B_{mem} would have substantial SHM, while
425 the total antigen-specific B_{mem} populations would have similar mutations between groups. Scenario #3
426 could also be resolved by SHM analysis, as cells experiencing less time in GCs would be expected to have
427 less SHM. SHM was analyzed for all groups (**Supp. Fig. 11B-C**). Overall SHM heavy chain (HC) mutation
428 counts of total antigen-specific B cells were similar between G1 and G2 (**Fig. 7C**), with > 98% of clones
429 containing HC SHM in both groups, consistent with the vast majority of the B_{mem} derived from the antigen-
430 specific B_{GC} responses observed in both groups post-prime (**Fig. 2H-I**). Notably, when BG18 type I BCRs
431 were examined, > 98% of clones also contained HC SHM in both groups (**Fig. 7C**). G2 did have more
432 BG18 type I BCRs that had 1-4 HC mutations at week 12 (**Fig. 7C**); however, all but one of these cells
433 belonged to clonal families with BCRs that had >5 HC mutations, making it unlikely that they were primed
434 just two weeks earlier (**Supp.Table 2**). These results suggested that scenario #2 was implausible to explain
435 the majority of the BG18 response in G2. In contrast, when SHM of BG18 type I BCRs was quantitatively
436 assessed, G2 had fewer HC mutations per BCR than G1 ($p = 0.0009$, **Fig. 7C**), while SHM of non-BG18
437 BCRs was indistinguishable between G1 and G2 (**Fig. 7C**). Thus, a parsimonious interpretation of the data
438 is that BG18 type I B cells from G2 likely participated in GC reactions for a shorter period of time after the
439 initial priming than did the BG18 type I cells from G1, based on SHM levels.
440 To examine the functional consequences of the SHM differences, a selection of BG18 type I BCRs
441 from each group were produced as IgG antibodies, and binding affinities were determined. Antibodies
442 from both G1 and G2 exhibited very high affinity for N332-GT5, and no significant difference was observed
443 between the groups (**Fig. 7D**). All antibodies were epitope-specific, as expected, exhibiting no binding to
444 N332-GT5KO (**Fig. 7D**). Affinity to three heterologous Env trimer boosting candidates[9,25] was determined.
445 100% of BG18-like antibodies from G1 had detectable affinity for heterologous booster candidate
446 BG505_B16, the most similar antigen to N332-GT5, while only 79% (11/14) of the antibodies from G2
447 bound BG505_B16. BG505_B16 affinities were significantly stronger for G1 antibodies compared to G2 (p
448 $= 0.016$, **Fig. 7D**). Affinities were also significantly stronger for G1 antibodies compared to G2 for
449 BG505_B11, the most native-like Env booster candidate tested ($p = 0.035$, **Fig. 7D**). Overall, these SHM
450 and binding data consistently indicate that BG18 type I precursors from G2 were primed by the initial
451 immunization but spent less time participating in the GC reaction compared to G1, with functional
452 consequences observed by reduced binding affinity for heterologous boosting candidates.
453
454
455 **DISCUSSION**
456 Despite their importance in generating quality immune responses to vaccination, the processes governing
457 recruitment of rare bnAb-precursor B cells, and competition between rare and common B cell specificities,
458 are only partially understood[6]. These processes have primarily been studied in mouse models using
459 precisely controlled frequencies of adoptively transferred rare B cells[4,9–12,60,61]. Here we explored
460 recruitment and differentiation of rare B cells in an outbred, non-transgenic, model using an HIV germline-
461 targeting priming immunogen and demonstrate that different antigen delivery strategies and adjuvants
462 can extensively impact the priming, expansion, differentiation, and affinity maturation of rare precursor B
463 cells.
464 Despite all six groups inducing antigen-specific GC responses, only ED SMNP (G1) drove early
465 recruitment of BG18 type I precursors detectable at week 3. After a booster immunization, BG18 type I
466 B_{mem} cells were identified in at least one animal from every group, indicating that recruitment of these cells
467 to GC reactions and subsequent differentiation to B_{mem} is possible under a variety of immunization
468 conditions. Most strikingly, a priming bolus immunization with SMNP (G2) recruited BG18 type I B cells to

469 GCs, despite very small GC reactions observable by week 3 post-prime, and these cells could be rapidly
470 expanded upon boosting.
471 Kinetics of naive B cell recruitment may play a large role in the results seen here, particularly the
472 early GC data. Finding BG18 type I cells in at least one animal in every group at week 12 indicates that
473 some recruitment of these rare precursors can occur under all six conditions tested, but is inconsistent at
474 best in most groups. The frequencies seen amongst the week 12 B_{mem} cells is likely more representative
475 of the true post-prime recruitment efficiency for each group. It is possible that in the week 3 GCs there are
476 BG18 type I cells present at such low frequencies that we could not yet detect them. Nevertheless, in the
477 case of the bolus immunization group the epitope-specific B_{GC} data suggest that these cells may enter
478 GCs later under those conditions. The SHM data also suggest that the BG18 type I cells from the bolus
479 group have spent less time in the GC than those after ED immunization, which is consistent with later
480 recruitment. Those outcomes are consistent with early T cell help likely playing a crucial role in the kinetics
481 of early GC development and diverse B cell recruitment to GCs[38,62,63]. This was evidenced by the most
482 robust early GC-T_{FH} and cT_{FH} responses being observed in G1, which may be driving many of the other
483 outcomes.
484 We previously estimated that it was conceivable that ~1.2 x 10^9 naïve B cells could be "screened"
485 in LNs for antigen-recognition under relatively optimized immunization conditions in humans[6]. We can
486 extend this calculation, using similar assumptions, to RMs using updated data. There are ~5 million B cells
487 per RM inguinal LN. We, and others, have shown that multiple LNs in a drainage region will uptake
488 antigen[39,64–67] and that after ED immunization with SMNP this may be 3-5 LNs in a specified region[39] (~20
489 million B cells). It has also now been shown that after SMNP immunization the antigen drains to deeper
490 LN clusters, probably tripling the number of LNs engaged (~60 million B cells)[68]. The immunizations in this
491 study were done bilaterally, doubling the number of LNs engaged (~120 million B cells). Naïve B cells are
492 constantly moving through lymphatics, and in humans exhibit a LN dwell time of 10-16 hours[69–71]. After a
493 bolus immunization it is reasonable to assume that naïve B cells can be recruited during the first 48-hours[72],
494 which would perhaps represent 4x turnover of the naive B cell population during that timeframe. The data
495 suggest that after ED immunization naïve B cells may be recruited for 2- to 3-weeks[37,38,73], which plausibly
496 represents 28 to 42x turnover of the naive B cell population per LN during that 2- to 3-weeks. Furthermore,
497 influx of cells into LNs after immunization can lead to swelling and 2- to 4-fold increased cell numbers[72].
498 Those estimations result in a calculated number of ~13 x 10^9 naive B cells potentially being "screened" *in*
499 *vivo* for antigen binding after ED SMNP immunization in RMs.
500 Although we do not know the true number of BG18 type I precursors that can bind to and be
501 activated by N332-GT5 in RMs, in humans, BG18 type I precursors were found at ~1 in 50 million naïve B
502 cells[12,25]. Based on previous precursor frequency calculations that number is likely to be 2-8-fold lower in
503 RMs (1 in 100-400 million[25]). Taken together, these calculations would indicate that between 32 and 130
504 BG18 type I naïve B cells are potentially screened for antigen binding in LNs after N332-GT5 ED
505 immunization with SMNP in RMs.
506 Experimentally, we observed that in G1 that there was a median of 3.5 BG18 type I clonal families
507 per animal (range 0-8, **Fig. 7A**) in the B_{mem} compartment. Using rarefaction analysis on the week 12 B_{mem}
508 sequencing results, we estimated that ~50% (range of 40-75%) of the B_{mem} repertoire was sampled in the
509 animals from G1 (**Supp. Fig. 7E**). This indicated that the true number of BG18 type I clonal families present
510 in each animal was likely double that observed experimentally (median 7, range 0-16). These calculations
511 were undertaken using assumptions based on experience with ED immunization in RMs, but the numbers
512 are likely much lower in non-SMNP and bolus immunization animals, which underscores the difficulty in
513 eliciting these types of rare responses in NHPs and likely humans as well.
514 When pSer modification was used to deliver a native HIV Env trimer in mice, increases in both
515 antigen-specific GC B cells and IgG titers were seen compared to normal bolus immunization[43]. The same

pSer trimer adjuvanted with SMNP led to slightly better total humoral responses, including development of autologous nAb titers, in NHPs, associated with the its extended release and valency attributes of pSer [45]. It was therefore unexpected that bolus immunization led to better priming of BG18 type I cells compared to pSer:alum SMNP herein. Even more unexpected was the poor recruitment of BG18 type I cells seen when delivering pSer modified N332-GT5 by ED. This group had some of the highest GC responses, but those large numbers of B_{GC} did not translate into efficient recruitment of rare BG18-like precursors. Despite this, the nano-alum group exhibited unique immunological characteristics that suggest that nano-alum may have a distinct mechanism of action compared to traditional alum and further study is warranted.

The other adjuvant tested, Amph-CpG, performed worse than SMNP in ED immunization. Amph-CpG has shown promise in modulating immune responses against SARS-CoV-2 vaccines in NHPs[50]. Further work is needed to elucidate how engaging different TLRs leads to differences in adjuvanticity compared to SMNP.

One of the more striking outcomes presented here was the large boosting response seen for the bolus immunization group, which inversely correlated with the circulating IgG titers pre-boost. The outcome implicated antibody feedback as a major factor in the booster immunization outcomes. Antibody feedback has recently seen a resurgence in research, in part due to observations surrounding antibody responses to COVID-19 vaccination[74–77]. Antibody feedback can exert influence through multiple mechanisms. One possibility is that the high level of circulating IgG leads to antigen clearance effectively lowering the dose of the boosting immunization. Antigen clearance traditionally occurs through Fc receptor mediated uptake of immune complexes by non-follicular antigen-presenting cells[77]. Another possibility was epitope masking by IgG produced by BG18 type I B cells. In a recent knock-in mouse study of N332-GT5 immunization, the authors found that excess antigen could overcome the antibody-dependent clearance of antigen by effectively depleting the circulating IgG and allow for better secondary GC responses[78]. Others have shown that IgG to dominant epitopes can lead to better responses to sub-dominant epitopes in subsequent immunizations by focusing the GC response[74,76,79–82]. ED or other slow delivery immunization strategies likely enhance priming of more diverse B cell responses due to engagement of this mechanism involving the earliest antibodies[37,38,73]. It is conceivable that in the bolus immunization group, the low circulating IgG titers of off-target but antigen-specific IgG could lead to immune complex formation and better uptake by follicular dendritic cells after booster immunization, while the lack of epitope-specific IgG allows for a focusing of the response on epitope[83]. Whereas after ED, the extremely high titers of antigen- and epitope-specific IgG led to both antigen clearance and masking of the N332 epitope on residual antigen. In the pSer:alum ED group, the epitope-specific response may have been low enough to minimize any epitope masking, but it is conceivable that the total IgG titers were sufficiently high as to lead to antigen clearance. It remains an interesting observation that although the circulating titers at week 10 predict the post-boost B_{mem} frequencies, there is no correlation with the antigen- and epitope-specific B_{GC} frequencies from week 10 to 12.

In mice, many vaccination strategies induce high titers of circulating antibodies after a single immunization, which allows antibody feedback to be a potentially major factor[77,78,80,82]. It would be expected that the impact of antibody feedback would be more modest in contexts of lower antibody responses. In large animal models and humans, single immunizations most often generate relatively low antibody responses, which are also often transient[38,84–86]. The experiments described herein include three features resulting in high antibody titers after the priming immunization. One feature is the nature of the antigen itself, which is highly immunogenic due in part to a substantial glycan hole[9,19,25,29]. Two additional features are the use of ED immunization and SMNP, which both enhance rapid induction of antibody responses. These features make this model system have characteristics wherein antibody feedback mechanisms may be more likely observed, compared to contexts where priming elicits low antibody titers.

563 We previously found that combining pSer:alum delivery and SMNP augmented induction of
564 autologous neutralizing responses in RMs to native-like HIV trimers over either vaccine strategy alone[45], in
565 contrast to the present study where pSer:alum delivery did not improve the recruitment of rare BG18-like
566 precursors. An important difference in these two scenarios, which may play an important role in the B cell
567 response, is epitope availability. The early antibody response to soluble native-like Env trimers if
568 dominantly focused on the irrelevant base of the immunogen [37,38,42]. Vaccine strategies like ED that amplify
569 the early antibody response against this epitope may promote capture of antigen on FDCs and allow more
570 time for rare precursors targeting other sites to be recruited to a GC. By contrast, N332-GT5 Env trimer is
571 engineered with a prominent glycan hole around the target BG18 epitope, relatively distant from the Env
572 base, and adoptive transfer models of rare precursor B cell recruitment by this immunogen have shown
573 that the Env trimer base is no longer dominant in this scenario, but rather B cells binding in the vicinity of
574 the new glycan hole epitope instead dominate[12]. In this situation, antibody feedback may hinder rather
575 than help the development of the desired on-target B cell response.
576 The comparison between ED and bolus immunization here is additionally valuable as it informs
577 ongoing clinical development of N332-GT5 as an HIV vaccine candidate. Currently, the first-in-human
578 clinical trial for both N332-GT5 and SMNP is ongoing (ClinicalTrials.gov Identifier: NCT06033209). In that
579 study, ED and bolus immunizations with N332-GT5 + SMNP are being compared head-to-head. The
580 results presented here will help inform the analysis of that trial and provide a benchmark for comparing
581 the priming efficiency in humans. Indeed, our results suggest that bolus immunization with suitably
582 designed germline-targeting trimer immunogens and appropriate adjuvants may suffice for inducing bnAb
583 precursor responses in humans. These data demonstrate that adjuvant selection is key, and the capacity
584 of SMNP to induce large GC responses recruiting highly diverse B cells, including very rare precursors, will
585 be an important component of any protein-based germline-targeting immunization regimen.
586 The next step for development of a germline-targeting vaccine to induce bnAbs will rely on
587 shepherding of the primed precursors towards bnAbs, and therefore the BG18-class B cells induced by
588 N332-GT5 must be able to engage more native-like HIV Env trimers, without being blocked by serum
589 antibodies. At this time, the *in vivo* affinity threshold for boosting the primed BG18 type I responses in
590 NHPs is not clear, but knock-in mouse data suggests that even modest affinities can lead to robust
591 boosting[9]. We hypothesize that BG18 type I cells after ED or bolus SMNP + N332-GT5 have sufficient
592 affinity to the tested immunogens as to be boosted *in vivo* by select heterologous Env trimers. Notably,
593 ED+SMNP priming elicited B cells with higher affinity for booster immunogen candidates, suggesting that
594 approach may allow for earlier introduction of native-like antigens in the immunization sequence.
595 In sum, here we demonstrated that both ED and bolus immunization can lead to priming and
596 expansion of rare BG18 type I B cells in NHPs when adjuvanted with SMNP and represent the first direct
597 study of rare B cell recruitment under multiple conditions in an outbred, non-transgenic, animal model. In
598 the context of germline-targeting immunizations, the quality of the B cells was higher in the ED group,
599 consistent with more rapid recruitment of B cells to GCs and more extensive SHM in GCs, along with
600 differential regulation of the rare B cell responses by the different concentrations of circulating IgG
601 generated by the different immunization conditions.
602
603

604 ## STAR METHODS
605
606 ### Adjuvant production and formulation
607 Alhydrogel aluminum hydroxide adjuvant was purchased from Invivogen and used as received.
608 SMNP adjuvant was synthesized and characterized as previously described[39]. Amph-CpG consisting of the
609 class B CpG 7909 sequence (5'-TCG TCG TTT TGT CGT TTT GTC GTT-3') conjugated at the 5′ end to a
610 diacyl lipid tail (ref [87])was prepared by solid phase synthesis by Axo Labs.
611 Nano-alum was generated by dispersing aluminum hydroxide adjuvant in the presence of a
612 phosphate-containing PEG-lipid surfactant. Alhydrogel (10 mg, Invivogen) was diluted to 1 mg/mL in
613 deionized water and combined with 10 mg of 1,2-distearoyl-sn-glycero-3-phosphoethanolamine-N-
614 [amino(polyethylene glycol (PEG))-2000] (Avanti Polar Lipids). The mixture was transferred to a 20 mL glass
615 scintillation vial and cooled to 4°C in ice water. While still on ice, the mixture was sonicated with a Misonix
616 Microson Ultrasonic Cell Disruptor XL2000 probe tip sonicator for 30 minutes, during which it transitioned
617 from opaque to opalescent. Care was taken to position the sonication probe deep enough in the mixture
618 to prevent foaming. Output power at the start of the sonication was set to ~20, with the power turned
619 down as sonication progressed and the solution transitioned from opaque to translucent. To remove
620 excess alum aggregates, the sonicated material was then incubated at 25°C for five days to enable
621 precipitation of any residual non-stabilized alum. The supernatant containing the suspended nano-alum
622 was collected, and nanoparticle formation was verified via dynamic light scattering on a Malvern Zetasizer
623 Nano instrument. Nano-alum used in this study was measured to have a Z-average diameter of ~70 nm
624 and a low PDI.
625
626 ### Protein production and pSer modification
627 For the expression of the N332-GT5 immunogen, a stable CHO cell line clone was developed utilizing the
628 Leap-In transposon expression system (ATUM, US10041077). The DNA sequence encoding the N332-GT5
629 trimer and its corresponding signal peptide was first synthesized. Subsequently, expression constructs
630 were designed and engineered based on the proprietary Leap-In transposon platform. The production of
631 the trimer protein involved comprehensive upstream cell culture and downstream purification process
632 development, followed by scale-up to large-scale cGMP manufacturing (details to be published in a
633 forthcoming article). With the exception of the signal peptide, the amino acid sequence of this trimer,
634 matches the N332-GT5 protein that was reported previously[25].
635 The N332-GT5 trimer used for pSer conjugation contained the C-terminal linker sequence
636 "GTKKKC", previously optimized for Env trimers and referred to as nohis8[43], placing a free terminal
637 cysteine for subsequent pSer peptide coupling. The trimer was co-transfected with furin into 293F cells
638 and purified using Galanthus nivalis lectin affinity chromatography (Vector Laboratories) followed by SEC
639 purification using Superdex 200 16/600 PG column (Cytiva).
640 Trimers that were used as SPR reagents were expressed with C-terminal 6xHis-tag and purified
641 using a HIS-TRAP column followed by size exclusion chromatography (SEC) on a Superdex 200 Increase
642 10/300 column (Cytiva) as described previously[25]. N332-GT5 and N332-GT5-KO trimers that were used as
643 biotinylated sorting reagents were expressed with a C-terminal His-tag and avi-tag, purified using a HIS-
644 TRAP column followed by SEC and biotinylated using a BirA biotin-protein ligase reaction kit (Avidity,
645 catalog no. BirA500) as described previously[25]. Compared to the immunogens, the N332-GT5 sorting
646 probes lacked the 241 and 289 glycosylation sites.
647 N332-GT5 trimers with a C-terminal Cys were conjugated with maleimide-functionalized pSer
648 peptide tags and characterized as previously described[43]. Briefly, peptides carrying 4 phosphoserines and
649 N-terminally functionalized with a maleimide group (mal-$pSer_4$) were produced by solid phase synthesis,
650 purified by HPLC, and their mass confirmed by matrix-assisted laser desorption/ionization-time of flight

651 mass spectrometry. N332-GT5-Cys trimers were gently reduced with tris(2-carbox- yethyl)phosphine then
652 reacted with 5 molar equivalents of mal-pSer4 in tris-buffered saline, followed by centrifugal filtration to
653 remove unconjugated peptide. The degree of modification of trimers was quantified using a Malachite
654 Green Phosphoprotein Phosphate Estimation Assay Kit (Thermo Scientific). Alum binding of pSer-
655 conjugated N332-GT5 was assessed by labeling the trimer with an AlexaFluor dye and assessing bound
656 protein following mixing with alum (loading) or following incubation of loaded alum with 10% mouse serum
657 in tris-buffered saline for 24 hr as previously described[43]. Antigenicity profiles of alum-bound pSer-N332-
658 GT5 were assessed by capturing alum particles on ELISA plates followed by addition of pSer-trimer to
659 allow binding, washing, and then probing with indicated dilutions of monoclonal antibodies as previously
660 described[42].
661
662 Mouse immunogenicity testing of nano-alum
663 All mouse studies were carried out at MIT under an IACUC-approved protocol following federal,
664 state, and local guidelines. Female BALB/c mice (Jackson Laboratory) 6-8 weeks of age were immunized
665 s.c. bilaterally at the tail base with alum/pSer-trimer or nano-alum/pSer-trimer. For flow cytometry analysis,
666 lymph nodes were harvested, crushed to form a single-cell suspension, and subjected to staining for
667 viability (Zombie Aqua Fixable Viability Kit, BioLegend), CD4 (BV711, BioLegend, RM4-5 clone), B220 (PE-
668 Cy7, BioLegend RA3-6B2 clone), CD38 (FITC, BioLegend 90 clone), CXCR5 (PE, BioLegend L138D7 clone),
669 PD-1 (BV421, BioLegend 29F.1A12 clone), and GL7 (PerCP-Cy5.5, BioLegend GL7 clone). Antigen-specific
670 staining was done using biotinylated trimers conjugated to either streptavidin-BV605 (BioLegend) or
671 streptavidin-APC (BioLegend). Analysis was performed on a Becton-Dickinson Symphony flow cytometer,
672 and the resulting data were processed using FlowJo software. Anti-trimer serum Ig titers were assessed
673 by ELISA. 96-well plates (Costar Corning) were coated overnight at 4°C with 1 μg/ml (50 μl/well) of
674 streptavidin in PBS. Coated plates were blocked with 2% BSA in PBS, and incubated overnight at 4°C.
675 Plates were then washed and incubated with 1 μg/ml biotinylated trimer in blocking buffer (2% BSA in
676 PBS) for 2 h at 25°C, following which serial dilutions of serum samples were added to the plates. After 2 h
677 incubation, plates were washed and incubated with HRP-conjugated anti-mouse IgG diluted 1:5,000 in
678 blocking buffer. The reaction mixture was incubated at 25°C for 30 min. Plates were washed and treated
679 with 50 μL TMB substrate for 10 minutes followed by addition 1M H_2SO_4 stop solution. Optical densities
680 were read on a microplate reader at 450 nm with background correction at 540 nm. Endpoint serum titers
681 were determined as the reciprocal of the highest serum dilution leading to a signal 0.1 OD units above
682 background.
683
684 Non-human Primates and Study Design
685 Adult Indian rhesus macaques (Macaca mulatta) were housed at the Emory National Primate
686 Research Center and maintained in accordance with NIH guidelines. All procedures were approved by the
687 Emory University Institutional Animal Care and Use Committee (IACUC) under protocols 202100128 and
688 201700666. Animal care facilities are accredited by the U.S. Department of Agriculture (USDA) and the
689 Association for Assessment and Accreditation of Laboratory Animal Care (AALAC) International. RMs for
690 this study were of mixed sex, an average age of 5.5 years, and a weight range of 4-7.2kgs at the time of
691 the priming immunization. Animals were pair housed for the duration of the study. Thirty-six NHPs were
692 assigned to one of six experimental groups—each group was comprised of 6 RMs. The immunizations
693 were as follows: Group 1 (ED SMNP), Group 2 (SMNP), Group 3 (ED Amph-CpG), Group 4 (ED pSer:alum
694 SMNP), Group 5 (pSer:alum SMNP), and Group 6 (pSer:nano-alum SMNP). Immunizations were
695 administered subcutaneously (s.c.) in the left and right mid-thighs. SMNP was dosed at 375mg per
696 injection site for all SMNP-containing groups. All alum-containing adjuvant (alum and Nanoalum) were
697 dosed at 500mg per injection site. This is the alum dose that has been previously tested in pSer-based

698 HIV Env immunizations in mice and RMs[43,45]. The Amph-CpG was administered at a dose of 2.5mg per
699 injection site which was the optimal dose determined from a previous RM immunization experiment using
700 SARS-CoV-2 RBD base protein immunogen[50].
701 Veterinarians performed fine need aspirates (FNAs) to bilaterally sample lymph nodes (LNs) in the
702 RMs. Palpation was used to identify draining LNs. A 22-gauge needle with an attached 3 ml syringe was
703 passed into the LN a maximum of five times. Samples were then placed into RPMI media with 10% FBS
704 and 1% Penicillin/Streptomycin. If red blood cell contamination was observed, an Ammonium Chloride-
705 Potassium lysing buffer was used. Samples were counted, frozen down, and stored in liquid nitrogen until
706 the time of analysis. Blood was collected throughout the study in NaCitrate CPT tubes (BD biosciences)
707 for peripheral blood mononuclear cells (PBMCs) and plasma isolation and frozen. Serum was collected via
708 serum clot tubes and frozen. Bone marrow aspirates were collected in heparin coated tube and analyzed
709 via ELISPOT fresh. Animals were treated with anesthesia (ketamine 5-10 mg/kg or telazol 3-6 mg/kg) and
710 analgesics for s.c. immunizations, LN FNA, bone marrow aspirates, and blood draws as per veterinarian
711 recommendations and IACUC approved protocols. After completion of the proposed study and approval
712 of the vet staff, animals were released to the center for reuse by other researchers.
713
714 ELISA analysis of serum IgG titers
715 Serum IgG titers were measured by ELISA. Nunc MaxiSorp plates were coated with streptavidin 18 hr at
716 4°C and blocked with 2% BSA in PBS. Blocked plates were washed with washing buffer (PBS with 0.05%
717 Tween-20) and incubated with Avi-tagged biotinylated antigen 18 hr at 4°C. Plates were washed again
718 and serial dilutions of sera were added to plates and incubated for 2 hr at 25°C, following which the plates
719 were washed and incubated with anti-rhesus IgG-HRP (BioRad). ELISA plates were developed with TMB
720 substrate and stopped by sulfuric acid 2 M. Absorbance values at 450 nm were measured on a Tecan
721 Infinite 200PRO plate reader, with a background correction wavelength of 540 nm.
722
723 Immunoglobulin DNA and repertoire sequencing (AIRR-Seq) sample preparation.
724 For immunoglobulin sequencing (AIRR-Seq), PBMCs were isolated from 15-20 ml of blood from each
725 animal. For immunoglobulin repertoire sequencing. Approximately 5 M PBMCs were lysed in QIAGEN
726 RLT buffer + 1% BME and stored at -80 C until RNA was purified using QIAGEN RNeasy kits. For
727 sequencing of the immunoglobulin DNA loci, 5 M PBMCs were snap frozen and stored at -80 C.
728
729 IGHD3-41 Genotyping
730 To genotype IGHD3-3 ("IGHD3.41"), we utilized a custom genomic IG targeted long-read Pacific
731 Biosciences single molecule real-time (SMRT) sequencing method (KAPA HyperExplore, Roche), following
732 previously published protocols[25,54,61,88] [1-4]. Briefly, genomic DNA was isolated from peripheral blood
733 mononuclear cells (PBMCs) collected from each animal using the DNeasy kit (Qiagen). DNA (~2.5 ug) was
734 sheared with g-tubes (Covaris); size selected >5-6 Kb (Blue Pippin/Pippin HT, Sage Science); End Repaired
735 and A-tailed (KAPA sequencing library protocol, Roche); and finally, sample-specific sequence barcodes
736 and universal primers were ligated. Initial PCR amplification (8-9 cycles) was conducted using PrimeSTAR
737 GXL polymerase (Takara), followed by size-selection and purification of amplified fragments 0.7X AMPure
738 PB beads (Pacific Biosciences). Target-enrichment was performed by hybridization of custom IGH/K/L
739 locus-specific oligonucleotide probes (KAPA HyperExplore, Roche). Oligo-bound fragments were
740 recovered using streptavidin beads (Roche), and additional PCR amplification (16-18 cycles) were
741 performed using PrimeSTAR GXL (Takara). Long-read sequencing libraries were prepared using the
742 SMRTbell Express Template Preparation Kit 2.0 (Pacific Biosciences). Resulting libraries were sequenced
743 on the Sequel IIe system.

HiFi reads for each animal were mapped to the RheMac10 reference genome (Mmul_10) using minimap2[89]. Phased single nucleotide variants representing two distinct alleles were resolved from HiFi reads spanning the IGHD3-3 gene (chr7: 168251081-168251167). At least 10 representative HiFi reads were required to include a given allele in the genotype of an animal.

AIRR-Seq library preparation:

The library preparation method was based on the protocol provided by Dr. Daniel Douek, NIAID/VRC[90,91] and the IgM constant region primer was based on Corcoran et al, 2016[92] and were described previously in Steichen et al, 2024[25]. RNA was extracted from sorted naive B cells in 350µL QIAGEN RLT buffer using the RNeasy Micro-DNase Digest protocol (QIAGEN) on QIAcube automation platforms (Valencia, CA). Clontech SMARTer cDNA template switching was used to perform the reverse transcription step. 8µL of RNA was mixed with 1 µL of 12µM 5′ CDS oligo(dT) primer for 3 seconds and incubated for 3 minutes at 72°C followed by at least 1 minute at 4°C. 8.5 µL of master mix comprising of 3.5 µL of 5x RT Buffer (250 mM Tris-HCl (pH 8.3), 375 mM KCl, 30 mM MgCl2), 1 µL Dithiothreitol, DTT (20 mM),1 µL dNTP Mix (10 mM), 1 µL RNAse Out (40U/µL), 1 µL SMARTer II A Oligo (12 µM), 1 µL Superscript II RT (200U/µL) was added to each reaction. After sealing and spinning the plates briefly, they were incubated for 90 minutes at 42°C and 10 minutes at 70°C. AMPure XP beads were used for purification of the first strand cDNA. For amplification of the rearranged BCR sequences, 19.3 µL of cDNA was mixed with 30.7 µL of master mix (25 µL of 2x KAPA Real-Time Library Amplification Kit (catalog# KK2702), 0.7 µL of 5PIIA (12 µM): forward primer and 5 µL of IgM primer (2 µM): reverse primer). The plates were sealed, vortexed for 5 seconds and centrifuged at 2000 RCF for 1 minute. Real-time PCR machine was used to visualize the amplification and the reaction was terminated in the exponential phase. The amplified BCRs were purified using the AMPure XP beads. Two more rounds of PCR amplification were performed for addition of barcodes and adapters. In the first round, 46 µL of master mix (25 µL of KAPA HotStart ReadyMix (catalog# KK2602), 2.5 µL of SYBR Green 1:10K and 18.5 µL of Nuclease-free water), 1 µL of P5_Seq BC_XX 5PIIA (10 µM), 1 µL of P7_i7_XX IgM (10 µM) and 2 µL of 1:10 diluted amplified rearranged BCR from previous PCR were mixed, sealed, vortexed and centrifuged. Real-time PCR amplification was performed and the resulting library was purified with AMPure XP beads. The last round of PCR amplification was performed for addition of the P5_Graft P5_Seq. Real-time PCR was carried out by mixing 44 µL of master mix (25 µL of KAPA HotStart ReadyMix (catalog# KK2602), 1 µL of P5_Graft P5_seq (10 µM): forward primer and 18 µL of Nuclease-free water), 1 µL of P7_i7_XX IgM (10 µM) (reverse primer) and 5 µL of amplified library from previous PCR followed by a final round of purification with AMPure XP beads. Agilent Bioanalyzer was used to assess the quality of the libraries and after pooling the libraries were sequenced on an Illumina MiSeq as 309 base paired-end runs. Primers used for AIRR-Seq library preparation and sequencing are listed below.

CDS Oligo dT	TTTTTTTTTTTTTTTTTTTTTTTTVN
SMARTer II A	AAGCAGTGGTATCAACGCAGAGTACATrGrGrG
5PIIA	AAGCAGTGGTATCAACGCAGAGT
P5_Graft P5_Seq	AATGATACGGCGACCACCGAGATCTACAC TCTTTCCCTA**CACGACGCTCTTCCGATCT**
P5_Seq BC_XX 5PIIA	CACGACGCTCTTCCGATCT (5' barcode) AAGCAGTGGTATCAACGCAGAGT
P7_i7_XX IgM	CAAGCAGAAGACGGCATACGAGAT (3' barcode) GGGGCATTCTCACAGGAGACGAGGGGGAAAAG
RhIgM	GGGGCATTCTCACAGGAGACGAGGGGGAAAAG
RhIgM Seq	GGGGCATTCTCACAGGAGACGAGGGGGAAAAG
Index RhIgM	CTTTTCCCCCTCGTCTCCTGTGAGAATGCCCC

780 **AIRR-Seq data analysis:**
781 Fastq files were demultiplexed using a custom script that searches for an exact match and trims the 5′
782 barcode followed by the 5′ RACE primer sequence with the corresponding number of upstream random
783 nucleotides. This script uses seqtk v1.2 {https://github.com/lh3/seqtk} for extracting reads. The resulting
784 demultiplexed files were processed by the Immcantation pipeline (docker container v4.4.0)[93,94]. The reads
785 were assembled using the AssemblePairs module followed by filtering with the FilterSeq module with -q
786 set to 20. The ParseHeaders module was used to add the sample name to the sequences. Duplicates were
787 removed using the CollapseSeq module with the –-uf set to the 5′ random nucleotide sequence. SplitSeq
788 was used to filter sequences with -DUPCOUNT of 2. IgBLAST v1.21.0[95] was used to annotate the
789 sequences using the germline database from Cirelli et al 2019[38]. The MakeDB module was used to create
790 ChangeO format files from the IgBLAST output. The functional sequences were selected using ParseDB
791 module to select productive sequences. The D gene usage frequencies were determined using the
792 countGenes function from alakazam v1.3.0 package[94].
793
794 **Activation-induced marker (AIM) and intracellular cytokine staining (ICS) assay to detect antigen-**
795 **specific CD4⁺ T cells**
796 Antigen-induced marker-based detection of antigen-specific T cells was performed similar to previously
797 described protocols[96,97]. Cryopreserved PBMCs were thawed and washed in RPMI media containing 10%
798 FBS, 1x penicillin/streptomycin and 1x GlutaMAX (R10 media). Cells were counted and then seeded at 1
799 million cells per well in a round-bottom 96-well plate. Cells were blocked with 0.5 µg/mL anti-CD40 mAb
800 (Miltenyi Biotec) and incubated with anti-CXCR5 and CCR7 for 15 minutes at 37°C. Then, cells were
801 stimulated for 24 hours with one of the following conditions: (1) 5 µg/mL N332-GT5 Env peptide pool
802 "Env"; (2) 1 ng/mL staphylococcal enterotoxin B (SEB) used as a positive control; or (3) DMSO as a
803 negative, unstimulated control plated in duplicate. N332-GT5 Env peptide pools consist of overlapping
804 15-mer peptides that cover the entire protein sequence and were resuspended in DMSO. An equimolar
805 amount of DMSO is present in both the peptide pool and the unstimulated, negative control. After 24
806 hours of incubation, intracellular transport inhibitors – 0.25 µL/well of GolgiPlug (BD Biosciences) and 0.25
807 µL/well of GolgiStop (BD Biosciences) – were added to the samples along with the AIM marker antibodies
808 (CD25, CD40L, CD69, OX40, 4-1BB) and incubated for 4 hours. After, cells were incubated for 15 min at
809 RT with FC Block (Biolegend) and Fixable Live/Dead Blue (Invitrogen). ells were washed with FACS buffer
810 (2% FBS in PBS) and stained with the surface antibodies for 30 minutes at 4°C. Following, cells were fixed
811 with 4% formaldehyde and permeabilized with a saponin-based buffer and subsequently stained with the
812 intracellular cytokine panel for 30 minutes at RT. Finally, the stained cells were washed and acquired on
813 the Cytek Aurora (Cytek Biosciences). Antibody panels and reagents are summarized in table below.
814 For data analysis, antigen-specific T cells were measured as background subtracted data, where the linear
815 averages of the DMSO background signal, calculated from duplicate wells for each sample, were deducted
816 from the stimulated signal. A minimum threshold for DMSO background signals was set at 0.005% and
817 the limit of quantitation (LOQ) was defined as the geometric mean of all DMSO samples. For each sample,
818 the stimulation index (SI) was calculated as the ratio between the AIM⁺ response in the stimulated condition
819 and the average DMSO response for the same sample. Samples with an SI lower than 2 for CD4 or 3 for
820 CD8 T cells responses and/or with a background subtracted response lower than the LOQ were considered
821 as non-responders. Non-responder samples were set at the baseline, which is the closest $\log_{10}$ value lower
822 than the LOQ.
823
824
825
826

827 AIM/ICS Staining Panel

Antibodies/ Reagents	Clone	Source	Catalog #	Dilution
LIVE/DEAD Fixable Blue	-	Invitrogen	L23105	1/500
GolgiPlug	-	BD Biosciences	555029	1/1000
GolgiStop	-	BD Biosciences	554724	1/1000
Fc Block	-	BioLegend	422302	1/20
Mouse anti-human CD40	HB14	Miltenyi	130-094-133	1:200
Mouse anti-human CXCR5 PE-Cy7	MU5UBEE	Thermo Fisher Scientific	25-9185-42	1:100
Mouse anti-human CCR7 BV650	G043H7	BioLegend	353233	1:100
Mouse anti-human CD69 PE-Cy5	FN50	BioLegend	310908	1:250
Mouse anti-human CD137 (4-1BB) BV421	4B4-1	BioLegend	309819	1:250
Mouse anti-human CD25 BV605	BC96	BioLegend	302631	1:250
Mouse anti-human CD40L BB515	24-31	BD Biosciences	568170	1:250
Mouse anti-human CD134 (OX40) PE	L106	BD Biosciences	340420	1:250
Mouse anti-human CD8 BUV496	RPA-T8	BD Biosciences	612943	1:100
Mouse anti-human CD14 APC-Cy7	M5E2	BioLegend	301820	1:100
Mouse anti-human CD16 APC-eFluor780	eBioCB16	Thermo Fisher Scientific	47-0168-42	1:100
Mouse anti-human CD20 APC-Cy7	2H7	BioLegend	302314	1:100
Mouse anti-human CD3 BUV395	SP34-2	BD Biosciences	564117	1:100
Mouse anti-human CD4 PerCP-Cy5.5	OKT4	BioLegend	317428	1:100
Mouse anti-human PD-1 BV785	EH12.2H7	BioLegend	329929	1:100
Mouse anti-human CD45RA PE-CF594	5H9	BD Biosciences	565419	1:100
Armenian Hamster anti-ICOS BV480	C398.4A	BD Biosciences	566087	1:100
Mouse anti-human IFN-γ BV750	B27	BD Biosciences	566357	1:100
Rat anti-human IL-2 BUV737	MQ1-17H12	BD Biosciences	612836	1:200
Mouse anti-human TNF-α BV711	MAb11	BioLegend	502940	1:200
Mouse anti-human Granzyme B Alexa Fluor 700	GB11	BD Biosciences	560213	1:1000
Mouse anti-human IL-21 Alexa Fluor 647	3A3-N2.1	BD Biosciences	560493	1:200

828

829 PBMC and FNA Flow Cytometry

830 Frozen PBMC and LN FNA samples were thawed in RPMI media with 10% FBS, 1% GlutaMAX,
831 and 1% Penicillin/Streptomycin (R10). The recovered cells were then stained with the appropriate antibody
832 panel. Fluorescent antigen probes were constructed by combining fluorophore-conjugated streptavidin
833 and biotinylated N332-GT5 (N332-GT5 WT) and N332-GT5 epitope knock-out (N332-GT5 KO) probes in
834 small increments across 45 minutes with an appropriate volume of PBS at room temperature (RT). Thawed
835 cells were incubated with KO probes for twenty minutes at 4°C then incubated with WT probes for thirty
836 minutes at 4°C. A master mix of surface staining antibodies was then added and incubated for thirty
837 minutes at 4°C (see below for PBMC and FNA panels). Cells were prepared for acquisition for either
838 analysis experiments on Cytek Aurora (Cytek Biosciences) or sorting experiments on BD FACSymphony S6
839 (BD Biosciences). For sorting experiments, 2 µg per 5 million cells of anti-human Total-Seq-C hashtag
840 antibodies were added to each sample following the surface staining master mix during the staining
841 protocol.

842 For analysis of bulk BGC and GC-TFH a threshold of 250 B cells and 500 CD4+ T cells was used,
843 respectively. For analysis of Env-binding BGC, a threshold of 75 BGC cells was used. LODs for antigen-

844 and epitope-specific B_{mem} and B_{GC} cells were determined by calculating the mean of 7 pre-immunizations
845 samples.
846
847 PBMC Staining Panel

Reagent	Clone	Catalog #	Dilution
AF647 Streptavidin	-	BioLegend (405237)	-
BV421 Streptavidin	-	BioLegend (405225)	-
PE Streptavidin	-	BioLegend (405245)	-
Viability APC-eFluor506	-	Thermo Fisher Scientific (65-0866-18)	1:500
CD8a APC-eFluor780	RPA-T8	BD Biosciences (563256)	1:100
CD16 APC-eFluor780	CB16	Thermo Fisher Scientific (47-0168-42)	1:100
CD14 APC-Cy7	M5E2	BioLegend (301820)	1:100
CD3 APC-Cy7	SP-34	BD Biosciences (557757)	1:100
CD20 BUV395	2H7	BD Biosciences (563781)	1:100
IgG BV605	G18-145	BD Biosciences (563246)	1:100
CD27 PE-Cy7	O323	Thermo Fisher Scientific (25-0279-42)	1:50
IgM PerCP-Cy5.5	G20-127	BD Biosciences (561285)	1:50
IgD AF488	polyclonal	Southern Biotech (2030-30)	1:50

848
849 FNA Staining Panel

Reagent	Clone	Catalog #	Dilution
AF647 Streptavidin	-	BioLegend (405237)	-
BV421 Streptavidin	-	BioLegend (405225)	-
PE Streptavidin	-	BioLegend (405245)	-
Viability APC-eFluor506	-	Thermo Fisher Scientific (65-0866-18)	1:500
CD4 BV711	OKT4	BioLegend (317440)	1:100
CD8a APC-eFluor780	RPA-T8	Thermo Fisher Scientific (47-0088-42)	1:100
CD16 APC-eFluor780	CB16	Thermo Fisher Scientific (47-0168-42)	1:100
CD20 AF488	2H7	BioLegend (302316)	1:100
CD38 PE-Cy5	OKT10	Produced in house	1:100
CD3 BUV395	SP-34	BD Biosciences (564117)	1:40
IgG BUV737	G18-145	BD Biosciences (612819)	1:40
IgM PerCP-Cy5.5	G20-127	BD Biosciences (561285)	1:40
PD1 BV605	EH12.2H7	BioLegend (329924)	1:20
CXCR5 PE-Cy7	Mu5UBEE	Thermo Fisher Scientific (25-9185-42)	1:20
CD71 PE-CF594	L01.1	BD Biosciences (Custom)	1:20

850
851 Single B cell sequencing
852 After sorting, antigen specific PBMC and LN FNA B cells were wash with PBS and loaded onto a Chromium
853 chip and controller following the manufacturers protocol (10X Genomics). Indexed V(D)J, Feature
854 Barcode, and Gene Expression libraries were prepared following the 10X Genomics protocol with the
855 Feature Barcoding Kit (10X Genomics) and sequenced on a NovaSeq 6000 (Illumina). Demultiplexing and
856 FASTQ generation were done using Cell Ranger v7.2 (10X Genomics). VDJ reads were assembled de novo
857 using Cell Ranger and contigs were aligned to a custom *Macaca mulatta* germline VDJ reference using

858 IgBLAST and the Change-O 1.3.0 package from the Immcantation framework[94]. Sequences were assigned
859 to animals using the MULTIseqDemux function in Seurat v4[98]. Inferred germline sequences
860 (CreateGermline.py) and clones (DefineClones.py) were determined with Change-O. SHM was quantified
861 using the observedMutations command in SHazaM package v1.2.0 comparing HC sequences to the
862 inferred germline sequences (masking the D gene sequences). For clonal abundance and diversity,
863 clonotypes for each animal were quantified using the countClones function in Alakazam package v1.3.0,
864 only animals that had 5 or more clones were included in abundance and diversity calculations. Clonal
865 richness (Chao1) was calculated using the iNEXT package v3.0.0 in R[99] , clonal richness was only calculated
866 for animals that had at least 1 sequence recovered at that timepoint.
867
868 ELISPOT
869 The antibody-secreting cells (ASCs) in NHP bone marrow were quantified using the enzyme-linked
870 immunosorbent spot (ELISpot) assay as described previously with slight modifications[100]. Briefly, 96-well
871 multi-screen HTS filter plates (MSHAN4B50, Millipore) were coated for 16 hours at 4°C with either 5µg/mL
872 of Goat Anti-Human Ig-UNLB (Southern Biotech, Cat# 2010-01) for capturing total rhesus IgG or 20µg/mL
873 of Galanthus Nivalis Lectin (Vector laboratories, Cat# L-1240) for capturing N332 antigen. The plates were
874 then washed four times with sterile PBS and blocked with R10 media for 2 hours in a 5% CO2 incubator at
875 37°C. For antigen capture, the GNL-coated plate was further incubated with 10µg/mL of N332 antigen for
876 2 hours at 37°C. Bone marrow (BM) mononuclear cells were harvested using Ficoll Paque Plus from 2 mL
877 of BM aspirates as reported (Kasturi SP et al 2020, Sci Immunol). 100µl of cells (5×106 cells/mL) were
878 added to the wells in the first row in duplicates (~333K cells), and serially diluted three-fold, and incubated
879 overnight for ~16 hours in a 5% CO2 incubator at 37°C. Following incubation, the plates were washed
880 four times with PBS followed by four washes with PBS containing 0.05% Tween 20 (PBS-T). Goat Anti-
881 Human IgG-biotin (Southern Biotech, Cat# 2045-08) was added at a dilution of 1:500 and incubated for
882 two hours at room temperature. Plates were washed with PBS followed by PBS-T four times each and
883 Avidin D-HRP (Vector Labs) was added at a dilution of 1:1000 and incubated for 1 hour at room
884 temperature. Finally, plates were washed four times in PBS-T followed by four washes with PBS, and spots
885 were developed for 5 minutes using a filtered 3-amino 9-ethylcarbazole (AEC) substrate (0.3 mg/mL AEC
886 in 0.1 M sodium acetate buffer, pH 5.0, with a 1:1000 dilution of 3% hydrogen peroxide). The reaction was
887 stopped by washing the plates with running tap water, and air-dried plates before imaging using the
888 Immunospot CTL counter and Image Acquisition 4.5 software (Cellular Technology). Total IgG+ ASC or
889 Env-specific ASCs/spots were counted manually using magnified images and reported as the absolute
890 number of ASCs per million BM cells or % of antigen specific ASCs as a fraction of total ASCs.
891
892 Antibody production
893 High-throughput antibody production was performed as previously described[61,101]. Briefly, antibodies were
894 produced using the ExpiCHO Expression System (Thermo Fisher) in baffled 96 deep-well blocks (Thomas
895 Scientific) according to manufacturer's instructions, with the following adjustments: the cell density was
896 increased to 10^7 viable cells/mL, cell culture volumes were increased to 1 mL/well, ExpiFectamine Reagent
897 (Thermo Fisher) volume was increased to 6 µL/well, and incubator shake speed was set to 1300 RPM. After
898 7 days incubation, supernatants were supplemented with 40 µL 1M Tris, pH 8.0, harvested by
899 centrifugation and purified using Protein A HP MultiTrap plates (GEHealthcare) per manufacturer's
900 instructions.
901
902 Antibody binding affinities
903 We measured kinetics and affinity of antibody-antigen interactions on Carterra LSA using CMDP Sensor
904 Chip (Carterra). This chip type has lower ligand capacity and excellent diffusion characteristics. It is

905 recommended for use when reducing avidity is necessary. 1x HBS-EP+ pH 7.4 was our running buffer (20x
906 stock from Teknova, Cat. No H8022) supplemented with BSA at 1mg/ml. We followed Carterra software
907 instructions to prepare chip surface for ligands capture. In a typical experiment about 500-700 RU of
908 capture antibody (SouthernBiothech Cat no 2047-01) in 10 mM Sodium Acetate pH 4.5 was amine
909 coupled. The critical detail here was the concentration range of the amine coupling reagents and capture
910 antibody. We used N-Hydroxysuccinimide (NHS) and 1-Ethyl-3-(3-dimethylaminopropyl)
911 carbodiimidehydrochloride (EDC) from Amine Coupling Kit (GE order code BR-1000-50). As per kit
912 instruction 22-0510-62 AG the NHS and EDC should be reconstituted in 10 ml of water each to give 11.5
913 mg/ml and 75 mg/ml respectively. However, the highest coupling levels of capture antibody were
914 achieved by using 10 times diluted NHS and EDC during surface preparation runs. Thus, in our runs the
915 concentrations of NHS and EDC were 1.15 mg/ml and 7.5 mg/ml. The activation time was reduced to
916 1min. The concentrated stocks of NHS and EDC could be stored frozen in -20C for up to 2 months without
917 noticeable loss of activity. The SouthernBiotech capture antibody was used at concentration 25ug/ml with
918 10 minutes contact time. Phosphoric Acid 1.7% was our regeneration solution with 60 seconds contact
919 time and injected three times per each cycle. Solution concentration of ligands was around 1 ug/ml and
920 contact time was 5 min. Raw sensograms were analyzed using Kinetics software (Carterra), interspot and
921 blank double referencing, Langmuir model. Analyte concentrations were quantified on NanoDrop 2000c
922 Spectrophotometer using Absorption signal at 280 nm. For best results analyte samples should be buffer
923 exchanged into the running buffer using dialysis. We typically cover broad range of affinities in our runs
924 and the best referencing practices are different depending on how fast the off-rate is for particular ligand.
925 For fast off-rate (faster than 9e-3 1/s) we use automated batch referencing that includes overlay y-aline
926 and higher analyte concentrations. For slow off-rates (9e-3 1/s or less) we use manual process referencing
927 that includes serial y-align and lower analyte concentrations. After automated data analysis by Kinetics
928 software, we also did additional filtering to remove datasets with highest response signals smaller than
929 signals from negative controls. This additional filtering could be performed automatically using R-script.
930
931 Statistical Analysis
932 Statistical tests were carried out using GraphPad Prism 10. For most graphs unpaired two-tailed Mann-
933 Whitney tests were used for the following comparisons (i) G1 vs 2, G1 vs 3, G1 vs 4, G1 vs 5, G1 vs 6, (ii)
934 G2 vs 5, G2 vs 6, (iii) G4 vs 5, (iv) G5 vs 6. Only (i) tests were done for the BG18 sequencing frequency
935 graphs except in Figure 3A were done using Fishers exact tests comparing each group to G1 individually.
936 P-values are listed if <0.1 or reported as NS if >0.1. Additional tests were carried out in Figure 4 comparing
937 each group to the pre-immunization samples using a Kruskal-Wallis test without correction. Those p-values
938 are represented by the following scale: NS > 0.05, * <0.05 ,** <0.01, *** <0.001, **** <0.0001. All p-values
939 reported in Figure 7 are from Mann-Whitney tests.
940
941 Material availability
942 This study did not generate new unique reagents
943
944 Data and code availability
945 • All sequencing files will be uploaded to SRA
946 • All original code will be publicly available on Github
947 • Any additional information required to reanalyze the data reported in this paper is available from
948 the lead author upon request
949
950
951

Acknowledgments

We thank Jennifer S Wood and the staff of the Emory National Primate Research Center. We are grateful to the Flow Cytometry and Next Generation Sequencing core facilities at La Jolla Institute for Immunology for their services.

Funding

This work was funded by the National Institute of Allergy and Infectious Diseases of the NIH (NIAID-NIH) under award CHAVD UM1AI144462. This research was funded in part by the Emory National Primate Research Center Grant Nos. ORIP/OD P51OD011132 and U42 PDP11023. The Emory National Primate Center is supported by the National Institutes of Health, Office of Research Infrastructure Programs/OD [P51OD011132 and U42 PDP11023]. The Emory Primate Genomics Core received funding from P51OD011132 and S10OD026799. The NovaSeq 6000 used in this work was funded by NIH grant S10OD025052.

Author Contributions

Conceptualization, P.J.M., D.J.I., and S.C.; Methodology, P.J.M., E.M.Z., K.A.R., A.A.U., S.S., A.P., S.P.K., C.T.W., S.E.B., D.J.I., and S.C.; Investigation, P.J.M., E.M.Z., K.A.R., J.M.S., M.S., K.N., K.K.M., L.M., A.A.U., S.S., A.P., O.K., A.L., P.G.L., I.P., A.M., O.L.R., K.S., S.S., M.L.S., E.B.A., W.P., J.G., and S.X.; Resources, K.A.R., J.M.S., K.N., N.P., E.G., N.A., M.K., D.L., S.E., B.S.H., D.L., V.R.L., E.B.A., W.P., J.G., S.X., D.C.C., S.P.K., C.T.W., S.E.B., G.S., W.R.S., D.J.I., and S.C.; Writing- Original Draft, P.J.M., D.J.I., and S.C.; Writing- Review & Editing, P.J.M., J.M.S., C.T.W., W.R.S., D.J.I., and S.C.; Supervision, S.P.K., C.T.W., S.E.B., G.S., W.R.S., D.J.I., and S.C.; Project Administration, P.J.M., L.M., D.C.C., D.J.I., S.C.; Funding Acquisition, C.T.W., S.E.B., G.S., W.R.S., D.J.I., and S.C..

Declaration of interests

D.J.I. and S.C. are inventors on a patent for the SMNP adjuvant (US11547672B2). K.A.R. and D.J.I. are inventors on patent applications for the synergistic combination of alum and SMNP adjuvants (PCT/US2022/074302 and US No. 17/816,045). D.J.I. and W.R.S. are named as inventors on a patent for pSer technology (US No. 11,224,648 B2). J.M.S. and W.R.S. are inventors on patent applications related to immunogens in this manuscript that have been filed by Scripps and IAVI. W.R.S. is an employee and shareholder of Moderna, Inc. All other authors declare no competing interests.

986 ## REFERENCES
987

988 1. Plotkin, S.A. (2010). Correlates of Protection Induced by Vaccination. Clin. Vaccine Immunol. 17,
989 1055–1065. https://doi.org/10.1128/cvi.00131-10.
990 2. Burton, D.R. (2023). Antiviral neutralizing antibodies: from in vitro to in vivo activity. Nat. Rev.
991 Immunol. 23, 720–734. https://doi.org/10.1038/s41577-023-00858-w.
992 3. Goldblatt, D., Alter, G., Crotty, S., and Plotkin, S.A. (2022). Correlates of protection against SARS-
993 CoV-2 infection and COVID-19 disease. Immunol. Rev. 310, 6–26.
994 https://doi.org/10.1111/imr.13091.
995 4. Abbott, R.K., Lee, J.H., Menis, S., Skog, P., Rossi, M., Ota, T., Kulp, D.W., Bhullar, D., Kalyuzhniy, O.,
996 Havenar-Daughton, C., et al. (2018). Precursor Frequency and Affinity Determine B Cell Competitive
997 Fitness in Germinal Centers, Tested with Germline-Targeting HIV Vaccine Immunogens. Immunity
998 48, 133-146.e6. https://doi.org/10.1016/j.immuni.2017.11.023.
999 5. Havenar-Daughton, C., Sarkar, A., Kulp, D.W., Toy, L., Hu, X., Deresa, I., Kalyuzhniy, O., Kaushik, K.,
1000 Upadhyay, A.A., Menis, S., et al. (2018). The human naive B cell repertoire contains distinct
1001 subclasses for a germline-targeting HIV-1 vaccine immunogen. Science Translational Medicine 10,
1002 eaat0381. https://doi.org/10.1126/scitranslmed.aat0381.
1003 6. Havenar-Daughton, C., Abbott, R.K., Schief, W.R., and Crotty, S. (2018). When designing vaccines,
1004 consider the starting material: the human B cell repertoire. Curr. Opin. Immunol. 53, 209–216.
1005 https://doi.org/10.1016/j.coi.2018.08.002.
1006 7. Lee, J.H., Toy, L., Kos, J.T., Safonova, Y., Schief, W.R., Havenar-Daughton, C., Watson, C.T., and
1007 Crotty, S. (2021). Vaccine genetics of IGHV1-2 VRC01-class broadly neutralizing antibody precursor
1008 naïve human B cells. npj Vaccines 6, 1–12. https://doi.org/10.1038/s41541-021-00376-7.
1009 8. Jardine, J.G., Kulp, D.W., Havenar-Daughton, C., Sarkar, A., Briney, B., Sok, D., Sesterhenn, F.,
1010 Ereño-Orbea, J., Kalyuzhniy, O., Deresa, I., et al. (2016). HIV-1 broadly neutralizing antibody
1011 precursor B cells revealed by germline-targeting immunogen. Science 351, 1458–1463.
1012 https://doi.org/10.1126/science.aad9195.
1013 9. Xie, Z., Lin, Y.-C., Steichen, J.M., Ozorowski, G., Kratochvil, S., Ray, R., Torres, J.L., Liguori, A.,
1014 Kalyuzhniy, O., Wang, X., et al. (2024). mRNA-LNP HIV-1 trimer boosters elicit precursors to broad
1015 neutralizing antibodies. Science 384, eadk0582. https://doi.org/10.1126/science.adk0582.
1016 10. Ray, R., Schiffner, T., Wang, X., Yan, Y., Rantalainen, K., Lee, C.-C.D., Parikh, S., Reyes, R.A., Dale,
1017 G.A., Lin, Y.-C., et al. (2024). Affinity gaps among B cells in germinal centers drive the selection of
1018 MPER precursors. Nat. Immunol. 25, 1083–1096. https://doi.org/10.1038/s41590-024-01844-7.
1019 11. Melzi, E., Willis, J.R., Ma, K.M., Lin, Y.-C., Kratochvil, S., Berndsen, Z.T., Landais, E.A., Kalyuzhniy, O.,
1020 Nair, U., Warner, J., et al. (2022). Membrane-bound mRNA immunogens lower the threshold to
1021 activate HIV Env V2 apex-directed broadly neutralizing B cell precursors in humanized mice.
1022 Immunity 55, 2168-2186.e6. https://doi.org/10.1016/j.immuni.2022.09.003.
1023 12. Steichen, J.M., Lin, Y.-C., Havenar-Daughton, C., Pecetta, S., Ozorowski, G., Willis, J.R., Toy, L., Sok,
1024 D., Liguori, A., Kratochvil, S., et al. (2019). A generalized HIV vaccine design strategy for priming of
1025 broadly neutralizing antibody responses. Science 366, eaax4380.
1026 https://doi.org/10.1126/science.aax4380.
1027 13. Burton, D.R. (2017). What Are the Most Powerful Immunogen Design Vaccine Strategies? Reverse
1028 Vaccinology 2.0 Shows Great Promise. Cold Spring Harb. Perspect. Biol. 9, a030262.
1029 https://doi.org/10.1101/cshperspect.a030262.
1030 14. Sanders, R.W., and Moore, J.P. (2024). Progress on priming HIV-1 immunity. Science 384, 738–739.
1031 https://doi.org/10.1126/science.adp3459.

1032 15. Haynes, B.F., Burton, D.R., and Mascola, J.R. (2019). Multiple roles for HIV broadly neutralizing
1033 antibodies. Sci. Transl. Med. 11, eaaz2686. https://doi.org/10.1126/scitranslmed.aaz2686.
1034 16. Lee, J.H., and Crotty, S. (2021). HIV vaccinology: 2021 update. Semin. Immunol. 51, 101470.
1035 https://doi.org/10.1016/j.smim.2021.101470.
1036 17. Medina-Ramírez, M., Garces, F., Escolano, A., Skog, P., Taeye, S.W. de, Moral-Sanchez, I.D.,
1037 McGuire, A.T., Yasmeen, A., Behrens, A.-J., Ozorowski, G., et al. (2017). Design and crystal structure
1038 of a native-like HIV-1 envelope trimer that engages multiple broadly neutralizing antibody precursors
1039 in vivo. J. Exp. Med. 214, 2573–2590. https://doi.org/10.1084/jem.20161160.
1040 18. McGuire, A.T., Hoot, S., Dreyer, A.M., Lippy, A., Stuart, A., Cohen, K.W., Jardine, J., Menis, S.,
1041 Scheid, J.F., West, A.P., et al. (2013). Engineering HIV envelope protein to activate germline B cell
1042 receptors of broadly neutralizing anti-CD4 binding site antibodies. J. Exp. Med. 210, 655–663.
1043 https://doi.org/10.1084/jem.20122824.
1044 19. Steichen, J.M., Kulp, D.W., Tokatlian, T., Escolano, A., Dosenovic, P., Stanfield, R.L., McCoy, L.E.,
1045 Ozorowski, G., Hu, X., Kalyuzhniy, O., et al. (2016). HIV Vaccine Design to Target Germline
1046 Precursors of Glycan-Dependent Broadly Neutralizing Antibodies. Immunity 45, 483–496.
1047 https://doi.org/10.1016/j.immuni.2016.08.016.
1048 20. Tian, M., Cheng, C., Chen, X., Duan, H., Cheng, H.-L., Dao, M., Sheng, Z., Kimble, M., Wang, L., Lin,
1049 S., et al. (2016). Induction of HIV Neutralizing Antibody Lineages in Mice with Diverse Precursor
1050 Repertoires. Cell 166, 1471-1484.e18. https://doi.org/10.1016/j.cell.2016.07.029.
1051 21. Sok, D., Briney, B., Jardine, J.G., Kulp, D.W., Menis, S., Pauthner, M., Wood, A., Lee, E.-C., Le, K.M.,
1052 Jones, M., et al. (2016). Priming HIV-1 broadly neutralizing antibody precursors in human Ig loci
1053 transgenic mice. Science 353, 1557–1560. https://doi.org/10.1126/science.aah3945.
1054 22. Jardine, J., Julien, J.-P., Menis, S., Ota, T., Kalyuzhniy, O., McGuire, A., Sok, D., Huang, P.-S.,
1055 MacPherson, S., Jones, M., et al. (2013). Rational HIV Immunogen Design to Target Specific
1056 Germline B Cell Receptors. Science 340, 711–716. https://doi.org/10.1126/science.1234150.
1057 23. Briney, B., Sok, D., Jardine, J.G., Kulp, D.W., Skog, P., Menis, S., Jacak, R., Kalyuzhniy, O., Val, N.
1058 de, Sesterhenn, F., et al. (2016). Tailored Immunogens Direct Affinity Maturation toward HIV
1059 Neutralizing Antibodies. Cell 166, 1459-1470.e11. https://doi.org/10.1016/j.cell.2016.08.005.
1060 24. Willis, J.R., Berndsen, Z.T., Ma, K.M., Steichen, J.M., Schiffner, T., Landais, E., Liguori, A., Kalyuzhniy,
1061 O., Allen, J.D., Baboo, S., et al. (2022). Human immunoglobulin repertoire analysis guides design of
1062 vaccine priming immunogens targeting HIV V2-apex broadly neutralizing antibody precursors.
1063 Immunity 55, 2149-2167.e9. https://doi.org/10.1016/j.immuni.2022.09.001.
1064 25. Steichen, J.M., Phung, I., Salcedo, E., Ozorowski, G., Willis, J.R., Baboo, S., Liguori, A., Cottrell, C.A.,
1065 Torres, J.L., Madden, P.J., et al. (2024). Vaccine priming of rare HIV broadly neutralizing antibody
1066 precursors in nonhuman primates. Science 384, eadj8321. https://doi.org/10.1126/science.adj8321.
1067 26. Leggat, D.J., Cohen, K.W., Willis, J.R., Fulp, W.J., deCamp, A.C., Kalyuzhniy, O., Cottrell, C.A.,
1068 Menis, S., Finak, G., Ballweber-Fleming, L., et al. (2022). Vaccination induces HIV broadly neutralizing
1069 antibody precursors in humans. Science 378, eadd6502. https://doi.org/10.1126/science.add6502.
1070 27. Andrabi, R., Pallesen, J., Allen, J.D., Song, G., Zhang, J., Val, N. de, Gegg, G., Porter, K., Su, C.-Y.,
1071 Pauthner, M., et al. (2019). The Chimpanzee SIV Envelope Trimer: Structure and Deployment as an
1072 HIV Vaccine Template. Cell Rep. 27, 2426-2441.e6. https://doi.org/10.1016/j.celrep.2019.04.082.
1073 28. Cheng, C., Xu, K., Kong, R., Chuang, G.-Y., Corrigan, A.R., Geng, H., Hill, K.R., Jafari, A.J., O'Dell,
1074 S., Ou, L., et al. (2019). Consistent elicitation of cross-clade HIV-neutralizing responses achieved in
1075 guinea pigs after fusion peptide priming by repetitive envelope trimer boosting. PLoS ONE 14,
1076 e0215163. https://doi.org/10.1371/journal.pone.0215163.
1077 29. Escolano, A., Steichen, J.M., Dosenovic, P., Kulp, D.W., Golijanin, J., Sok, D., Freund, N.T., Gitlin,
1078 A.D., Oliveira, T., Araki, T., et al. (2016). Sequential Immunization Elicits Broadly Neutralizing Anti-

1079 HIV-1 Antibodies in Ig Knockin Mice. Cell 166, 1445-1458.e12.
1080 https://doi.org/10.1016/j.cell.2016.07.030.
1081 30. Bernat, N.V., Corcoran, M., Nowak, I., Kaduk, M., Dopico, X.C., Narang, S., Maisonasse, P.,
1082 Dereuddre-Bosquet, N., Murrell, B., and Hedestam, G.B.K. (2021). Rhesus and cynomolgus macaque
1083 immunoglobulin heavy-chain genotyping yields comprehensive databases of germline VDJ alleles.
1084 Immunity 54, 355-366.e4. https://doi.org/10.1016/j.immuni.2020.12.018.
1085 31. Chernyshev, M., Kaduk, M., Corcoran, M., and Hedestam, G.B.K. (2022). VDJ Gene Usage in IgM
1086 Repertoires of Rhesus and Cynomolgus Macaques. Front. Immunol. 12, 815680.
1087 https://doi.org/10.3389/fimmu.2021.815680.
1088 32. Backlund, C., Jalili-Firoozinezhad, S., Kim, B., and Irvine, D.J. (2023). Biomaterials-Mediated
1089 Engineering of the Immune System. Annu. Rev. Immunol. 41, 153–179.
1090 https://doi.org/10.1146/annurev-immunol-101721-040259.
1091 33. Bhagchandani, S., Johnson, J.A., and Irvine, D.J. (2021). Evolution of Toll-like receptor 7/8 agonist
1092 therapeutics and their delivery approaches: From antiviral formulations to vaccine adjuvants.
1093 Advanced Drug Delivery Reviews 175, 113803. https://doi.org/10.1016/j.addr.2021.05.013.
1094 34. Pulendran, B., Arunachalam, P.S., and O'Hagan, D.T. (2021). Emerging concepts in the science of
1095 vaccine adjuvants. Nat. Rev. Drug Discov. 20, 454–475. https://doi.org/10.1038/s41573-021-00163-
1096 y.
1097 35. Singh, A., Boggiano, C., Eller, M.A., Maciel, M., Marovich, M.A., Mehra, V.L., Mo, A.X., Singleton,
1098 K.L., and Leitner, W.W. (2023). Optimizing the Immunogenicity of HIV Vaccines by Adjuvants –
1099 NIAID Workshop Report. Vaccine 41, 4439–4446. https://doi.org/10.1016/j.vaccine.2023.06.029.
1100 36. Lavelle, E.C., and McEntee, C.P. (2024). Vaccine adjuvants: Tailoring innate recognition to send the
1101 right message. Immunity 57, 772–789. https://doi.org/10.1016/j.immuni.2024.03.015.
1102 37. Lee, J.H., Sutton, H.J., Cottrell, C.A., Phung, I., Ozorowski, G., Sewall, L.M., Nedellec, R., Nakao, C.,
1103 Silva, M., Richey, S.T., et al. (2022). Long-primed germinal centres with enduring affinity maturation
1104 and clonal migration. Nature 609, 998–1004. https://doi.org/10.1038/s41586-022-05216-9.
1105 38. Cirelli, K.M., Carnathan, D.G., Nogal, B., Martin, J.T., Rodriguez, O.L., Upadhyay, A.A., Enemuo,
1106 C.A., Gebru, E.H., Choe, Y., Viviano, F., et al. (2019). Slow Delivery Immunization Enhances HIV
1107 Neutralizing Antibody and Germinal Center Responses via Modulation of Immunodominance. Cell
1108 177, 1153-1171.e28. https://doi.org/10.1016/j.cell.2019.04.012.
1109 39. Silva, M., Kato, Y., Melo, M.B., Phung, I., Freeman, B.L., Li, Z., Roh, K., Wijnbergen, J.W.V., Watkins,
1110 H., Enemuo, C.A., et al. (2021). A particulate saponin/TLR agonist vaccine adjuvant alters lymph flow
1111 and modulates adaptive immunity. Sci. Immunol. 6, eabf1152.
1112 https://doi.org/10.1126/sciimmunol.abf1152.
1113 40. Ramezani-Rad, P., Marina-Zárate, E., Maiorino, L., Myers, A., Michaels, K.K., Pires, I.S., Bloom, N.I.,
1114 Lopez, P.G., Cottrell, C.A., Burton, I., et al. (2024). Dose-dependent regulation of immune memory
1115 responses against HIV by saponin monophosphoryl lipid A nanoparticle adjuvant. bioRxiv,
1116 2024.07.31.604373. https://doi.org/10.1101/2024.07.31.604373.
1117 41. Cirelli, K.M., and Crotty, S. (2017). Germinal center enhancement by extended antigen availability.
1118 Curr. Opin. Immunol. 47, 64–69. https://doi.org/10.1016/j.coi.2017.06.008.
1119 42. Moyer, T.J., Kato, Y., Abraham, W., Chang, J.Y.H., Kulp, D.W., Watson, N., Turner, H.L., Menis, S.,
1120 Abbott, R.K., Bhiman, J.N., et al. (2020). Engineered immunogen binding to alum adjuvant enhances
1121 humoral immunity. Nat. Med. 26, 430–440. https://doi.org/10.1038/s41591-020-0753-3.
1122 43. Rodrigues, K.A., Cottrell, C.A., Steichen, J.M., Groschel, B., Abraham, W., Suh, H., Agarwal, Y., Ni,
1123 K., Chang, J.Y.H., Yousefpour, P., et al. (2023). Optimization of an alum-anchored clinical HIV vaccine
1124 candidate. npj Vaccines 8, 117. https://doi.org/10.1038/s41541-023-00711-0.

1125 44. Rodrigues, K.A., Rodriguez-Aponte, S.A., Dalvie, N.C., Lee, J.H., Abraham, W., Carnathan, D.G.,
1126 Jimenez, L.E., Ngo, J.T., Chang, J.Y.H., Zhang, Z., et al. (2021). Phosphate-mediated coanchoring of
1127 RBD immunogens and molecular adjuvants to alum potentiates humoral immunity against SARS-
1128 CoV-2. Sci. Adv. 7, eabj6538. https://doi.org/10.1126/sciadv.abj6538.
1129 45. Phung, I., Rodrigues, K.A., Marina-Zárate, E., Maiorino, L., Pahar, B., Lee, W.-H., Melo, M., Kaur, A.,
1130 Allers, C., Fahlberg, M., et al. (2023). A combined adjuvant approach primes robust germinal center
1131 responses and humoral immunity in non-human primates. Nat. Commun. 14, 7107.
1132 https://doi.org/10.1038/s41467-023-42923-x.
1133 46. Chang, J.Y.H., Agarwal, Y., Rodrigues, K.A., Momin, N., Ni, K., Read, B.J., Moyer, T.J., Mehta, N.K.,
1134 Silva, M., Suh, H., et al. (2022). Co-Anchoring of Engineered Immunogen and Immunostimulatory
1135 Cytokines to Alum Promotes Enhanced-Humoral Immunity. Adv. Ther. 5, 2100235.
1136 https://doi.org/10.1002/adtp.202100235.
1137 47. Morefield, G.L., HogenEsch, H., Robinson, J.P., and Hem, S.L. (2004). Distribution of adsorbed
1138 antigen in mono-valent and combination vaccines. Vaccine 22, 1973–1984.
1139 https://doi.org/10.1016/j.vaccine.2003.10.040.
1140 48. Raponi, A., Brewer, J.M., Garside, P., and Laera, D. (2021). Nanoalum adjuvanted vaccines: small
1141 details make a big difference. Semin. Immunol. 56, 101544.
1142 https://doi.org/10.1016/j.smim.2021.101544.
1143 49. Steinbuck, M.P., Seenappa, L.M., Jakubowski, A., McNeil, L.K., Haqq, C.M., and DeMuth, P.C.
1144 (2021). A lymph node–targeted Amphiphile vaccine induces potent cellular and humoral immunity to
1145 SARS-CoV-2. Sci. Adv. 7, eabe5819. https://doi.org/10.1126/sciadv.abe5819.
1146 50. Seenappa, L.M., Jakubowski, A., Steinbuck, M.P., Palmer, E., Haqq, C.M., Carter, C., Fontenot, J.,
1147 Villinger, F., McNeil, L.K., and DeMuth, P.C. (2022). Amphiphile-CpG vaccination induces potent
1148 lymph node activation and COVID-19 immunity in mice and non-human primates. npj Vaccines 7,
1149 128. https://doi.org/10.1038/s41541-022-00560-3.
1150 51. Crotty, S. (2019). T Follicular Helper Cell Biology: A Decade of Discovery and Diseases. Immunity 50,
1151 1132–1148. https://doi.org/10.1016/j.immuni.2019.04.011.
1152 52. Corcoran, M.M., and Hedestam, G.B.K. (2024). Adaptive immune receptor germline gene variation.
1153 Curr. Opin. Immunol. 87, 102429. https://doi.org/10.1016/j.coi.2024.102429.
1154 53. Engelbrecht, E., Rodriguez, O.L., Shields, K., Schultze, S., Tieri, D., Jana, U., Yaari, G., Lees, W.D.,
1155 Smith, M.L., and Watson, C.T. (2024). Resolving haplotype variation and complex genetic
1156 architecture in the human immunoglobulin kappa chain locus in individuals of diverse ancestry.
1157 Genes Immun. 25, 297–306. https://doi.org/10.1038/s41435-024-00279-2.
1158 54. Gibson, W.S., Rodriguez, O.L., Shields, K., Silver, C.A., Dorgham, A., Emery, M., Deikus, G., Sebra,
1159 R., Eichler, E.E., Bashir, A., et al. (2023). Characterization of the immunoglobulin lambda chain locus
1160 from diverse populations reveals extensive genetic variation. Genes Immun. 24, 21–31.
1161 https://doi.org/10.1038/s41435-022-00188-2.
1162 55. Pennell, M., Rodriguez, O.L., Watson, C.T., and Greiff, V. (2023). The evolutionary and functional
1163 significance of germline immunoglobulin gene variation. Trends Immunol. 44, 7–21.
1164 https://doi.org/10.1016/j.it.2022.11.001.
1165 56. Avnir, Y., Watson, C.T., Glanville, J., Peterson, E.C., Tallarico, A.S., Bennett, A.S., Qin, K., Fu, Y.,
1166 Huang, C.-Y., Beigel, J.H., et al. (2016). IGHV1-69 polymorphism modulates anti-influenza antibody
1167 repertoires, correlates with IGHV utilization shifts and varies by ethnicity. Sci. Rep. 6, 20842.
1168 https://doi.org/10.1038/srep20842.
1169 57. Rodriguez, O.L., Safonova, Y., Silver, C.A., Shields, K., Gibson, W.S., Kos, J.T., Tieri, D., Ke, H.,
1170 Jackson, K.J.L., Boyd, S.D., et al. (2023). Genetic variation in the immunoglobulin heavy chain locus

1171 shapes the human antibody repertoire. Nat. Commun. 14, 4419. https://doi.org/10.1038/s41467-
1172 023-40070-x.
1173 58. deCamp, A.C., Corcoran, M.M., Fulp, W.J., Willis, J.R., Cottrell, C.A., Bader, D.L.V., Kalyuzhniy, O.,
1174 Leggat, D.J., Cohen, K.W., Hyrien, O., et al. (2024). Human immunoglobulin gene allelic variation
1175 impacts germline-targeting vaccine priming. npj Vaccines 9, 58. https://doi.org/10.1038/s41541-
1176 024-00811-5.
1177 59. Bernat, N.V., Corcoran, M., Hardt, U., Kaduk, M., Phad, G.E., Martin, M., and Hedestam, G.B.K.
1178 (2019). High-Quality Library Preparation for NGS-Based Immunoglobulin Germline Gene Inference
1179 and Repertoire Expression Analysis. Frontiers in Immunology 10.
1180 60. Kato, Y., Abbott, R.K., Freeman, B.L., Haupt, S., Groschel, B., Silva, M., Menis, S., Irvine, D.J., Schief,
1181 W.R., and Crotty, S. (2020). Multifaceted Effects of Antigen Valency on B Cell Response Composition
1182 and Differentiation In Vivo. Immunity 53, 548-563.e8. https://doi.org/10.1016/j.immuni.2020.08.001.
1183 61. Schiffner, T., Phung, I., Ray, R., Irimia, A., Tian, M., Swanson, O., Lee, J.H., Lee, C.-C.D., Marina-
1184 Zárate, E., Cho, S.Y., et al. (2024). Vaccination induces broadly neutralizing antibody precursors to
1185 HIV gp41. Nat. Immunol. 25, 1073–1082. https://doi.org/10.1038/s41590-024-01833-w.
1186 62. Havenar-Daughton, C., Lee, J.H., and Crotty, S. (2017). Tfh cells and HIV bnAbs, an
1187 immunodominance model of the HIV neutralizing antibody generation problem. Immunol. Rev. 275,
1188 49–61. https://doi.org/10.1111/imr.12512.
1189 63. Lee, J.H., Hu, J.K., Georgeson, E., Nakao, C., Groschel, B., Dileepan, T., Jenkins, M.K., Seumois, G.,
1190 Vijayanand, P., Schief, W.R., et al. (2020). Modulating the quantity of HIV Env-specific CD4 T cell
1191 help promotes rare B cell responses in germinal centers. J. Exp. Med. 218, e20201254.
1192 https://doi.org/10.1084/jem.20201254.
1193 64. Ols, S., Yang, L., Thompson, E.A., Pushparaj, P., Tran, K., Liang, F., Lin, A., Eriksson, B., Hedestam,
1194 G.B.K., Wyatt, R.T., et al. (2020). Route of Vaccine Administration Alters Antigen Trafficking but Not
1195 Innate or Adaptive Immunity. Cell Rep. 30, 3964-3971.e7.
1196 https://doi.org/10.1016/j.celrep.2020.02.111.
1197 65. Liang, F., Lindgren, G., Lin, A., Thompson, E.A., Ols, S., Röhss, J., John, S., Hassett, K., Yuzhakov,
1198 O., Bahl, K., et al. (2017). Efficient Targeting and Activation of Antigen-Presenting Cells In Vivo after
1199 Modified mRNA Vaccine Administration in Rhesus Macaques. Mol. Ther. 25, 2635–2647.
1200 https://doi.org/10.1016/j.ymthe.2017.08.006.
1201 66. Lindsay, K.E., Bhosle, S.M., Zurla, C., Beyersdorf, J., Rogers, K.A., Vanover, D., Xiao, P., Araínga, M.,
1202 Shirreff, L.M., Pitard, B., et al. (2019). Visualization of early events in mRNA vaccine delivery in non-
1203 human primates via PET–CT and near-infrared imaging. Nat. Biomed. Eng. 3, 371–380.
1204 https://doi.org/10.1038/s41551-019-0378-3.
1205 67. Buckley, M., Araínga, M., Maiorino, L., Pires, I.S., Kim, B.J., Michaels, K.K., Dye, J., Qureshi, K.,
1206 Zhang, Y., Mak, H., et al. (2024). Visualizing lipid nanoparticle trafficking for mRNA vaccine delivery
1207 in non-human primates. bioRxiv, 2024.06.21.600088. https://doi.org/10.1101/2024.06.21.600088.
1208 68. Yousefpour, P., Zhang, Y.J., Maiorino, L., Melo, M.B., Ramirez, M.A.A., Kumarapperuma, S.C., Xiao,
1209 P., Silva, M., Li, N., Michaels, K.K., et al. (2024). Modulation of antigen delivery and lymph node
1210 activation in non-human primates by saponin adjuvant SMNP.
1211 https://doi.org/10.1101/2024.08.28.608716.
1212 69. Schmidt, T.H., Bannard, O., Gray, E.E., and Cyster, J.G. (2013). CXCR4 promotes B cell egress from
1213 Peyer's patches. J. Exp. Med. 210, 1099–1107. https://doi.org/10.1084/jem.20122574.
1214 70. Tomura, M., Yoshida, N., Tanaka, J., Karasawa, S., Miwa, Y., Miyawaki, A., and Kanagawa, O. (2008).
1215 Monitoring cellular movement in vivo with photoconvertible fluorescence protein "Kaede"
1216 transgenic mice. Proc. Natl. Acad. Sci. 105, 10871–10876.
1217 https://doi.org/10.1073/pnas.0802278105.

1218 71. Ganusov, V.V., and Auerbach, J. (2014). Mathematical Modeling Reveals Kinetics of Lymphocyte
1219 Recirculation in the Whole Organism. PLoS Comput. Biol. 10, e1003586.
1220 https://doi.org/10.1371/journal.pcbi.1003586.
1221 72. Turner, J.S., Benet, Z.L., and Grigorova, I.L. (2017). Antigen Acquisition Enables Newly Arriving B
1222 Cells To Enter Ongoing Immunization-Induced Germinal Centers. J. Immunol. 199, 1301–1307.
1223 https://doi.org/10.4049/jimmunol.1700267.
1224 73. Tam, H.H., Melo, M.B., Kang, M., Pelet, J.M., Ruda, V.M., Foley, M.H., Hu, J.K., Kumari, S.,
1225 Crampton, J., Baldeon, A.D., et al. (2016). Sustained antigen availability during germinal center
1226 initiation enhances antibody responses to vaccination. Proc. Natl. Acad. Sci. 113, E6639–E6648.
1227 https://doi.org/10.1073/pnas.1606050113.
1228 74. Zarnitsyna, V.I., Lavine, J., Ellebedy, A., Ahmed, R., and Antia, R. (2016). Multi-epitope Models
1229 Explain How Pre-existing Antibodies Affect the Generation of Broadly Protective Responses to
1230 Influenza. PLoS Pathog. 12, e1005692. https://doi.org/10.1371/journal.ppat.1005692.
1231 75. Toellner, K.-M., Sze, D.M.-Y., and Zhang, Y. (2018). What Are the Primary Limitations in B-Cell
1232 Affinity Maturation, and How Much Affinity Maturation Can We Drive with Vaccination? A Role for
1233 Antibody Feedback. Cold Spring Harb. Perspect. Biol. 10, a028795.
1234 https://doi.org/10.1101/cshperspect.a028795.
1235 76. Schaefer-Babajew, D., Wang, Z., Muecksch, F., Cho, A., Loewe, M., Cipolla, M., Raspe, R., Johnson,
1236 B., Canis, M., DaSilva, J., et al. (2023). Antibody feedback regulates immune memory after SARS-
1237 CoV-2 mRNA vaccination. Nature 613, 735–742. https://doi.org/10.1038/s41586-022-05609-w.
1238 77. Cyster, J.G., and Wilson, P.C. (2024). Antibody modulation of B cell responses—Incorporating
1239 positive and negative feedback. Immunity 57, 1466–1481.
1240 https://doi.org/10.1016/j.immuni.2024.06.009.
1241 78. Tas, J.M.J., Koo, J.-H., Lin, Y.-C., Xie, Z., Steichen, J.M., Jackson, A.M., Hauser, B.M., Wang, X.,
1242 Cottrell, C.A., Torres, J.L., et al. (2022). Antibodies from primary humoral responses modulate the
1243 recruitment of naive B cells during secondary responses. Immunity 55, 1856-1871.e6.
1244 https://doi.org/10.1016/j.immuni.2022.07.020.
1245 79. Dvorscek, A.R., McKenzie, C.I., Stäheli, V.C., Ding, Z., White, J., Fabb, S.A., Lim, L., O'Donnell, K.,
1246 Pitt, C., Christ, D., et al. (2024). Conversion of vaccines from low to high immunogenicity by
1247 antibodies with epitope complementarity. Immunity. https://doi.org/10.1016/j.immuni.2024.08.017.
1248 80. McNamara, H.A., Idris, A.H., Sutton, H.J., Vistein, R., Flynn, B.J., Cai, Y., Wiehe, K., Lyke, K.E.,
1249 Chatterjee, D., KC, N., et al. (2020). Antibody Feedback Limits the Expansion of B Cell Responses to
1250 Malaria Vaccination but Drives Diversification of the Humoral Response. Cell Host Microbe 28, 572-
1251 585.e7. https://doi.org/10.1016/j.chom.2020.07.001.
1252 81. Meyer-Hermann, M. (2019). Injection of Antibodies against Immunodominant Epitopes Tunes
1253 Germinal Centers to Generate Broadly Neutralizing Antibodies. Cell Rep. 29, 1066-1073.e5.
1254 https://doi.org/10.1016/j.celrep.2019.09.058.
1255 82. Schiepers, A., Wout, M.F.L. van't, Hobbs, A., Mesin, L., and Victora, G.D. (2024). Opposing effects of
1256 pre-existing antibody and memory T cell help on the dynamics of recall germinal centers. Immunity.
1257 https://doi.org/10.1016/j.immuni.2024.05.009.
1258 83. Heesters, B.A., Myers, R.C., and Carroll, M.C. (2014). Follicular dendritic cells: dynamic antigen
1259 libraries. Nat. Rev. Immunol. 14, 495–504. https://doi.org/10.1038/nri3689.
1260 84. Keating, G.M., and Noble, S. (2003). Recombinant Hepatitis B Vaccine (Engerix-B®). Drugs 63,
1261 1021–1051. https://doi.org/10.2165/00003495-200363100-00006.
1262 85. Wright, J.G., Plikaytis, B.D., Rose, C.E., Parker, S.D., Babcock, J., Keitel, W., Sahly, H.E., Poland,
1263 G.A., Jacobson, R.M., Keyserling, H.L., et al. (2014). Effect of reduced dose schedules and

1264 intramuscular injection of anthrax vaccine adsorbed on immunological response and safety profile: A
1265 randomized trial. Vaccine 32, 1019–1028. https://doi.org/10.1016/j.vaccine.2013.10.039.
1266 86. Plotkin, S.A. (2018). Plotkin's Vaccines (Seventh Edition) S. A. Plotkin, P. A. Offit, W. A. Orenstein,
1267 and K. M. Edwards, eds.
1268 87. Liu, H., Moynihan, K.D., Zheng, Y., Szeto, G.L., Li, A.V., Huang, B., Egeren, D.S.V., Park, C., and
1269 Irvine, D.J. (2014). Structure-based programming of lymph-node targeting in molecular vaccines.
1270 Nature 507, 519–522. https://doi.org/10.1038/nature12978.
1271 88. Rodriguez, O.L., Gibson, W.S., Parks, T., Emery, M., Powell, J., Strahl, M., Deikus, G., Auckland, K.,
1272 Eichler, E.E., Marasco, W.A., et al. (2020). A Novel Framework for Characterizing Genomic Haplotype
1273 Diversity in the Human Immunoglobulin Heavy Chain Locus. Front. Immunol. 11, 2136.
1274 https://doi.org/10.3389/fimmu.2020.02136.
1275 89. Li, H. (2018). Minimap2: pairwise alignment for nucleotide sequences. Bioinformatics 34, 3094–3100.
1276 https://doi.org/10.1093/bioinformatics/bty191.
1277 90. Huang, J., Kang, B.H., Ishida, E., Zhou, T., Griesman, T., Sheng, Z., Wu, F., Doria-Rose, N.A., Zhang,
1278 B., McKee, K., et al. (2016). Identification of a CD4-Binding-Site Antibody to HIV that Evolved Near-
1279 Pan Neutralization Breadth. Immunity 45, 1108–1121. https://doi.org/10.1016/j.immuni.2016.10.027.
1280 91. Francica, J.R., Sheng, Z., Zhang, Z., Nishimura, Y., Shingai, M., Ramesh, A., Keele, B.F., Schmidt,
1281 S.D., Flynn, B.J., Darko, S., et al. (2015). Analysis of immunoglobulin transcripts and hypermutation
1282 following SHIVAD8 infection and protein-plus-adjuvant immunization. Nat. Commun. 6, 6565.
1283 https://doi.org/10.1038/ncomms7565.
1284 92. Corcoran, M.M., Phad, G.E., Bernat, N.V., Stahl-Hennig, C., Sumida, N., Persson, M.A.A., Martin, M.,
1285 and Hedestam, G.B.K. (2016). Production of individualized V gene databases reveals high levels of
1286 immunoglobulin genetic diversity. Nat. Commun. 7, 13642. https://doi.org/10.1038/ncomms13642.
1287 93. Heiden, J.A.V., Yaari, G., Uduman, M., Stern, J.N.H., O'Connor, K.C., Hafler, D.A., Vigneault, F., and
1288 Kleinstein, S.H. (2014). pRESTO: a toolkit for processing high-throughput sequencing raw reads of
1289 lymphocyte receptor repertoires. Bioinformatics 30, 1930–1932.
1290 https://doi.org/10.1093/bioinformatics/btu138.
1291 94. Gupta, N.T., Heiden, J.A.V., Uduman, M., Gadala-Maria, D., Yaari, G., and Kleinstein, S.H. (2015).
1292 Change-O: a toolkit for analyzing large-scale B cell immunoglobulin repertoire sequencing data.
1293 Bioinformatics 31, 3356–3358. https://doi.org/10.1093/bioinformatics/btv359.
1294 95. Ye, J., Ma, N., Madden, T.L., and Ostell, J.M. (2013). IgBLAST: an immunoglobulin variable domain
1295 sequence analysis tool. Nucleic Acids Res. 41, W34–W40. https://doi.org/10.1093/nar/gkt382.
1296 96. Havenar-Daughton, C., Reiss, S.M., Carnathan, D.G., Wu, J.E., Kendric, K., Peña, A.T. de la, Kasturi,
1297 S.P., Dan, J.M., Bothwell, M., Sanders, R.W., et al. (2016). Cytokine-Independent Detection of
1298 Antigen-Specific Germinal Center T Follicular Helper Cells in Immunized Nonhuman Primates Using
1299 a Live Cell Activation-Induced Marker Technique. J Immunol 197, 994–1002.
1300 https://doi.org/10.4049/jimmunol.1600320.
1301 97. Reiss, S., Baxter, A.E., Cirelli, K.M., Dan, J.M., Morou, A., Daigneault, A., Brassard, N., Silvestri, G.,
1302 Routy, J.-P., Havenar-Daughton, C., et al. (2017). Comparative analysis of activation induced marker
1303 (AIM) assays for sensitive identification of antigen-specific CD4 T cells. Plos One 12, e0186998.
1304 https://doi.org/10.1371/journal.pone.0186998.
1305 98. Hao, Y., Stuart, T., Kowalski, M.H., Choudhary, S., Hoffman, P., Hartman, A., Srivastava, A., Molla, G.,
1306 Madad, S., Fernandez-Granda, C., et al. (2024). Dictionary learning for integrative, multimodal and
1307 scalable single-cell analysis. Nat. Biotechnol. 42, 293–304. https://doi.org/10.1038/s41587-023-
1308 01767-y.

99. Hsieh, T.C., Ma, K.H., and Chao, A. (2016). iNEXT: an R package for rarefaction and extrapolation of species diversity (Hill numbers). Methods Ecol. Evol. 7, 1451–1456. https://doi.org/10.1111/2041-210x.12613.
100. Kasturi, S.P., Rasheed, M.A.U., Havenar-Daughton, C., Pham, M., Legere, T., Sher, Z.J., Kovalenkov, Y., Gumber, S., Huang, J.Y., Gottardo, R., et al. (2020). 3M-052, a synthetic TLR-7/8 agonist, induces durable HIV-1 envelope–specific plasma cells and humoral immunity in nonhuman primates. Sci. Immunol. 5. https://doi.org/10.1126/sciimmunol.abb1025.
101. Huang, D., Abbott, R.K., Havenar-Daughton, C., Skog, P.D., Al-Kolla, R., Groschel, B., Blane, T.R., Menis, S., Tran, J.T., Thinnes, T.C., et al. (2020). B cells expressing authentic naive human VRC01-class BCRs can be recruited to germinal centers and affinity mature in multiple independent mouse models. Proc. Natl. Acad. Sci. 117, 22920–22931. https://doi.org/10.1073/pnas.2004489117.

1355 ## FIGURE LEGENDS

1356

1357 **Figure 1: Study schematic.** Study schematic showing seven immunization groups and sampling types and
1358 timepoints (n =6 for each)

1359

1360 **Figure 2: Escalating dose immunization and SMNP prime larger GC responses. A)** Flow cytometry
1361 gating of B_{GC} cells ($CD38^{-}CD71^{+}$). **B)** B_{GC} cell frequency ($CD38^{-}CD71^{+}$) as a percentage of total B cells
1362 ($CD20^{+}$). **C)** Area under the curve (AUC) of B_{GC} cell frequency as a percentage of total B cells post-priming
1363 (weeks 3-9) immunization. **D)** Flow cytometry gating of GC-T_{FH} cells (PD-$1^{Hi}CXCR5^{+}$). **E)** GC-T_{FH} cell
1364 frequency as a percentage of total $CD4^{+}$ cells. **F)** AUC of GC-T_{FH} cell frequency as a percentage of total
1365 $CD4^{+}$ cells post-priming (week 3-9) immunization. **G)** Flow cytometry gating of N332-GT5 antigen specific
1366 B_{GC} cells (N332-GT5-$AF647^{+}$N332-GT5-$BV421^{+}$; N332-$GT5^{++}$). **H)** Antigen-specific B_{GC} cell frequency
1367 (N332-GT5-$AF647^{+}$N332-GT5-$BV421^{+}$) as a percentage of total B cells ($CD20^{+}$). **I)** Area under the curve
1368 (AUC) of antigen-specific B_{GC} cell frequency as a percentage of total B cells post-priming (weeks 3-9)
1369 immunization. **J)** Flow cytometry gating of N332-GT5 epitope specific B_{GC} cells (N332-GT5-$AF647^{+}$N332-
1370 GT5-$BV421^{+}$N332-GT5KO-PE^{-}). **K)** Epitope-specific B_{GC} cell frequency (N332-GT5-$AF647^{+}$N332-GT5-
1371 $BV421^{+}$N332-GT5KO-PE^{-}) as a percentage of total B cells ($CD20^{+}$). **I)** Area under the curve (AUC) of
1372 epitope-specific B_{GC} cell frequency as a percentage of total B cells post-priming (weeks 3-9) immunization.
1373 Triangles in longitudinal graphs represent time of immunizations. Mean and SEM or geometric mean and
1374 geometric SD are plotted depending on the scale in all longitudinal figures and median was plotted in all
1375 per animal figures. Statistical significance was tested using unpaired two-tailed Mann-Whitney tests with
1376 the p-values listed on each graph representative of the tests carried out, NS listed when p-value was >0.1.
1377 Gray regions (H, K) represent B_{GC} LOD determined using pre-immunization samples.

1378

1379 **Figure 3: Escalating dose adjuvanted with SMNP leads to a larger, more diverse, composition of BCRs**
1380 **3-weeks post-prime. A)** Frequency of BG18 type I B_{GC} cells from week 3 among total B cells, plotted per
1381 animal. Numbers below indicate total number of paired BCR sequences recovered from each group and
1382 the total number of BG18 type I BCRs recovered. All cells are from week LN FNAs. **B)** Clonal richness of
1383 the BCR sequences recovered from epitope specific B_{GC} cells plotted as the Chao1 index on a per animal
1384 basis. Chao was calculated for all animals that had at least 1 sequence recovered. **C)** Clonal abundance
1385 curves for each group. Clonal abundance was calculated per animal then the mean abundance for each
1386 clone rank was plotted for each group. Animals with fewer than 5 total clones were excluded from
1387 abundance calculations. **D)** Cumulative abundance of the top 5 most abundant clones plotted per animal.
1388 Animals with fewer than 5 total clones were excluded from abundance calculations. **E)** Percentage of each
1389 Ig isotype making up the total BCR sequences isolated from each group. The lines in all per animal graphs
1390 represent medians. Statistical significance was tested using unpaired two-tailed Mann-Whitney tests with
1391 the p-values listed on each graph representative of the tests carried out except for A) where multiple
1392 Fisher's exact tests were used to compare each group directly to G1, NS listed when p-value was >0.1.

1393

1394 **Figure 4: Vaccine-elicited T cell and serum IgG responses. A)** Representative flow cytometry gating of
1395 an AIM assay performed at week 2 using N332-GT5 (Env) overlapping peptide pools or a DMSO control
1396 (unstimulated). **B)** Frequency of AIM^{+} ($CD40L^{+}OX40^{+}$) T cells out of total $CD4^{+}$ T cells. **C)** Representative
1397 flow cytometry gating of an AIM assay performed at week 2 using N332-GT5 (Env) overlapping peptide
1398 pools. Red dots are Env+ cells. **D)** Frequency of AIM^{+} ($CD40L^{+}OX40^{+}$) cT_{FH} cells out of total $CD4^{+}$ cT_{FH} cells.
1399 **E)** Representative flow cytometry gating of an AIM assay performed at week 2 using N332-GT5 (Env)
1400 overlapping peptide pools or a DMSO control (unstimulated). **F)** Frequency of $AIM^{+}ICS^{+}$ ($CD40L^{+}IL21^{+}$) T
1401 cells out of total $CD4^{+}$ T cells. **G)** Representative flow cytometry gating of an AIM assay performed at week

2 using N332-GT5 overlapping peptide pools. **H)** Frequency of AIM$^+$ICS$^+$ (CD69$^+$IFNg$^+$) T cells out of total CD8$^+$ T cells. **I)** Longitudinal area under the curve (AUC) of total antigen-specific serum IgG measured by ELISA. **J)** AUC of antigen-specific serum IgG at week 10 plotted by animal. **K)** Longitudinal area under the curve (AUC) of total epitope-specific serum IgG measured by ELISA. **L)** AUC of epitope-specific serum IgG at week 10 plotted by animal. Mean and SD are plotted in I and K, lines in all other graphs are median values. Pre-immunization time point included in all AIM/ICS assays. Statistical significance was tested using unpaired two-tailed Mann-Whitney tests with the p-values listed on each graph representative of the tests carried out, NS listed when p-value was >0.1. The row of asterixis in B, D, F, and H above the Y-axis indicate statistical significance for each group compared to the pre-immunizations samples using the following scale: NS > 0.05, * <0.05 ,** <0.01, *** <0.001, **** <0.0001.

Figure 5: Antigen-specific B_{mem} responses. A) Representative flow cytometry gating showing N332-GT5 antigen specific (N332-GT5-AF647$^+$N332-GT5-BV421$^+$) B_{mem} cells. **B)** Frequency of antigen-specific B_{mem} cells of total B cells from PBMCs over time for each group. **C)** Representative flow cytometry gating showing N332-GT5 epitope specific (N332-GT5-AF647$^+$N332-GT5-BV421$^+$N332-GT5KO-PE$^-$) B_{mem}. **D)** Frequency of epitope specific B_{mem} cells of total B cells over time for each group. **E)** Week 10 and week 12 antigen specific B_{mem} frequency plotted per animal. **F)** Fold change of week 12 antigen specific B_{mem} frequency over the week 10 antigen specific B_{mem} frequency. **G)** Week 10 and week 12 epitope specific B_{mem} frequency plotted per animal. **H)** Fold change of week 12 epitope specific B_{mem} frequency over the week 10 epitope specific B_{mem} frequency. **I)** Frequency of BG18 type I BCRs that are B_{mem} cells among total B cells plotted per animal at week 12. Numbers below indicate total number of paired BCR sequences recovered from each group and the total number of BG18 type I BCRs recovered. **J)** Clonal richness of the BCR sequences recovered from epitope specific B_{mem} cells from week 12 plotted as the Chao1 index on a per animal basis. Chao was calculated for all animals that had at least 1 sequence recovered. **K)** Clonal abundance curves for each group from sequences at week 12. Clonal abundance was calculated per animal then the mean abundance for each clone rank was plotted for each group. Animals with fewer than 5 total clones were excluded from abundance calculations. **L)** Cumulative abundance of the top 5 most abundant clones plotted per animal. The lines in all per animal graphs represent medians. **M)** Frequency of IGHD3-41 usage in IgM$^+$ naïve B cells for 35 of the 36 animals plotted by specific genotype. Statistical significance was tested using unpaired two-tailed Mann-Whitney tests with the p-values listed on each graph representative of the tests carried out, NS listed when p-value was >0.1. Gray regions (B, D, E, G) represent B_{mem} LOD determined using pre-immunization samples.

Figure 6: Level of antigen specific circulating IgG predict boost outcomes A) AUC of antigen-specific serum IgG at week 12 plotted by animal. **B)** Fold change increase in serum IgG from week 10 to 12 calculated by taking week 12 AUC over week 10 AUC. **C)** AUC of epitope-specific serum IgG at week 12 plotted by animal. **D)** Fold change from week 10 to 12 for N332-GT5 epitope specific serum IgG. **E)** Correlation between fold change increase from week 10 to 12 and week 10 AUC. r and p-value are from pearson correlation analysis. **F)** Correlation between fold change increase for antigen-specific B_{mem} from week 10 to 12 and week 10 IgG AUC. r and p-value are from pearson correlation analysis. **G)** N332-GT5 specific BM-B_{PC} measured from bone marrow aspirates by ELISpot assay at weeks 10 and 16. **H)** Fold change from week 10 to 12 for BM-B_{PC}. Statistical significance was tested using unpaired two-tailed Mann-Whitney tests with the p-values listed on each graph representative of the tests carried, NS listed when p-value was >0.1.

Figure 7: BG18 type I BCRs have more SHM and higher affinity for boosting candidates. A) Quantitation of BG18 clones in each group and the number of IGHV genes used by those clones. **B)** Graph of the

1449 percentage of BG18 type I clones for each group that use the specified IGHV genes. **C)** Heavy chain
1450 nucleotide mutations plotted on a per cell basis for each group. Both total recovered BCRs and BG18 type
1451 I BCRs are shown with the number of sequences in each, the median mutations listed, and the percent of
1452 all sequences with at least 1 mutation. Statistical significance was tested using unpaired two-tailed Mann-
1453 Whitney test. **D)** Binding affinities (Apparent K_D) for a random subset of BG18 type I BCRs expressed from
1454 groups 1 and 2 to N332-GT5 and three potential boosting immunogens obtained by capturing IgG as the
1455 ligand and flowing trimers as analyte. Number and percent of binders are listed for each comparison (G1:
1456 n = 8, G2: n = 14). Dotted line represents the limit of detection for this assay. Statistical significance was
1457 tested between groups using unpaired two-tailed Mann-Whitney tests.
1458
1459
1460

SUPPLEMENTARY FIGURE LEGENDS

Supplementary Figure 1: pSer modification and antigenicity. A) Schematic of pSer peptide coupling to c-terminal Cys at the base of Env trimers and subsequent binding to aluminum hydroxide particles. **B)** Fluorescently-labeled pSer-conjugated or unmodified N332-GT5 trimers were mixed with alum in TBS, and the fraction of protein bound to alum was assessed after initial 30-minute adsorption ("Loading") or after 24-hour incubation in 10% mouse serum at 37°C by fluorescence spectroscopy. **C)** Antigenicity profiling ELISA assessing binding of serial dilutions of the indicated mAbs to pSer-N332-GT5 adsorbed to plate-immobilized alum. **D)** Area-under-the-curve values for mAb binding vs. antibody concentration from data shown in (**C**). Mean and SD are plotted. Statistical significance was tested using two-way ANOVA with Sidak's multiple comparisons test in (**B**). * $p < 0.05$, ****$p < 0.0001$.

Supplementary Figure 2: Nano-alum synthesis and characterization. A) Schematic of nano-alum formulation and binding with pSer-trimers. **B)** Number-average particle size of nano-alum determined by dynamic light scattering. C) TEM image of neat Alhydrogel and cryoEM image of nano-alum. **D)** Photographs illustrating physical appearance of sedimented alum solution vs. stable opalescent nano-alum solution. **E)** CryoEM image of pSer-trimer mixed with nano-alum showing trimers decorating individual aluminum hydroxide nanocrystals. F-H) BALB/c mice (n = 5 animals/group) were immunized with 5 µg pSer-trimer adsorbed to 50 µg Alhydrogel (alum) or 50 µg nano-alum. Shown are flow cytometry analyses of total GC B cells **(F)** and trimer-specific GC B cells **(G)** on day 14 and serum IgG titers determined by ELISA over time (H). Statistical significance determined by two-tailed t test in **(F, G)** and two-way ANOVA in (H). ns, not significant; **, $p < 0.01$; ***, $p < 0.001$.

Supplementary Figure 3: Amph-CpG adjuvant. A) Molecular structure of Amph-CpG.

Supplementary Figure 4: Germinal center flow cytometry gating. A) Gating strategy for LN FNA analysis. GC-T_{FH} gating and B_{GC} gates used for quantification are shown with antigen- and epitope-specific gates. Epitope-specific B_{GC} cells were sorted. **B)** Antigen-specific non-GC B cell frequency (N332-GT5-AF647$^+$N332-GT5-BV421$^+$) as a percentage of total B cells (CD20$^+$). Geometric mean and SD are shown for each group at week 3 and 9. **C)** Antigen-specific non-GC B cell frequency (N332-GT5-AF647$^+$N332-GT5-BV421$^+$N332-GT5KO-PE$^-$) as a percentage of total B cells (CD20$^+$). Geometric mean and SD are shown for each group at week 3 and 9.

Supplementary Figure 5: BG18 sequencing. A) Sequence alignment of germline BG18 H-CDR3 with macaque IGHD3-41 and sequence definition of BG18 type I BCRs. **B)** Frequency of BG18$_{short}$ B_{GC} cells among total B cells, plotted per animal. Numbers below indicate total number of paired BCR sequences recovered from each group and the total number of BG18$_{short}$ BCRs recovered. **C)** Frequency of potential BG18 type III B_{GC} cells among total B cells, plotted per animal. Numbers below indicate total number of paired BCR sequences recovered from each group and the total number of potential BG18 type III BCRs recovered. **D)** Simpson diversity index of BCR sequences plotted per animal.

Supplementary Figure 6: AIM ICS gating and data. A) Flow cytometry gating for AIM ICS T cell assay. **B)** Frequency of AIM$^+$ (CD40L$^+$OX40$^+$) T cells out of total CD4$^+$ T cells. **C)** Frequency of AIM$^+$ICS$^+$ (CD40L$^+$IFNγ$^+$) T cells out of total CD4$^+$ T cells. **D)** Frequency of AIM$^+$ICS$^+$ (CD40L$^+$GzmB$^+$) T cells out of total CD4$^+$ T cells. **E)** Frequency of AIM$^+$ICS$^+$ (CD40L$^+$IL2$^+$) T cells out of total CD4$^+$ T cells. **F)** Frequency of AIM$^+$ICS$^+$ (CD40L$^+$TNFα$^+$) T cells out of total CD4$^+$ T cells. **G)** Frequency of AIM$^+$ (OX40$^+$41BB$^+$) cT_{FH} cells out of total CD4$^+$ cT_{FH} cells.

1508
1509 **Supplementary Figure 7: ELISA data and B_{GC} correlations. A)** Longitudinal endpoint titer curves of total
1510 antigen-specific serum IgG measured by ELISA. **B)** Longitudinal endpoint titer curves of total epitope-
1511 specific serum IgG measured by ELISA. Geometric mean and SD are plotted for each group at each time
1512 point on a Log(titer) axis. **C)** Correlation between total post-prime antigen-specific B_{GC} and week 10
1513 antigen-specific IgG AUC. r and p-value are from pearson correlation analysis run with all groups included
1514 or excluding G6. **D)** Correlation between total post-prime epitope-specific B_{GC} and week 10 epitope-
1515 specific IgG AUC. r and p-value are from pearson correlation analysis run with all groups included or
1516 excluding G6.
1517
1518 **Supplementary Figure 8: B_{mem} flow cytometry and sequencing. A)** Flow cytometry gating strategy for
1519 isolating epitope-specific B_{mem} cells from PBMCs. **B)** Frequency of $BG18_{short}$ B_{GC} cells among total B cells,
1520 plotted per animal. Numbers below indicate total number of paired BCR sequences recovered from each
1521 group and the total number of $BG18_{short}$ BCRs recovered. **C)** Frequency of potential BG18 type III B_{GC} cells
1522 among total B cells, plotted per animal. Numbers below indicate total number of paired BCR sequences
1523 recovered from each group and the total number of potential BG18 type III BCRs recovered. **D)** Simpson
1524 diversity index of BCR sequences plotted per animal. Statistical significance was tested using unpaired
1525 two-tailed Mann-Whitney tests with the p-values listed on each graph representative of the tests carried
1526 out, NS listed when p-value was >0.1. **E)** iNext plots showing the results of rarefaction analysis performed
1527 on the week 12 B_{mem} sequences to determine the % sequence coverage based on the number and clonality
1528 of the recovered sequences. Each group is plotted separately with each line representing a single animal.
1529 Only animals that had more than 5 unique clones were included in the analysis.
1530
1531 **Supplementary Figure 9: IGHD3-41 Immunogenetics. A)** IGHD3-41 genotype distribution for each
1532 animal separated by group. **B)** Week 12 BG18 type I B_{mem} frequency plotted by genotype and group. Each
1533 dot represents an individual animal. **C)** Week 12 BG18 type I B_{mem} frequency plotted by genotype for all
1534 42 animals together. Statistical significance was tested using ANOVA with the p-values listed on each
1535 graph. For B) p-values represent within-group comparisons.
1536
1537 **Supplementary Figure 10: Serum IgG correlations and B_{PC}. A)** Correlation between epitope-specific fold
1538 change increase from week 10 to 12 and epitope-specific week 10 AUC. r and p-value are from pearson
1539 correlation analysis. **B-C)** Total IgG^+ BM-B_{PC} measured from bone marrow aspirates by ELISpot assay at
1540 weeks 10 and 16.
1541
1542 **Supplementary Figure 11: Light chain usage and SHM across groups. A)** Graph of the distribution of
1543 IGHK and IGHL genes used by BG18 type I clones in groups 1 and 2. **B)** Heavy chain nucleotide
1544 mutations plotted for each group of total week 12 B_{mem} cells. Number of sequences, median mutation
1545 count, and percentage of all cells with 1 or more mutations are listed below graphs. **C)** Heavy chain
1546 nucleotide mutations plotted for each group of week 12 BG18 type I B_{mem}. Number of sequences,
1547 median mutation count, and percentage of all cells with 1 or more mutations are listed below graphs

1548

Fig.1

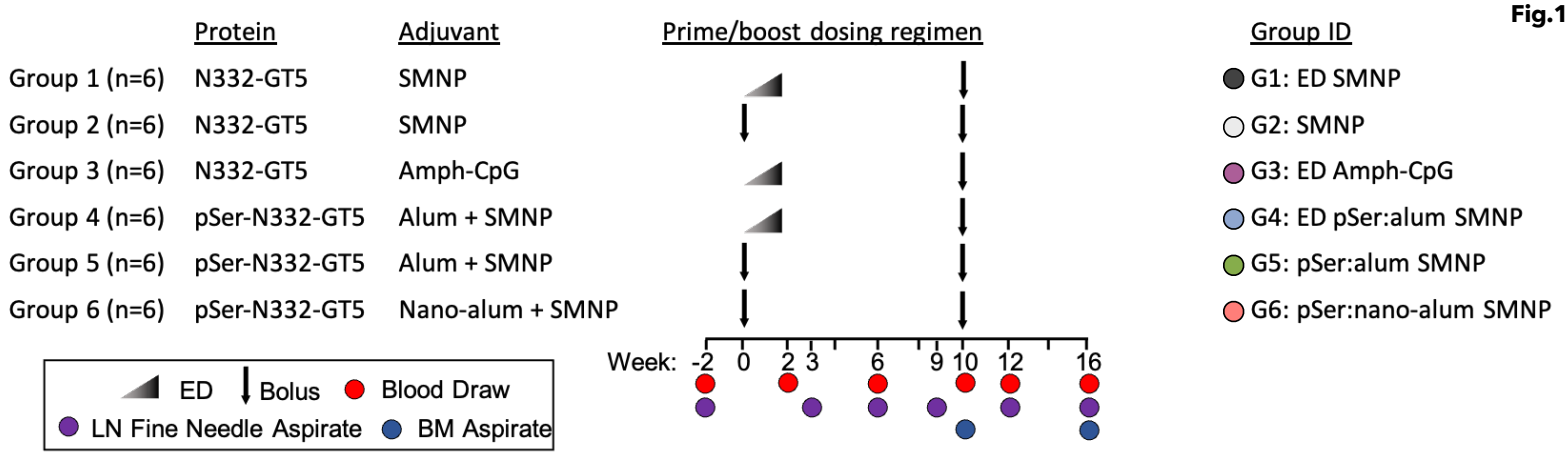
Protein
Adjuvant
Prime/boost dosing regimen
Group ID
Group 1 (n=6) N332-GT5 SMNP
Group 2 (n=6) N332-GT5 SMNP
Group 3 (n=6) N332-GT5 Amph-CpG
Group 4 (n=6) pSer-N332-GT5 Alum + SMNP
Group 5 (n=6) pSer-N332-GT5 Alum + SMNP
Group 6 (n=6) pSer-N332-GT5 Nano-alum + SMNP
G1: ED SMNP
G2: SMNP
G3: ED Amph-CpG
G4: ED pSer:alum SMNP
G5: pSer:alum SMNP
G6: pSer:nano-alum SMNP
Week: -2 0 2 3 6 9 10 12 16
ED
Bolus
Blood Draw
LN Fine Needle Aspirate
BM Aspirate

Fig.2

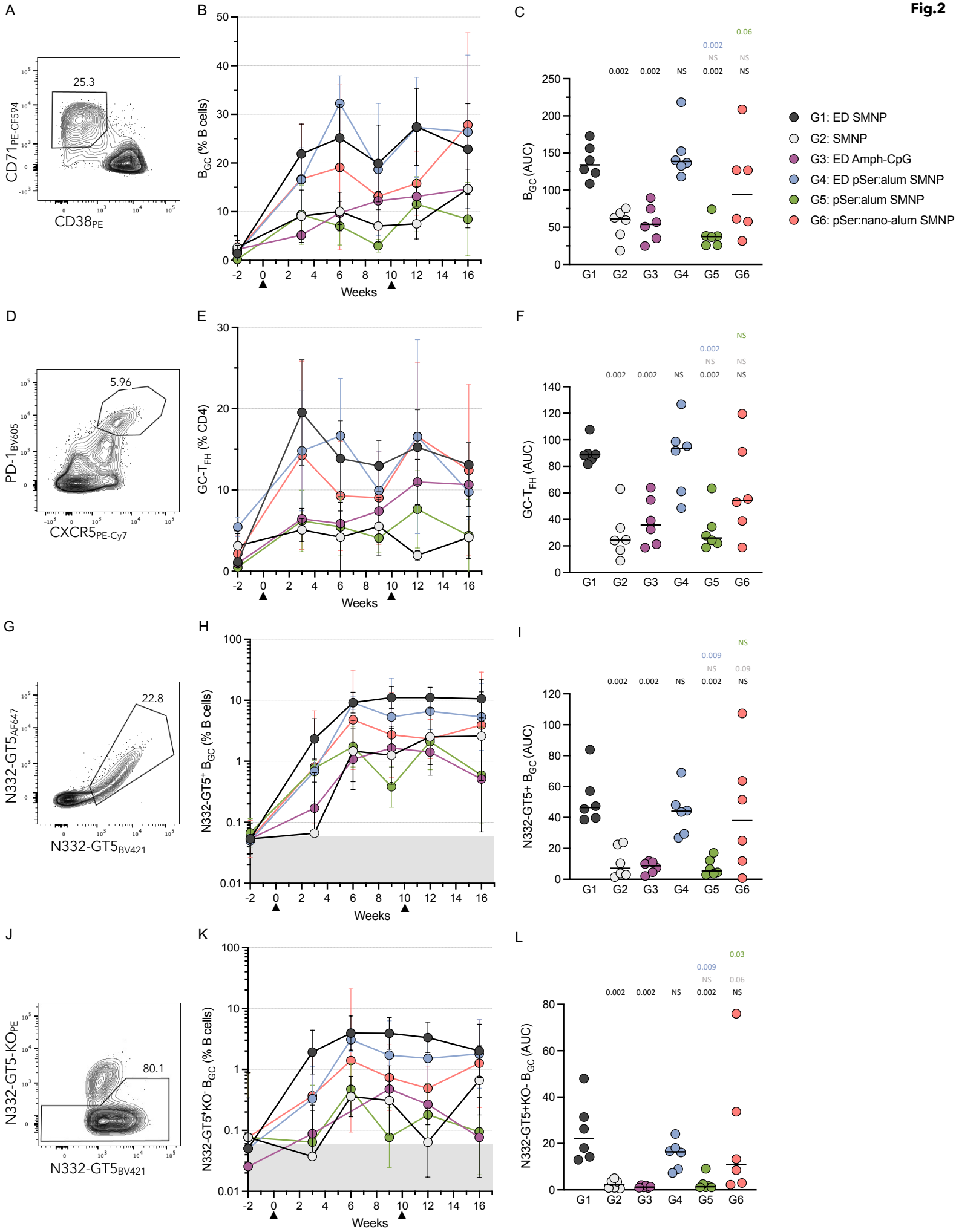
A
25.3
CD71PE-CF594
CD38PE
B
BGC (% B cells)
Weeks
C
BGC (AUC)
0.002
0.002
NS
0.002
NS
0.002
NS
NS
0.06
G1
G2
G3
G4
G5
G6
G1: ED SMNP
G2: SMNP
G3: ED Amph-CpG
G4: ED pSer:alum SMNP
G5: pSer:alum SMNP
G6: pSer:nano-alum SMNP
D
5.96
PD-1BV605
CXCR5PE-Cy7
E
GC-TFH (% CD4)
Weeks
F
GC-TFH (AUC)
0.002
0.002
NS
0.002
NS
0.002
NS
NS
NS
G
22.8
N332-GT5AF647
N332-GT5BV421
H
N332-GT5+ BGC (% B cells)
Weeks
I
N332-GT5+ BGC (AUC)
0.002
0.002
NS
0.002
NS
0.009
NS
0.09
NS
J
80.1
N332-GT5-KOPE
N332-GT5BV421
K
N332-GT5+KO- BGC (% B cells)
Weeks
L
N332-GT5+KO- BGC (AUC)
0.002
0.002
NS
0.002
NS
0.009
NS
0.06
0.03

Fig.3

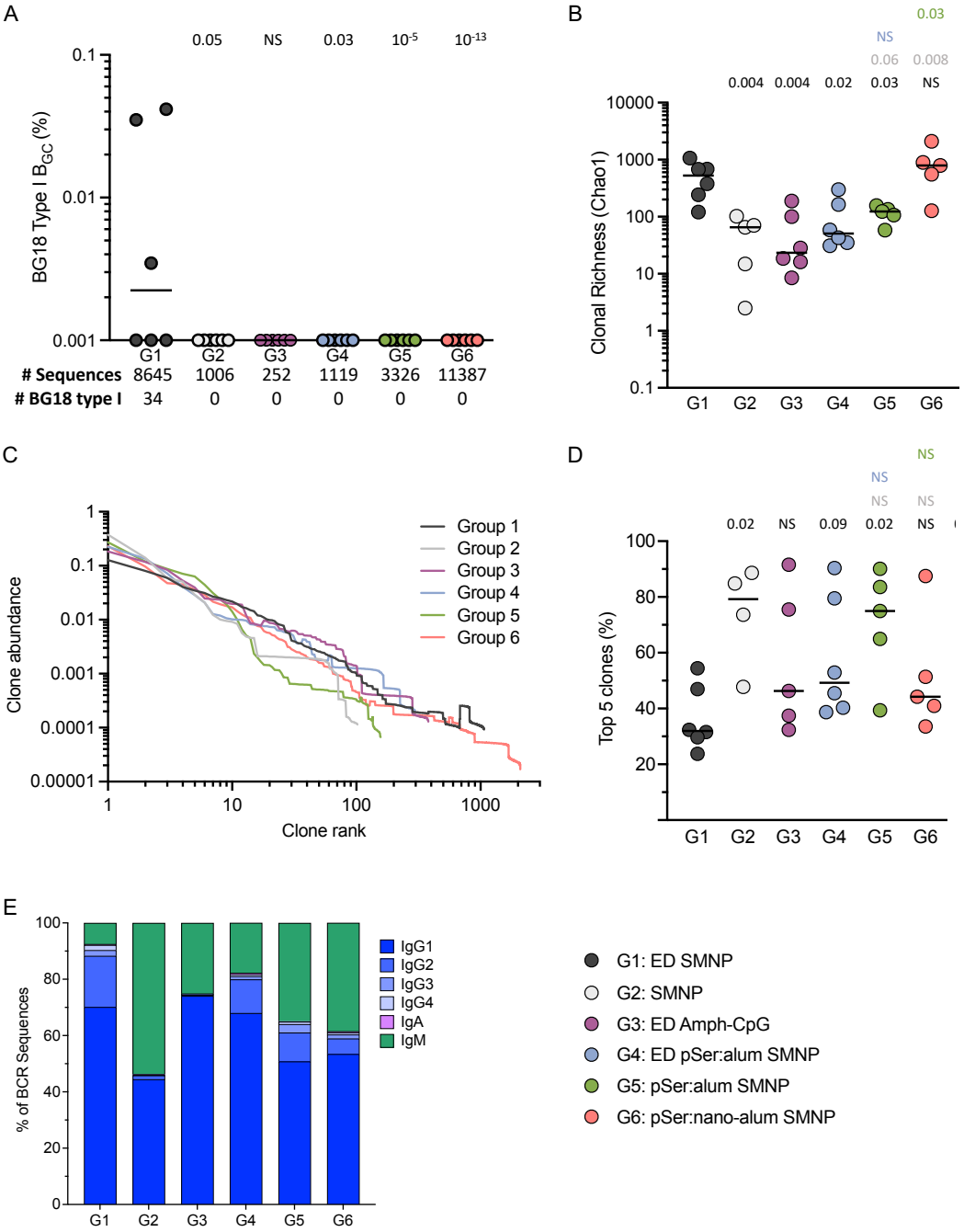
A
0.05
NS
0.03
10-5
10-13
BG18 Type I BGC (%)
0.1
0.01
0.001
G1 G2 G3 G4 G5 G6
Sequences 8645 1006 252 1119 3326 11387
BG18 type I 34 0 0 0 0 0
B
0.03
NS
0.06
0.008
0.004
0.004
0.02
0.03
NS
Clonal Richness (Chao1)
10000
1000
100
10
1
0.1
G1 G2 G3 G4 G5 G6
C
Clone abundance
1
0.1
0.01
0.001
0.0001
0.00001
1
10
100
1000
Clone rank
Group 1
Group 2
Group 3
Group 4
Group 5
Group 6
D
NS
NS
NS
NS
0.02
NS
0.09
0.02
NS
Top 5 clones (%)
100
80
60
40
20
G1 G2 G3 G4 G5 G6
E
% of BCR Sequences
100
80
60
40
20
0
G1 G2 G3 G4 G5 G6
IgG1
IgG2
IgG3
IgG4
IgA
IgM
G1: ED SMNP
G2: SMNP
G3: ED Amph-CpG
G4: ED pSer:alum SMNP
G5: pSer:alum SMNP
G6: pSer:nano-alum SMNP

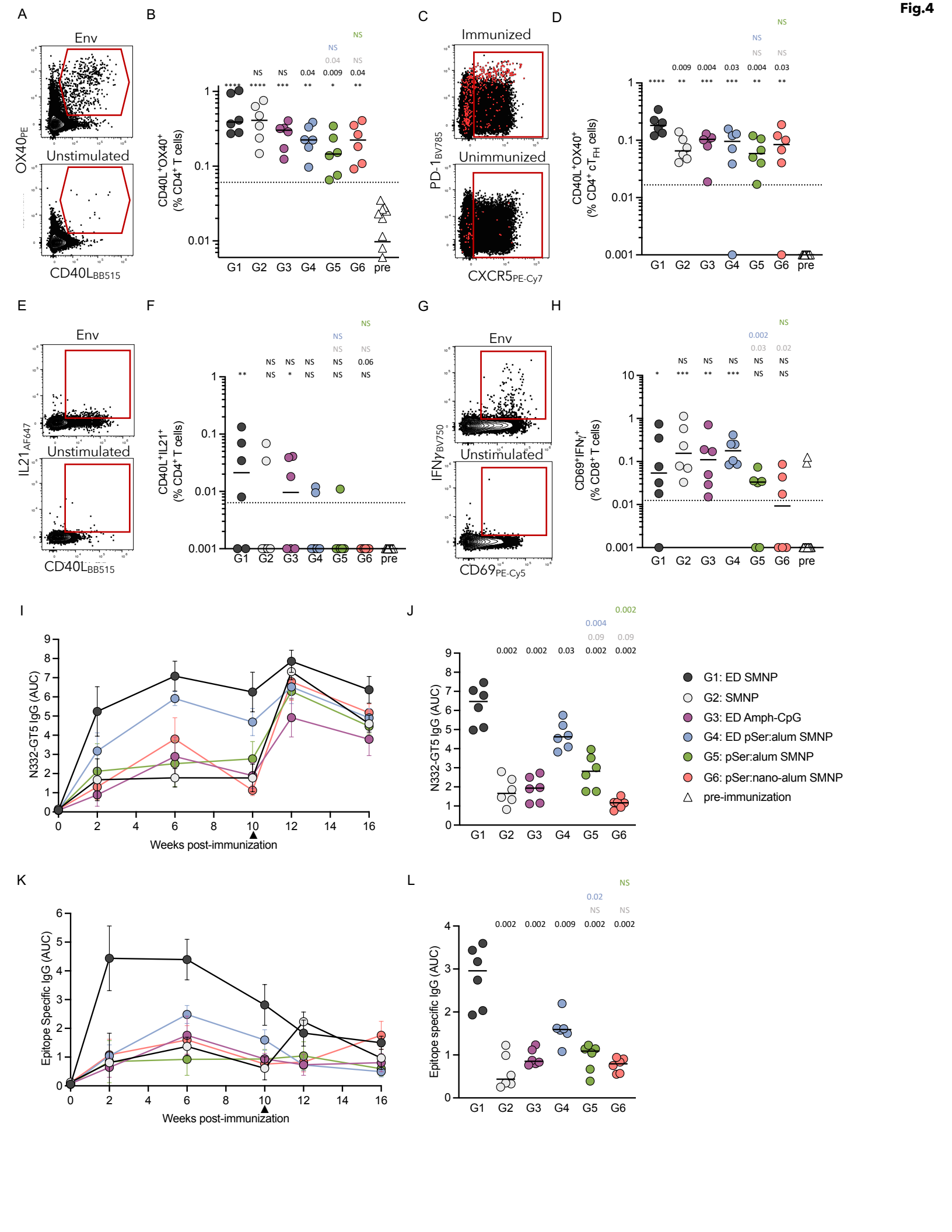
A
Env
Unstimulated
OX40PE
CD40LBB515
B
CD40L+OX40+ (% CD4+ T cells)
G1 G2 G3 G4 G5 G6 pre
C
Immunized
Unimmunized
PD-1BV785
CXCR5PE-Cy7
D
CD40L+OX40+ (% CD4+ cTFH cells)
E
IL21AF647
F
CD40L+IL21+ (% CD4+ T cells)
G
IFNγBV750
CD69PE-Cy5
H
CD69+IFNγ+ (% CD8+ T cells)
I
N332-GT5 IgG (AUC)
Weeks post-immunization
J
G1: ED SMNP
G2: SMNP
G3: ED Amph-CpG
G4: ED pSer:alum SMNP
G5: pSer:alum SMNP
G6: pSer:nano-alum SMNP
pre-immunization
K
Epitope Specific IgG (AUC)
L
Epitope specific IgG (AUC)

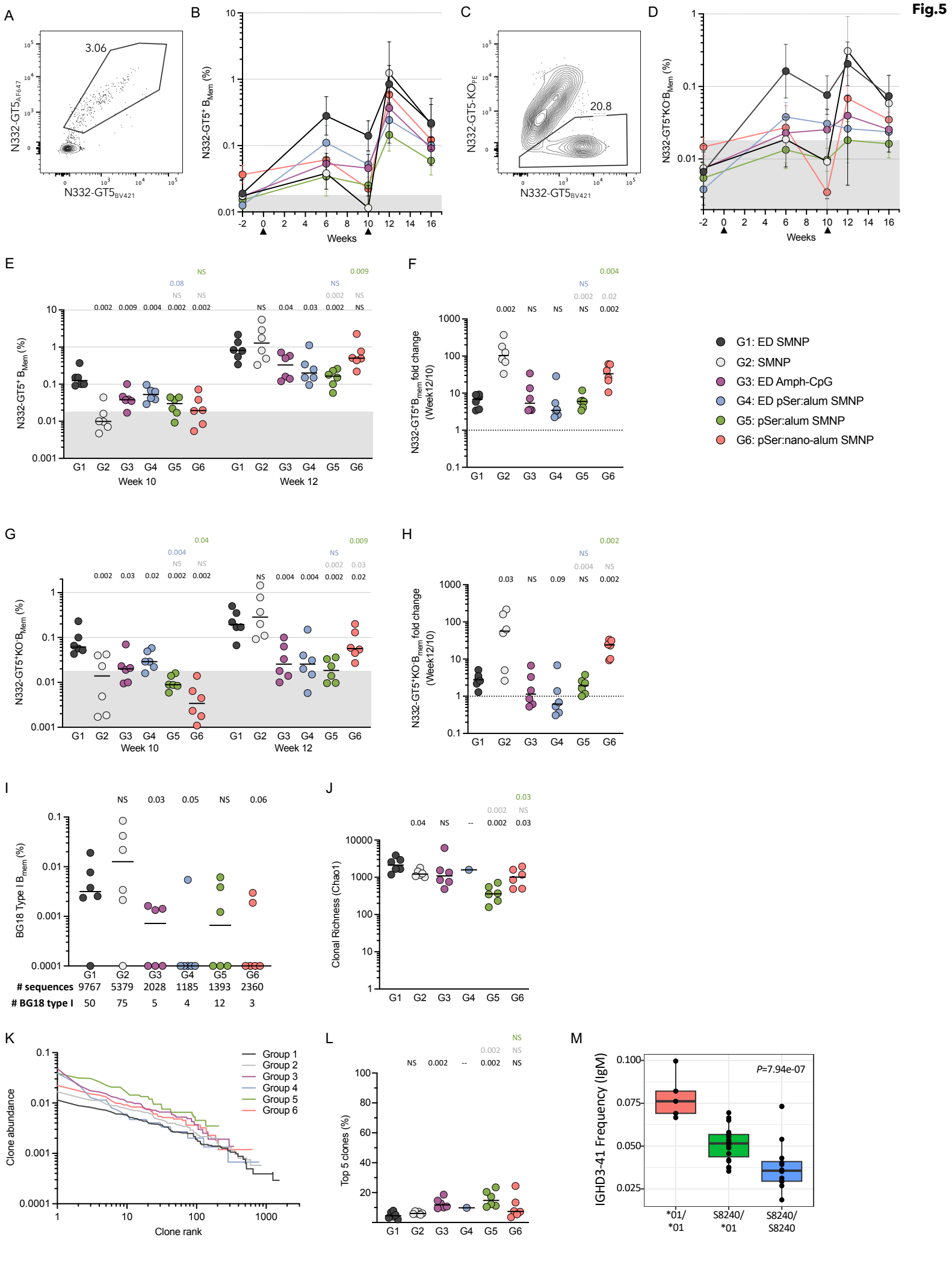
Fig.5
A
3.06
N332-GT5AF647
N332-GT5BV421
B
N332-GT5+ BMem (%)
Weeks
C
20.8
N332-GT5-KOPE
N332-GT5BV421
D
N332-GT5+KO-BMem (%)
Weeks
E
N332-GT5+ BMem (%)
Week 10
Week 12
F
N332-GT5+Bmem fold change (Week12/10)
G1: ED SMNP
G2: SMNP
G3: ED Amph-CpG
G4: ED pSer:alum SMNP
G5: pSer:alum SMNP
G6: pSer:nano-alum SMNP
G
N332-GT5+KO-BMem (%)
Week 10
Week 12
H
N332-GT5+KO-Bmem fold change (Week12/10)
I
BG18 Type I Bmem (%)
sequences 9767 5379 2028 1185 1393 2360
BG18 type I 50 75 5 4 12 3
J
Clonal Richness (Chao1)
K
Clone abundance
Clone rank
Group 1
Group 2
Group 3
Group 4
Group 5
Group 6
L
Top 5 clones (%)
M
IGHD3-41 Frequency (IgM)
P=7.94e-07
*01/ *01
S8240/ *01
S8240/ S8240

Fig.6

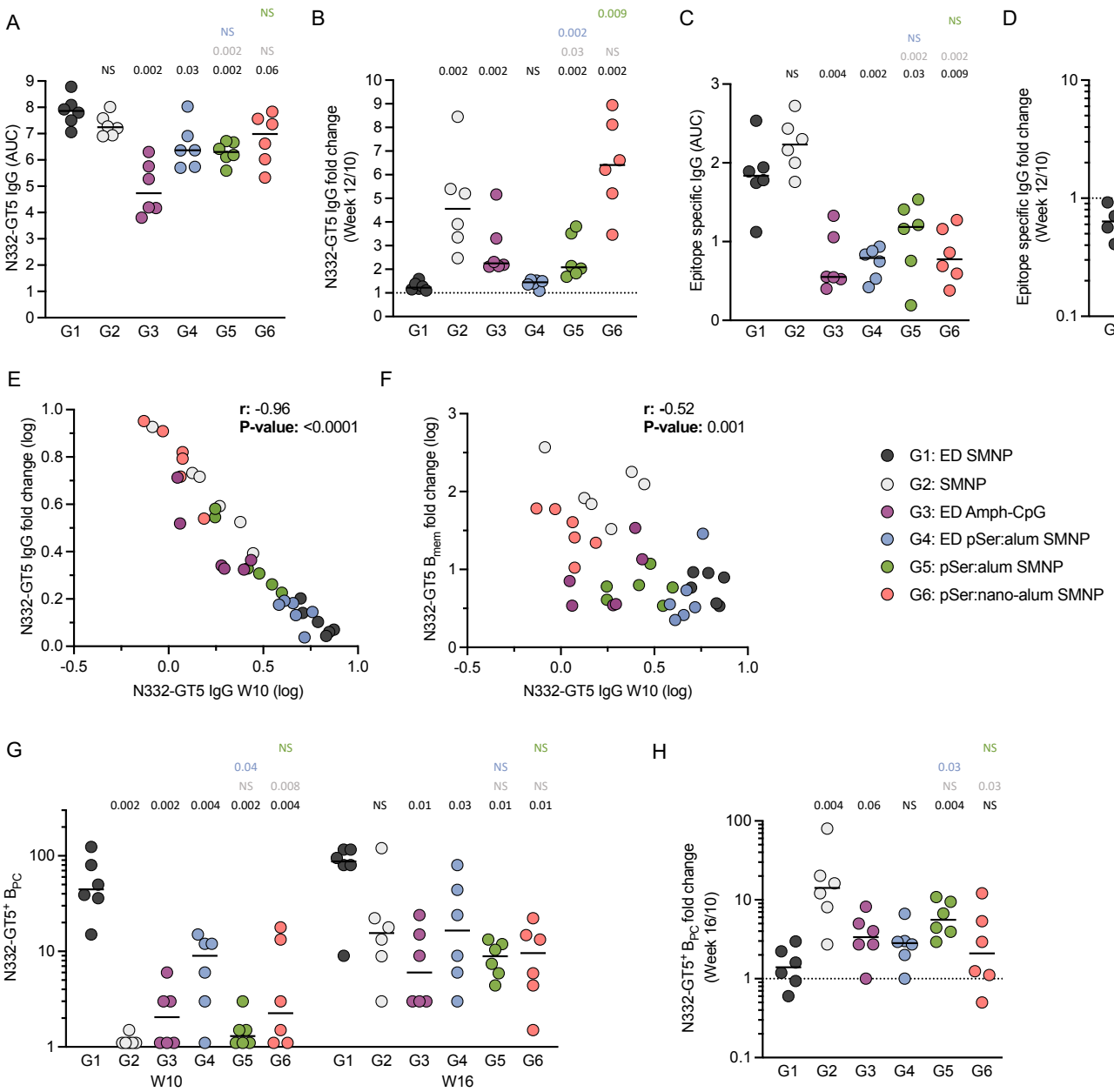
A
N332-GT5 IgG (AUC)
NS 0.002 0.03 0.002 0.06
NS NS 0.002 NS
G1 G2 G3 G4 G5 G6
B
N332-GT5 IgG fold change (Week 12/10)
0.002 0.002 NS 0.002 0.002
0.002 0.03 NS
0.009
C
Epitope specific IgG (AUC)
NS 0.004 0.002 0.03 0.009
NS 0.002 0.002
NS
D
Epitope specific IgG fold change (Week 12/10)
0.002 NS NS 0.06 0.06
0.06 0.009 0.002
NS
E
N332-GT5 IgG fold change (log)
N332-GT5 IgG W10 (log)
r: -0.96
P-value: <0.0001
F
N332-GT5 B$_{mem}$ fold change (log)
N332-GT5 IgG W10 (log)
r: -0.52
P-value: 0.001
G1: ED SMNP
G2: SMNP
G3: ED Amph-CpG
G4: ED pSer:alum SMNP
G5: pSer:alum SMNP
G6: pSer:nano-alum SMNP
G
N332-GT5$^+$ B$_{PC}$
0.002 0.002 0.004 0.002 0.004
NS 0.008
0.04
NS
NS 0.01 0.03 0.01 0.01
NS NS
NS
W10
W16
H
N332-GT5$^+$ B$_{PC}$ fold change (Week 16/10)
0.004 0.06 NS 0.004 NS
NS 0.03
0.03
NS

Fig.7

A

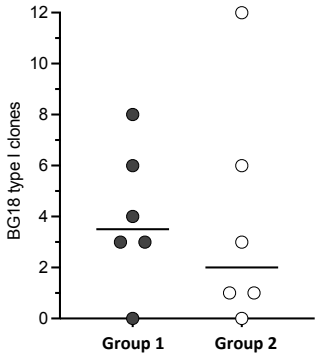

	Group 1	Group 2
# Clones	27	23
# IGHV genes	19	18

B

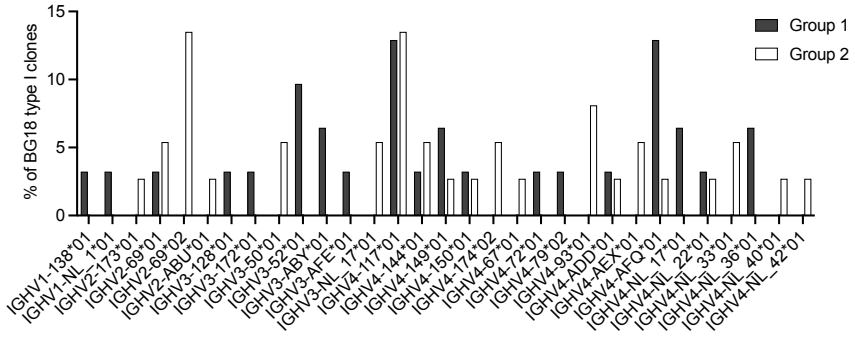

C

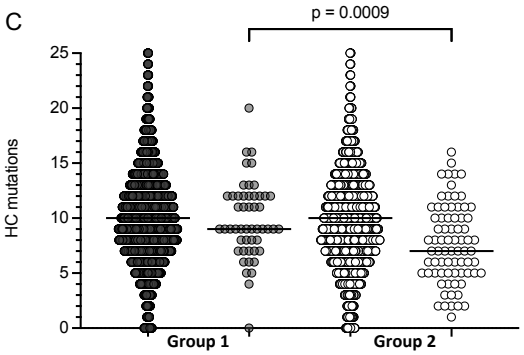

Cells	All	BG18	All	BG18
N	9278	50	5048	75
Median	10	9	10	7
% Mutated	98.6	98.0	98.4	100

D

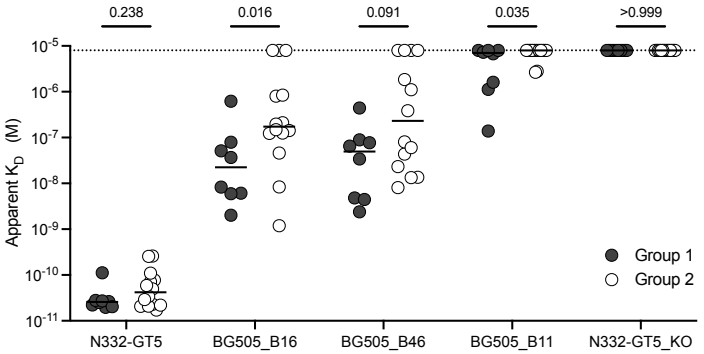

	N332-GT5		BG505_B16		BG505_B46		BG505_B11		N332-GT5_KO	
# Binders	7	14	8	11	8	10	5	2	0	0
% Binders	87.5	100	100	78.6	100	71.4	62.5	14.3	0	0

Supplementary Fig.1

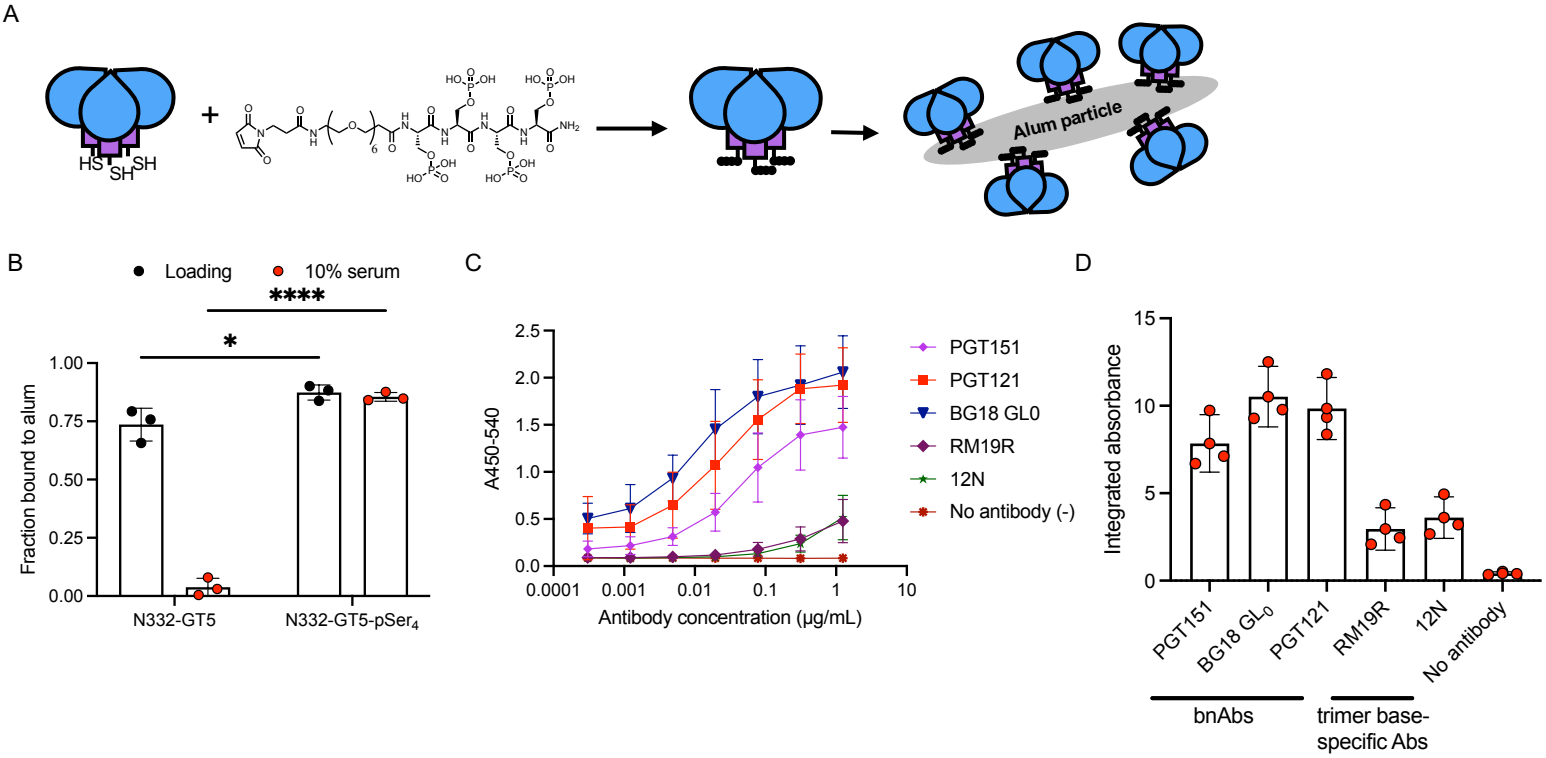

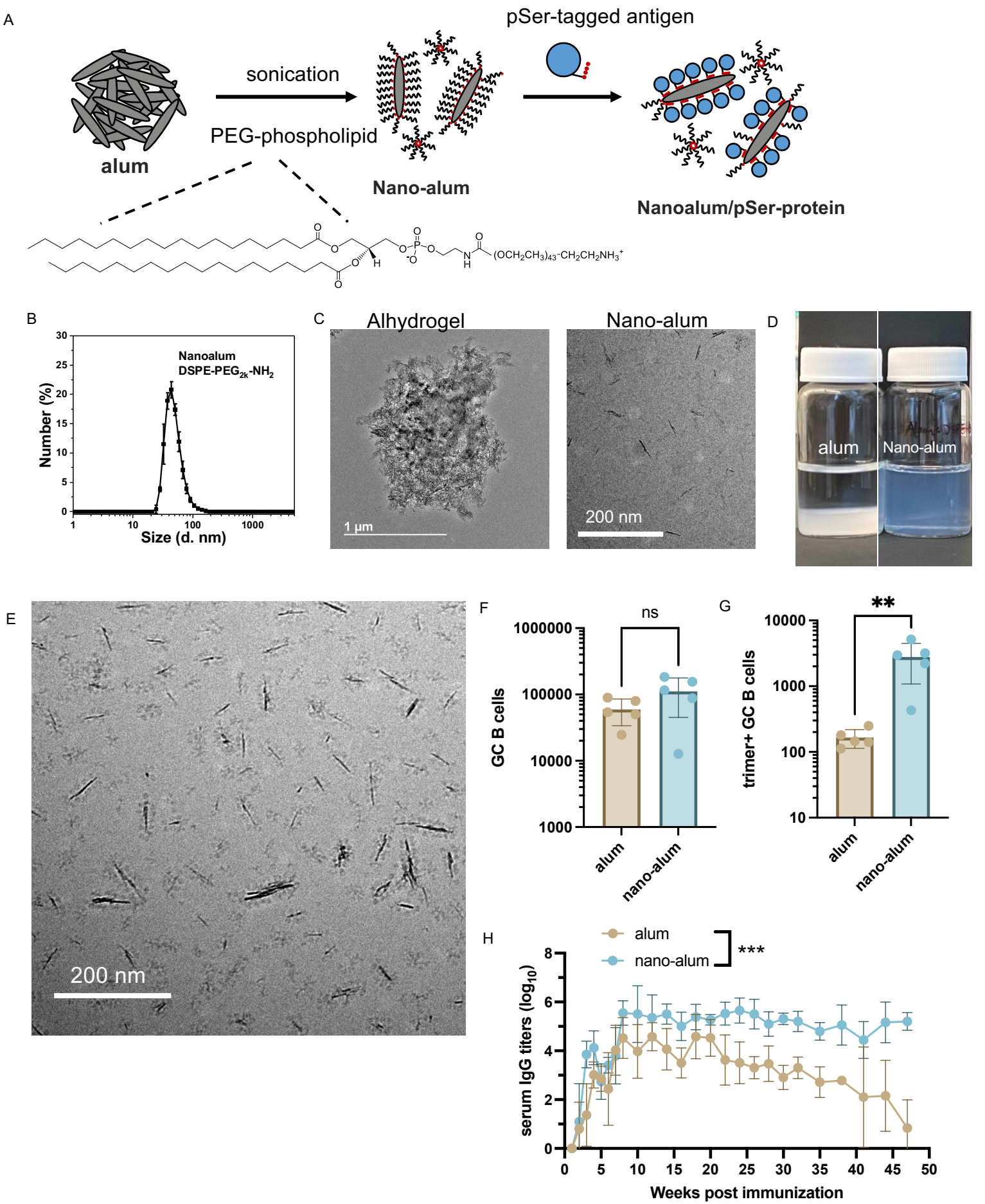
A
pSer-tagged antigen
sonication
PEG-phospholipid
alum
Nano-alum
Nanoalum/pSer-protein
B
Nanoalum
DSPE-PEG2k-NH2
Number (%)
Size (d. nm)
C
Alhydrogel
Nano-alum
1 μm
200 nm
D
alum
Nano-alum
E
200 nm
F
ns
GC B cells
alum
nano-alum
G
**
trimer+ GC B cells
alum
nano-alum
H
alum
nano-alum
***
serum IgG titers (log10)
Weeks post immunization

Supplementary Fig.3

A

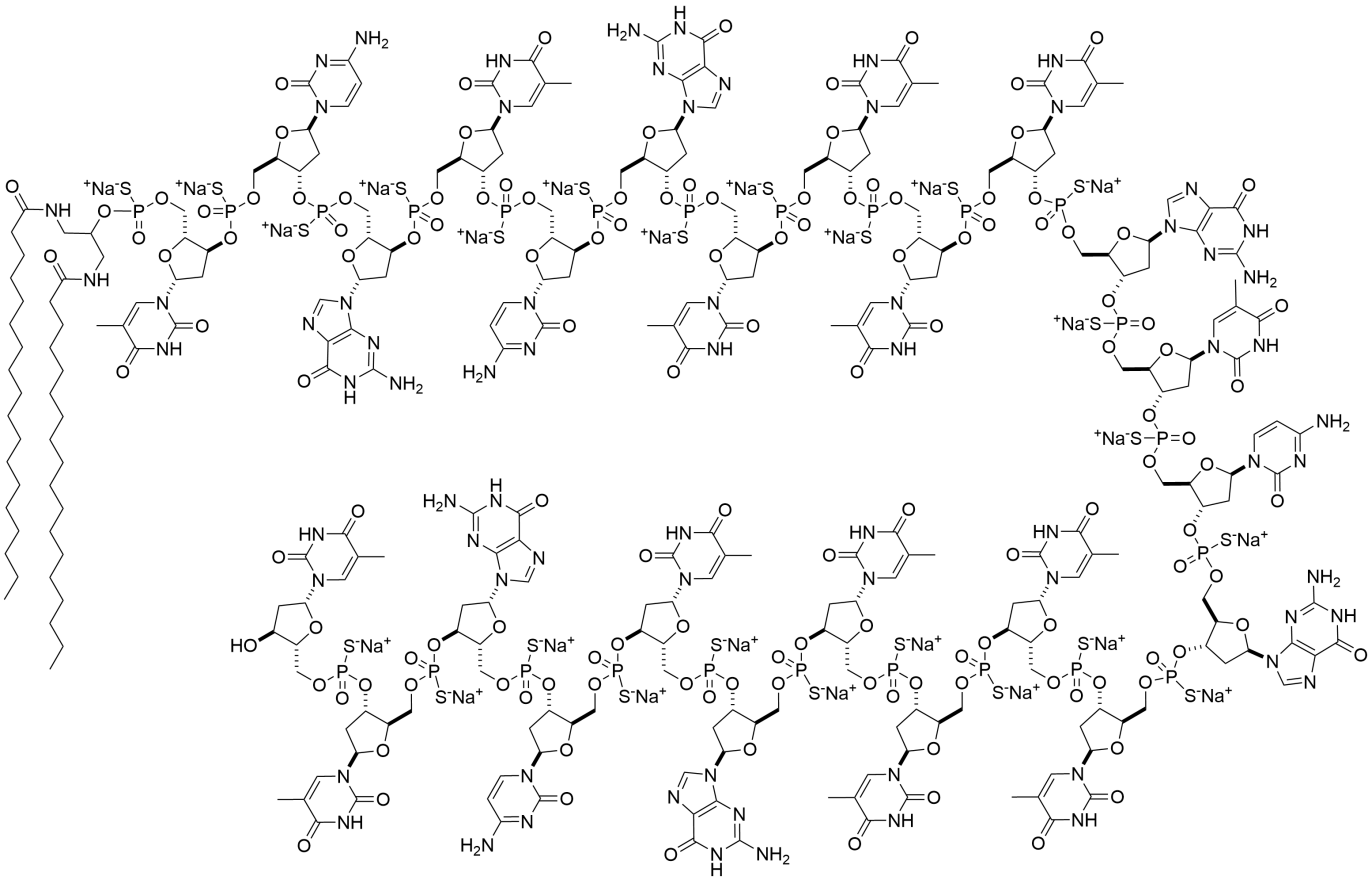

Supplementary Fig.4

A

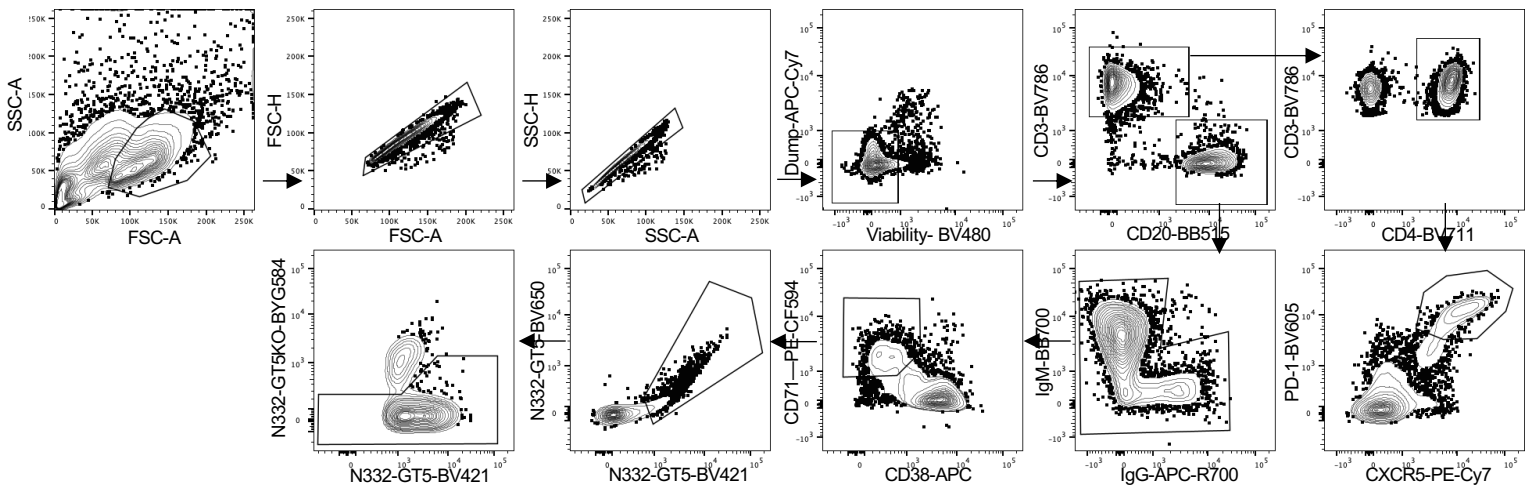

B

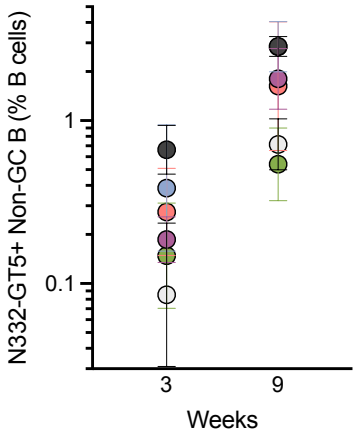

C

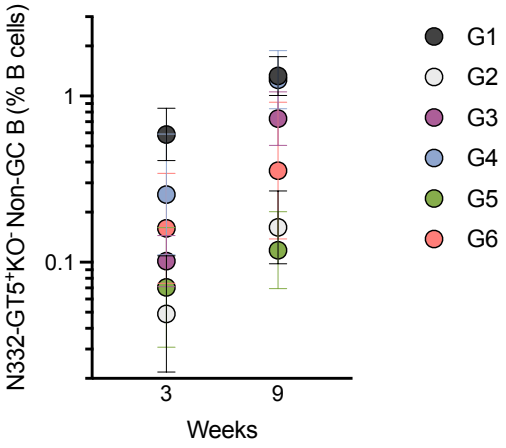

Supplementary Fig.5

A

D gene in BG18 reading frame

Glu at D+2

```
ARNAITIFGVVIIGEYYYYGMDV   BG18 germline HCDR3
    ITIFGVVII             Human IGHD3-3
    ITIFGVVIT             Macaque IGHD3-41 reading frame 3
        GVLQFLEWLLY       Macaque IGHD3-41 reading frame 1
```

BG18 type I Sequence definition

1. HCDR3 >= 22AA
2. IGHD3-41
3. "G.....E" found within HCDR3

B

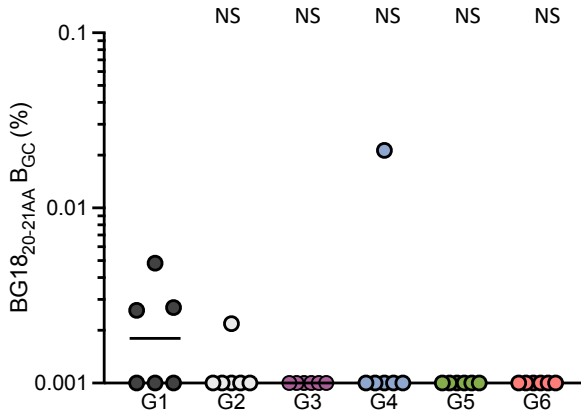

	G1	G2	G3	G4	G5	G6
# Sequences	8645	1006	252	1119	3326	11387
# BG18$_{20\text{-}21AA}$ type I	11	1	0	1	0	0

C

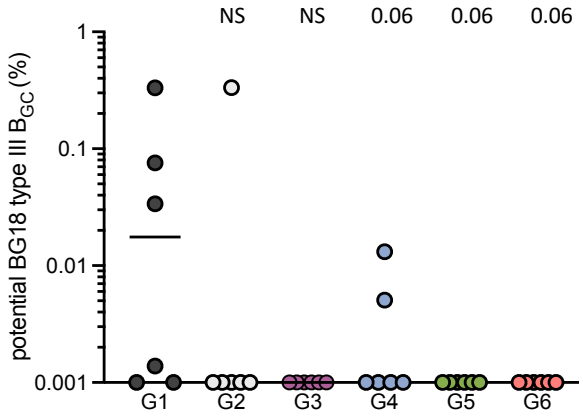

	G1	G2	G3	G4	G5	G6
# Sequences	8645	1006	252	1119	3326	11387
# potential BG18 type III	325	112	0	8	0	0

D

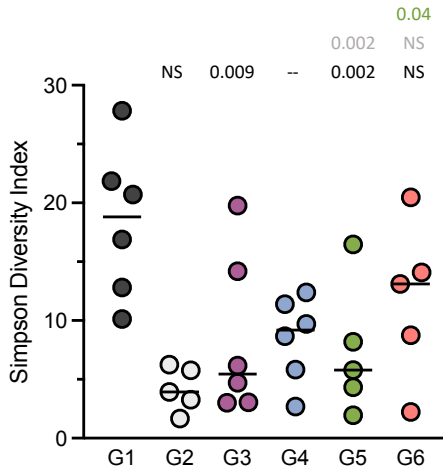

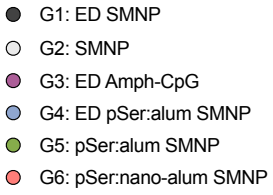

Supplementary Fig.6

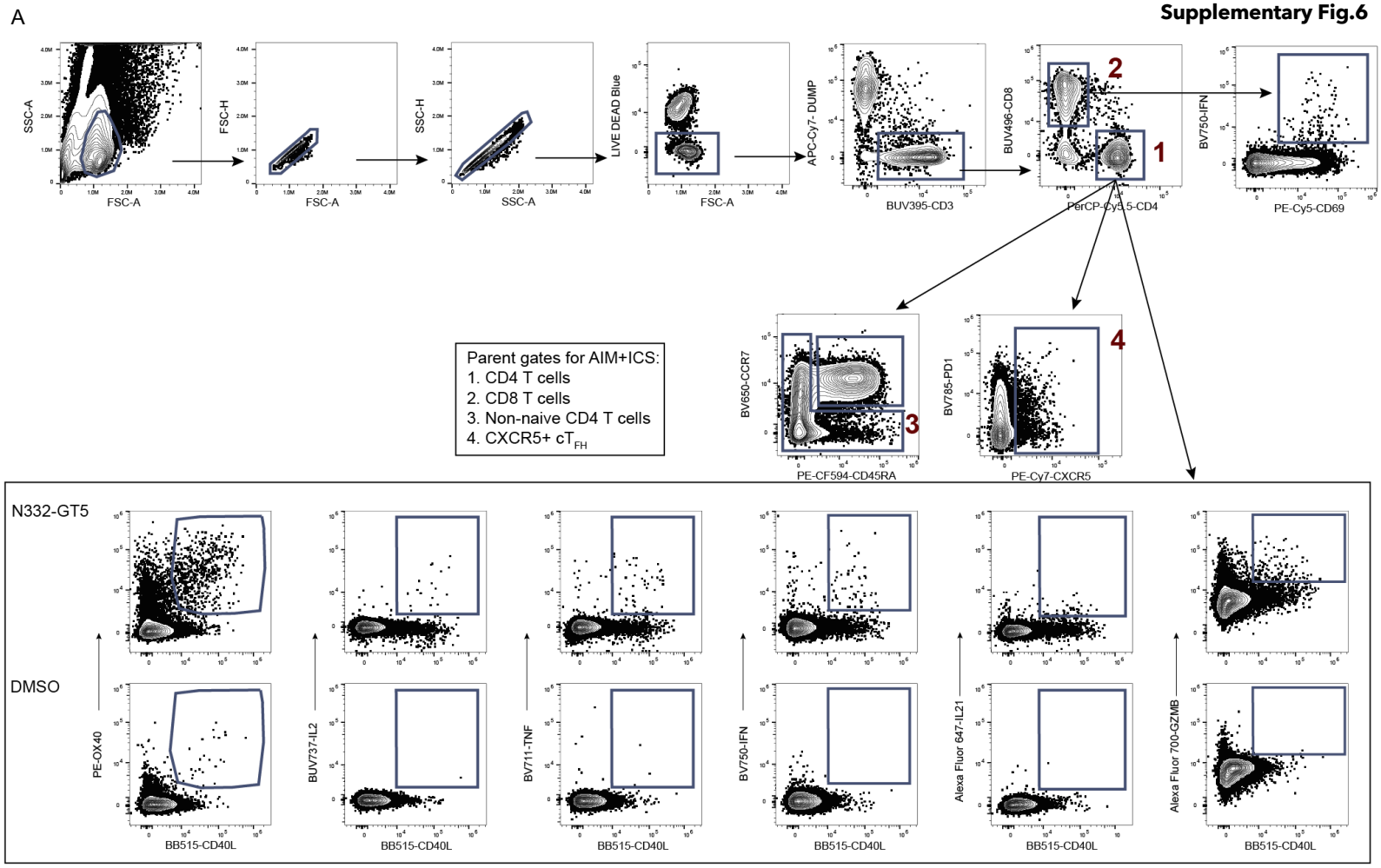

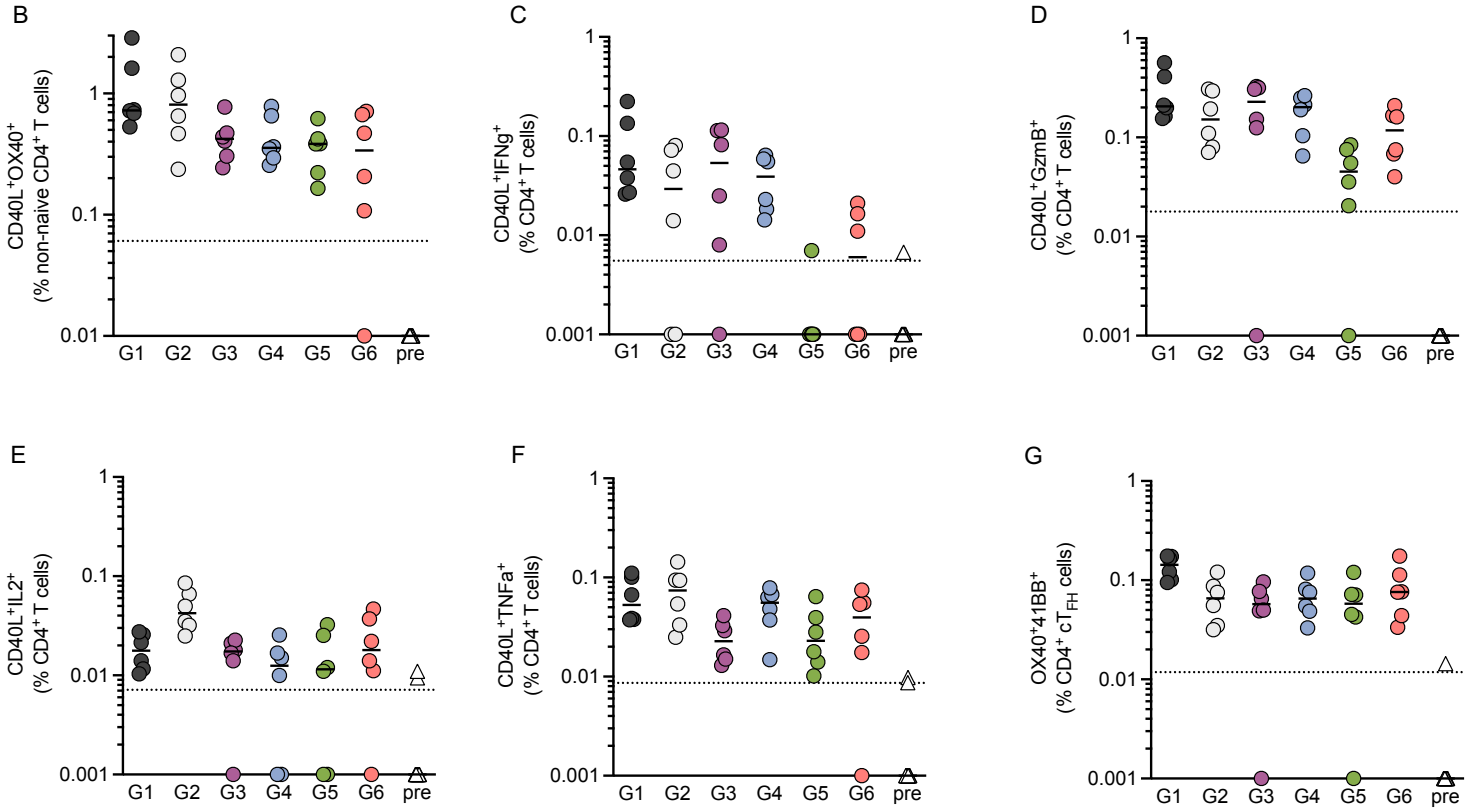

Supplementary Fig.7

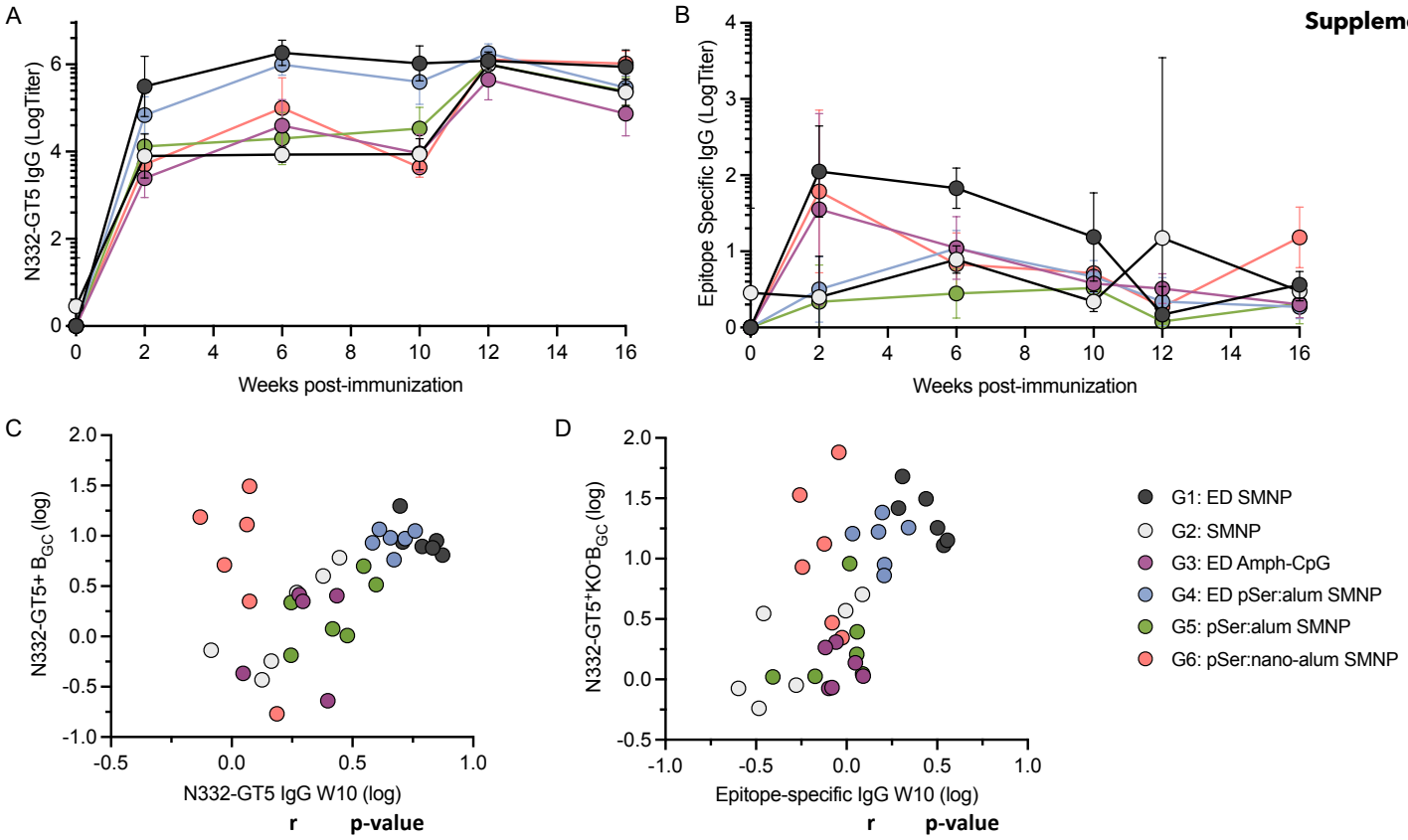

	r	p-value
All groups	0.41	0.015
Excluding G6	0.80	<0.0001

	r	p-value
All groups	0.57	0.0003
Excluding G6	0.76	<0.0001

Supplementary Fig.8

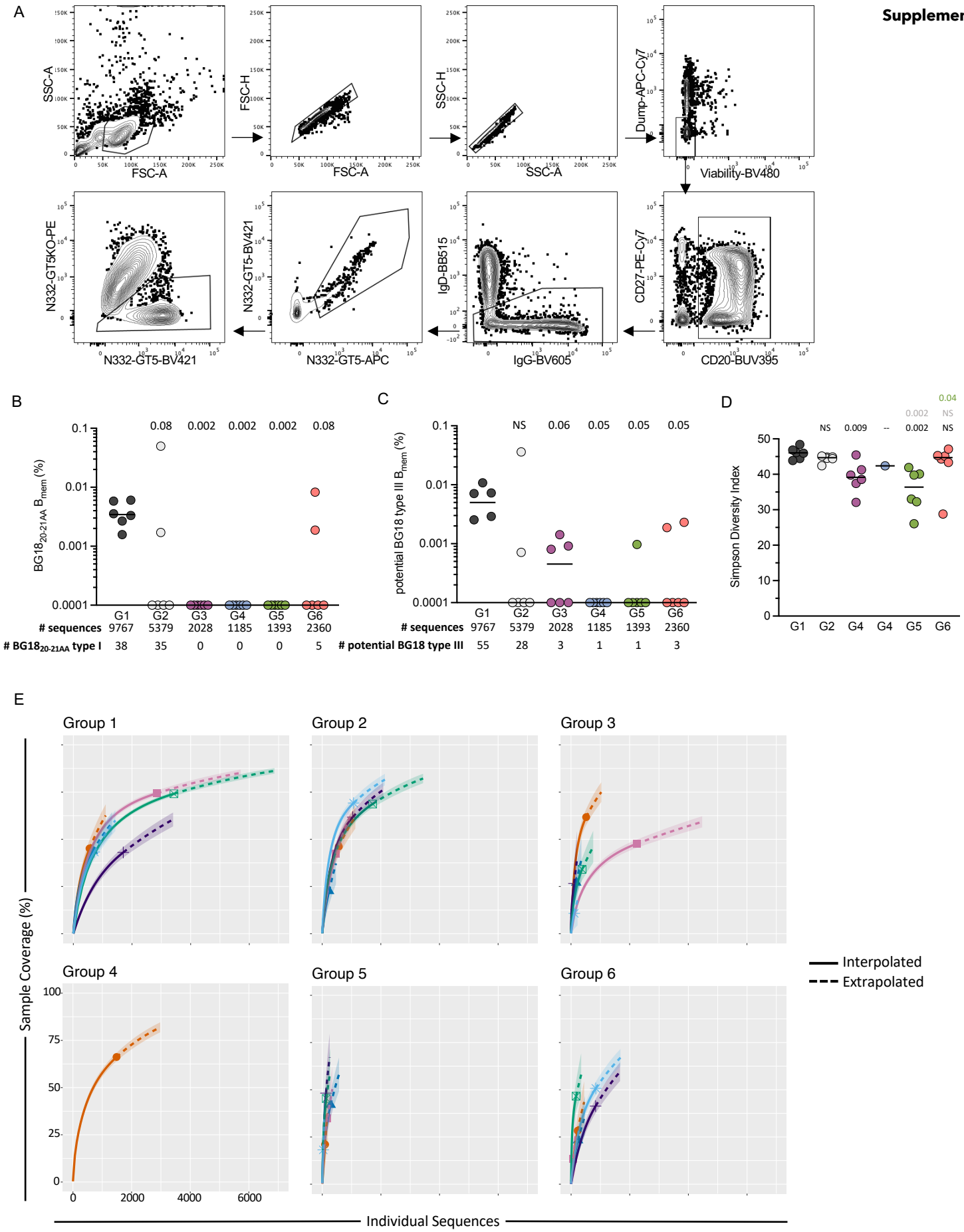

Supplementary Fig.9

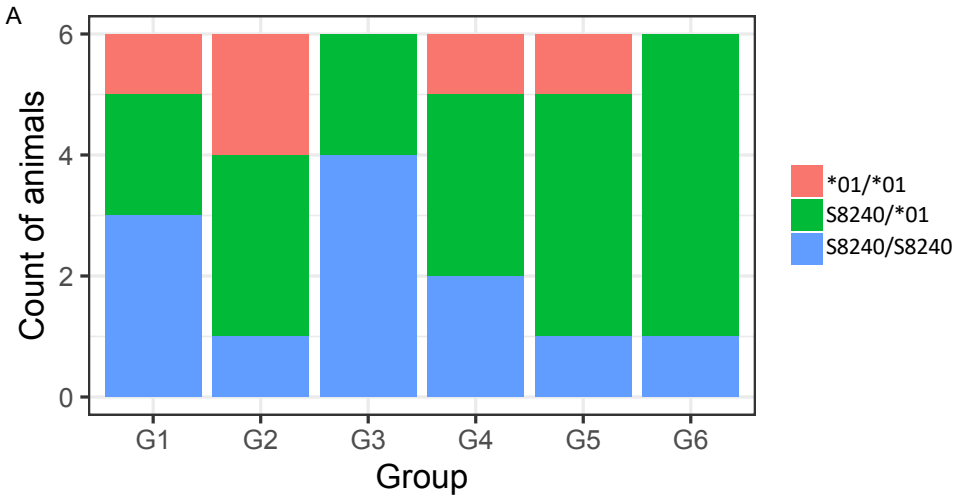

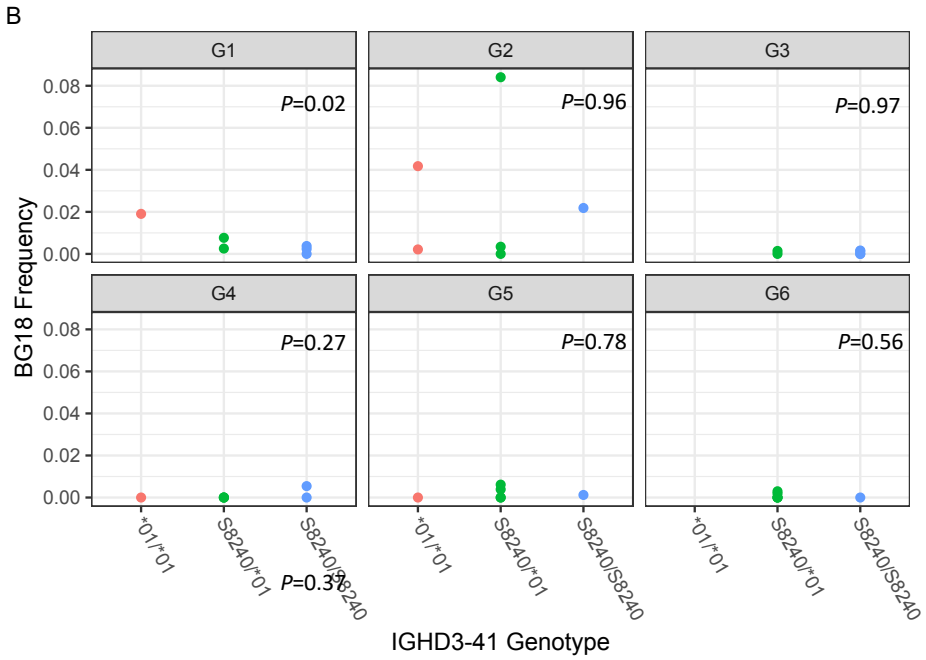

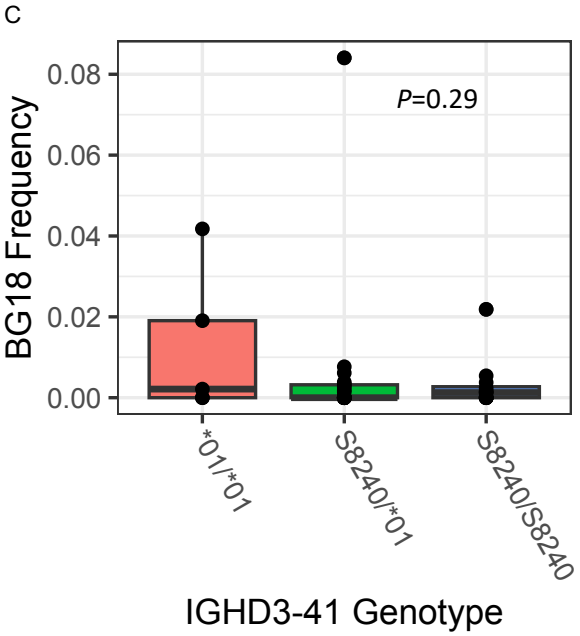

Supplementary Fig.10

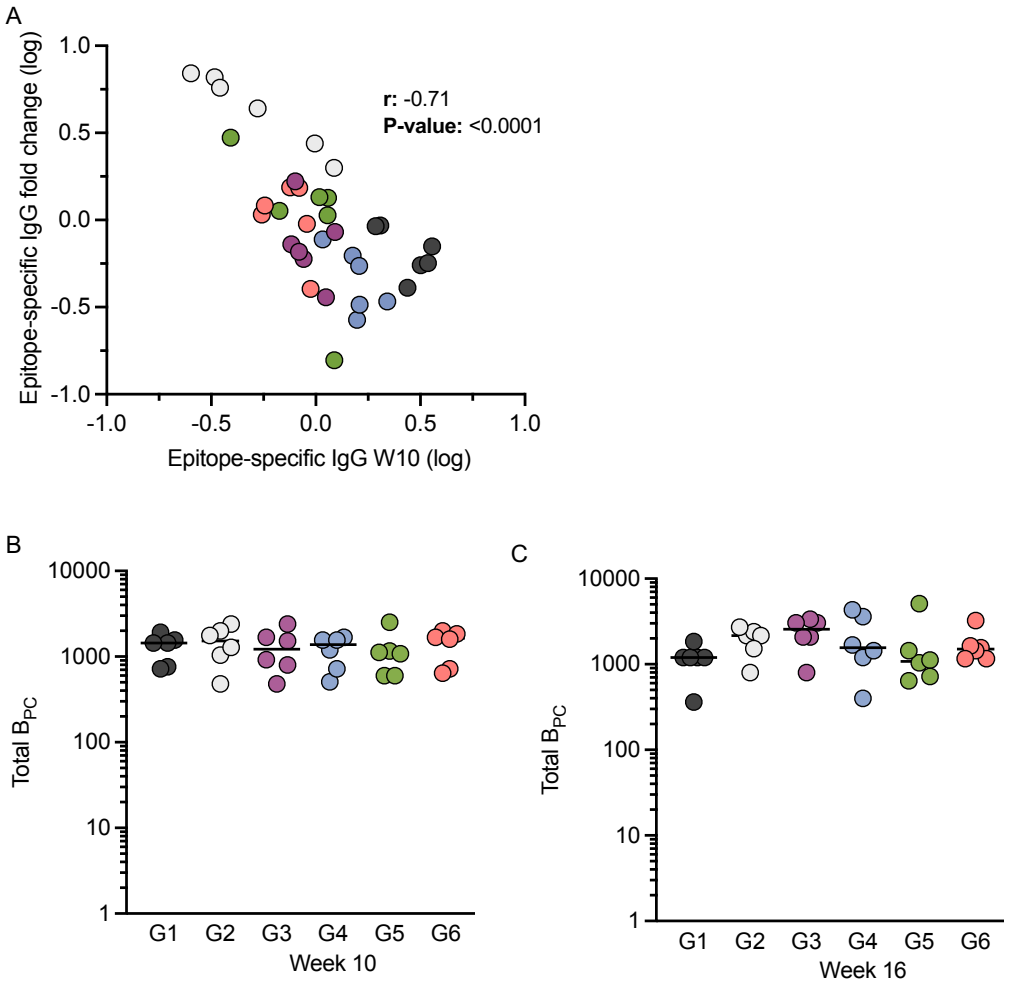

A

Supplementary Fig.11

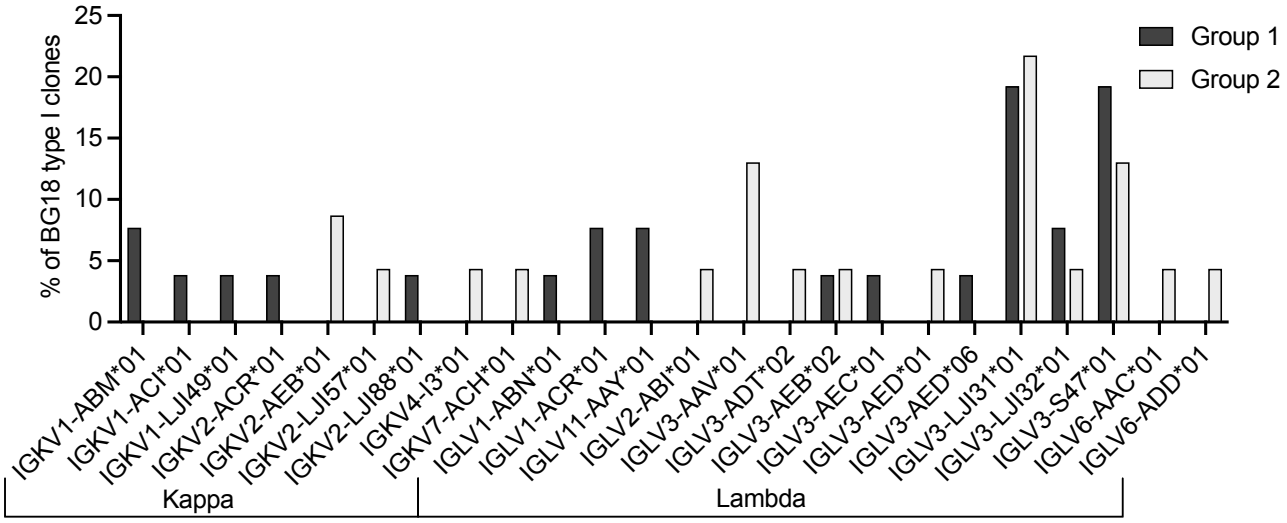

B

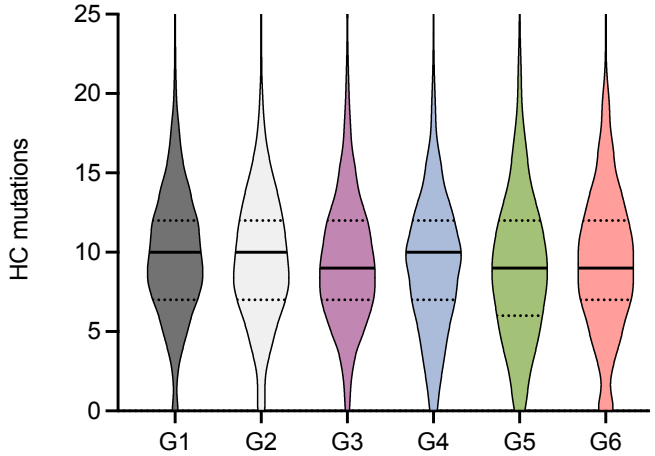

	G1	G2	G3	G4	G5	G6
N	9278	5048	2024	827	1014	2337
Median	10	10	9	10	9	9
% Mutated	98.6	98.4	99.0	97.9	97.5	95.9

C

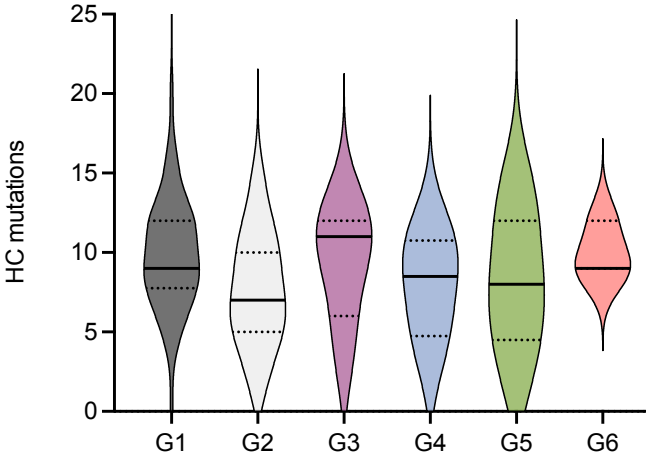

	G1	G2	G3	G4	G5	G6
N	50	75	5	4	12	3
Median	9	7	11	8.5	8	9
% Mutated	98.0	100	100	100	100	100

Supplementary Table 1. Week 3 BG18 type I B_{GC} sequences

NHP	Clone	VH	D	JH	HCDR3	HCDR3 length	HC nucleotide mutations	VL/VK	JL/JK	LCDR3	LC nucleotide mutations
RHu20	18604	IGHV3-52*01	IGHD3-41*01	IGHJ5-2*01,IGHJ5-5*01	CARNGITIFGLVILGEFYNSLDVW	22	1	IGLV3-AEC*01	IGLJ3*01	CQSADSSGNHPVF	2
	20527	IGHV1-NL_1*01_S2052	IGHD3-41*01	IGHJ6*01,IGHJ6-6*01	CARDGITIFGLVIFGESDYYGLDSW	23	0	IGLV3-S47*01_S0001	IGLJ3*01	CQVWDISSDHPVF	1
		IGHV1-NL_1*01_S2052	IGHD3-41*01	IGHJ6*01,IGHJ6-6*01	CARDVITIFGLVILGESDYYGLDSW	23	3	IGLV3-S47*01_S0001	IGLJ3*01	CQVWDISSDHPVF	1
		IGHV1-NL_1*01_S2052	IGHD3-41*01	IGHJ6*01,IGHJ6-6*01	CARDGITIFGLVIFGESDYYGLDSW	23	0	IGLV3-S47*01_S0001	IGLJ3*01	CQVWDISSDHPVF	3
		IGHV1-NL_1*01_S2052	IGHD3-41*01	IGHJ6*01,IGHJ6-6*01	CAGDGFTIFGLVILGESDYSGLDSW	23	4	IGLV3-S47*01_S0001	IGLJ3*01	CQVWDITSDHPVF	1
		IGHV1-NL_1*01_S2052	IGHD3-41*01	IGHJ6*01,IGHJ6-6*01	CARDGITVFGLVIFGESDYYGLDSW	23	1	IGLV3-S47*01_S0001	IGLJ3*01	CQVWDISSDHPVF	0
	20528	IGHV4-149*01_S0794	IGHD3-41*01	IGHJ6*01,IGHJ6-6*01	CARDLLEIFGLVIFGEVDYYGLDSW	23	3	IGKV1-LJI49*01	IGKJ1-I1*01	CQQFNIYPRTF	1
		IGHV4-149*01_S0794	IGHD3-41*01	IGHJ6*01,IGHJ6-6*01	CARDLLEIFGLVIFGEVDYYGLDSW	23	0	IGKV1-LJI49*01	IGKJ1-I1*01	CQQRNSYPRTF	2
		IGHV4-149*01_S0794	IGHD3-41*01	IGHJ6*01,IGHJ6-6*01	CARDLLEIFGLVIFGEVDYYGLDSW	23	1	IGKV1-LJI49*01	IGKJ1-I1*01	CQQRNSYPRTF	2
		IGHV4-149*01_S0794	IGHD3-41*01	IGHJ6*01,IGHJ6-6*01	CARDLLEIFGLVIFGEVDYYGLDSW	23	0	IGKV1-LJI49*01	IGKJ1-I1*01	CQQHNTYPRTF	4
		IGHV4-149*01_S0794	IGHD3-41*01	IGHJ6*01,IGHJ6-6*01	CARDLLEIFGLVIFGEVDYYDLDSW	23	2	IGKV1-LJI49*01	IGKJ1-I1*01	CQQRNSYPRTF	1
		IGHV4-149*01_S0794	IGHD3-41*01	IGHJ6*01,IGHJ6-6*01	CARDLLEIFGLVIFGEVDYYGLDSW	23	3	IGKV1-ABZ*01	IGKJ1-I1*01	CQQRNSYPRTF	2
		IGHV4-149*01_S0794	IGHD3-41*01	IGHJ6*01,IGHJ6-6*01	SARDLLEIFGLVIFGEVDYYGLDSW	23	7	IGKV1-LJI49*01	IGKJ1-I1*01	CQQRNSYPRTF	1
RQh20	18554	IGHV4-79*01	IGHD3-41*01_S8240	IGHJ3*01,IGHJ3-2*01	CARGDTIFGVVITPESSEAFDFW	22	2	IGLV6-AAC*01,IGLV6-AAC*02	IGLJ3-S3*01	CQSYDSYNVLF	2
		IGHV4-79*01	IGHD3-41*01_S8240	IGHJ3*01,IGHJ3-2*01	CARGDTIFGVVITPESSEAFDFW	22	2	IGLV6-AAC*05,IGLV6-AAC*05_S8052	IGLJ3-S3*01	CQSYDSYNVLF	2
	20295	IGHV4-NL_21*01_S4478	IGHD3-41*01_S8240	IGHJ1*01,IGHJ1-1*01	CARGGGRIGVLQFLEWLSETEYFEFW	24	0	IGLV3-AED*06	IGLJ3*01	CQVWDSSSDHWVF	6
		IGHV4-NL_21*01_S4478	IGHD3-41*01_S8240	IGHJ1*01,IGHJ1-1*01	CARGGGRIGVLQFLEWLSETEYFEFW	24	0	IGLV3-AED*06	IGLJ3*01	CQVWDSSSDHWVF	5
	20774	IGHV4-NL_22*01_S6977	IGHD3-41*01_S8240	IGHJ6*01,IGHJ6-6*01	CAREGGSVFGVVIFTEFNYYGLDSW	23	0	IGLV3-LJI31*01	IGLJ1-S1*01	CQVWDSSSKYYIF	0
RRt20	18555	IGHV4-NL_22*01_S6977	IGHD3-41*01_S8240	IGHJ2*01,IGHJ2-I1*01	CATLGITIFGVVIFGELDWYFDLW	22	0	IGLV1-LJI69*01	IGLJ2-S2*01	CSAWDSSLSALF	1
		IGHV4-NL_22*01_S6977	IGHD3-41*01_S8240	IGHJ2*01,IGHJ2-I1*01	CATLGITIFGVVIFGELDWYFDLW	22	2	IGLV1-LJI69*01	IGLJ2-S2*01	CSAWDSSLSGLF	2
		IGHV4-NL_22*01_S6977	IGHD3-41*01_S8240	IGHJ2*01,IGHJ2-I1*01	CATLGITIFGVVIFGEVDWYFDLW	22	4	IGLV1-LJI69*01	IGLJ2-S2*01	CSAWDSSLSGLF	1
		IGHV4-NL_22*01_S6977	IGHD3-41*01_S8240	IGHJ2*01,IGHJ2-I1*01	CATLGITIFGVLIFGELDWYFDLW	22	5	IGLV1-LJI69*01	IGLJ2-S2*01	CSAWDSSLSGLF	0
		IGHV4-NL_22*01_S6977	IGHD3-41*01_S8240	IGHJ2*01,IGHJ2-I1*01	CATLGITIFGVVIFGELDWYFDLW	22	2	IGLV1-LJI69*01	IGLJ2-S2*01	CSAWDSSLSGLF	0
		IGHV4-NL_22*01_S6977	IGHD3-41*01_S8240	IGHJ2*01,IGHJ2-I1*01	CATLGITIFGVVIFGEVDWYFDLW	22	1	IGLV1-LJI69*01	IGLJ2-S2*01	CSAWDSSLSGLF	1
		IGHV4-NL_22*01_S6977	IGHD3-41*01_S8240	IGHJ2*01,IGHJ2-I1*01	CATLGITIFGVVIFGELDWYFDLW	22	0	IGLV1-LJI69*01	IGLJ2-S2*01	CSAWDSSLSGLF	0
		IGHV4-NL_22*01_S6977	IGHD3-41*01_S8240	IGHJ2*01,IGHJ2-I1*01	CATLGITIFGVVIFGELDWYFDLW	22	3	IGLV1-LJI69*01	IGLJ2-S2*01	CSVWDSSLSGLF	0
		IGHV4-NL_22*01_S6977	IGHD3-41*01_S8240	IGHJ2*01,IGHJ2-I1*01	CATLGITIFGVVIFGELDWYFDLW	22	1	IGLV1-LJI69*01	IGLJ2-S2*01	CSAWDSSLSGLF	1
		IGHV4-NL_22*01_S6977	IGHD3-41*01_S8240	IGHJ2*01,IGHJ2-I1*01	CATLGITIFGVVIFGELDWYFDLW	22	0	IGLV1-LJI69*01	IGLJ2-S2*01	CSAWDSSLSGLF	2
		IGHV4-NL_22*01_S6977	IGHD3-41*01_S8240	IGHJ2*01,IGHJ2-I1*01	CATLGITIFGVVIFGELDWYFDLW	22	0	IGLV1-LJI69*01	IGLJ2-S2*01	CSAWDSSLSGLF	1
		IGHV4-NL_22*01_S6977	IGHD3-41*01_S8240	IGHJ2*01,IGHJ2-I1*01	CTTLGITIFGVVIFGELDWYFDLW	22	0	IGLV1-LJI69*01	IGLJ2-S2*01	CSAWDSSLSGLF	1
		IGHV4-NL_22*01_S6977	IGHD3-41*01_S8240	IGHJ2*01,IGHJ2-I1*01	CATLGITIFGMVIFGEVDWYFDLW	22	2	IGLV1-LJI69*01	IGLJ2-S2*01	CSAWDSSLSGLF	1
		IGHV4-NL_22*01_S6977	IGHD3-41*01_S8240	IGHJ2*01,IGHJ2-I1*01	CATLGITIFGVVIFGELDWYFDLW	22	0	IGLV1-LJI69*01	IGLJ2-S2*01	CSTWDSSLSGLF	0
		IGHV4-NL_22*01_S6977	IGHD3-41*01_S8240	IGHJ2*01,IGHJ2*01_S5087,IGHJ2-I1*01	CATLGITIFGVVIFGELDWYFDFW	22	2	IGLV1-LJI69*01	IGLJ2-S2*01	CSAWDSSLSGLF	0
		IGHV4-NL_22*01_S6977	IGHD3-41*01_S8240	IGHJ2*01,IGHJ2-I1*01	CATLGITIFGVIIFGEVDWYFDLW	22	2	IGLV1-LJI69*01	IGLJ2-S2*01	CSVWDSSLSGLF	1

Supplementary Table 2. Week 12 BG18 type I B_{mem} sequences

	NHP	Clone	VH	D	JH	HCDR3	HCDR3 length	HC nucleotide mutations	VL/VK	JL/JK	LCDR3	LC nucleotide mutations
G1	RHu20	20511	IGHV3-AFE*01_S4619	IGHD3-41*01	IGHJ6*01	CARNLRKIFGVVILGESEDYGLDSW	23	15	IGLV3-S47*01_S0001	IGLJ1-S1*01	CQLWDSNNDHYIF	10
		20512	IGHV4-AFQ*01	IGHD3-41*01	IGHJ6*01	CARIRITIFGVVALKETEENGLDSW	23	9	IGLV3-S47*01_S0001	IGLJ3-S3*01	CQVWDISSDHVLF	4
		20513	IGHV4-AFQ*01_S2532	IGHD3-41*01	IGHJ6*01	CARGHITIFGVVILGEIDYYGLDSW	23	13	IGLV3-LJI32*01	IGLJ3-S3*01	CQVWDSSSSHLVLF	10
		20517	IGHV4-150*01_S9374	IGHD3-41*01	IGHJ6*01	CARESITIFGLVTFREFNYNGLDSW	23	16	IGLV3-LJI31*01_S0001	IGLJ3*01	CQVWDISSDHHRIF	5
			IGHV4-150*01_S9374	IGHD3-41*01	IGHJ6*01	CARDNIAIFGLVFREFNYNGLDSW	23	9	IGLV3-LJI31*01_S0001	IGLJ3*01	CQVWDNNTYYQIF	5
			IGHV4-150*01_S9374	IGHD3-41*01	IGHJ6*01	CARESITIFGLVTFREFNYNGLDSW	23	8	IGLV3-LJI31*01_S0001	IGLJ3*01	CQVWDSSSDHRIF	7
			IGHV4-150*01_S9374	IGHD3-41*01	IGHJ6*01	CARDSIGIFGLLEFREFNYYGLDSW	23	13	IGLV3-LJI31*01_S0001	IGLJ3*01	CQVWDSSSDHRVF	4
		20518	IGHV3-52*01	IGHD3-41*01	IGHJ5-2*01	CARNSITIFGVVIFKEYWLHSLDVW	23	11	IGLV3-S47*01_S0001	IGLJ3*01	CQVWDISSDHPVF	6
			IGHV3-52*01	IGHD3-41*01	IGHJ5-2*01	CARTSITIFGVIIFKEYWYNSLDVW	23	7	IGLV3-S47*01_S0001	IGLJ3*01	CQVWDISSDHPVF	4
		20527	IGHV1-NL_1*01_S2052	IGHD3-41*01	IGHJ6*01	CSRERITIFGVVILGETDYHGLDSW	23	5	IGLV3-S47*01_S0001	IGLJ3*01	CQVWDISSDHPVF	5
			IGHV1-NL_1*01_S2052	IGHD3-41*01	IGHJ6*01	CSRERVTIFGVVIFGETEYHGLDSW	23	7	IGLV3-S47*01_S0001	IGLJ3*01	CQVWDNTNDHPVF	8
		20528	IGHV4-149*01_S0794	IGHD3-41*01	IGHJ6*01	CARDLLEIFGLLIFGEVENYGLDSW	23	9	IGKV1-LJI49*01	IGKJ1-I1*01	CQQCESDPRTF	9
			IGHV4-149*01_S0794	IGHD3-41*01	IGHJ6*01	CARDLLEIFGLLIFGEVENYGLDSW	23	15	IGKV1-LJI49*01	IGKJ1-I1*01	CQQCNSDPRTF	9
	RQh20	20383	IGHV2-69*01_S5121	IGHD3-41*01_S8240	IGHJ5-4*02	CARLHISVWGVIQFSEWSEEDNWFNVW	25	9	IGLV1-ABN*01	IGLJ3-S3*01	CATWDDSLSGVLF	8
			IGHV2-69*01_S5121	IGHD3-41*01_S8240	IGHJ5-4*02	CARLHISVWGVIQFSEWSEEDNWFDVW	25	7	IGLV1-ABN*01	IGLJ3-S3*01	CAAWDDSLSGVLF	2
		20774	IGHV4-NL_22*01_S6977	IGHD3-41*01_S8240	IGHJ6*01	CAREGGSVFGVLIFDEVNYHGLDSW	23	9	IGLV3-LJI31*01	IGLJ1-S1*01	CQVWDSSSEYYIF	8
			IGHV4-NL_22*01_S6977	IGHD3-41*01_S8240	IGHJ6*01	CAREGGSVFGVLIFDEVNYHGLDSW	23	6	IGLV3-LJI31*01	IGLJ1*01	CQVWDDSSEYHIF	11
		20775	IGHV3-128*01	IGHD3-41*01_S8240	IGHJ1*01	CTRVGIKIFGVVLLGEFDRDFFDFW	23	9	IGLV3-LJI31*01_S0001	IGLJ2-S2*01	CQVWDSDSDHVLF	4
		20776	IGHV4-72*01_S2051	IGHD3-41*01_S8240	IGHJ4*01	CARHNRESFGVLQFLEWILKGFDYW	23	6	IGLV3-LJI31*01_S0001	IGLJ2-S2*01	CQVWDNSGDHISF	5
			IGHV4-72*01_S2051	IGHD3-41*01_S8240	IGHJ4*01	CARHIRESFGLSQFLEWVLKGFDYW	23	8	IGLV3-LJI31*01_S0001	IGLJ3-S3*01	CQVWDNSGDHVSF	9
	RRt20	20415	IGHV4-NL_17*01_S0936	IGHD3-41*01_S8240	IGHJ5-1*01	CARDDGGITVFGVVDFGEIDENNRFDVW	25	12	IGLV1-ACR*01	IGLJ3-S3*01	CSAWDSSLSTVLF	10
			IGHV4-NL_17*01_S0936	IGHD3-41*01_S8240	IGHJ5-1*01	CAREGGITIFGVVAFGELDEDNRPDVW	25	12	IGLV1-ACR*01	IGLJ3-S3*01	CSAWDSSLSTVLF	7
		20728	IGHV4-NL_36*01_S0936	IGHD3-41*01_S8240	IGHJ6*01	CVRAQTSIYGVVIFGEFDWNGLDSW	23	11	IGLV11-AAY*01	IGLJ3*01	CQVYDSSSNWVVF	8
		20740	IGHV3-ABY*01_S4607	IGHD3-41*01	IGHJ5-1*01	CTREGRGLFGLVVFSEWEDNGFDVW	23	12	IGKV1-ABM*01	IGKJ3-I3*01	CQHYYSTPFTF	5
			IGHV3-ABY*01_S4607	IGHD3-41*01	IGHJ5-1*01	CTREGRGLFGLVVFSEWEDNGFDVW	23	12	IGKV1-ABM*01	IGKJ3-I3*01	CQHYYSTPFTF	5
	RTo20	12661	IGHV4-79*02_S9501	IGHD3-41*01_S8240	IGHJ5-4*02	CARGHRITVFGVIIFGEIGGENNWFDVW	26	20	IGKV2-LJI88*01	IGKJ4-I4*01	CMQTLQTPLTF	5
		20364	IGHV4-144*01_S3008	IGHD3-41*01_S8240	IGHJ5-4*02	CSRNGGITIFGVVIFGEFQTNNWFDVW	25	11	IGLV3-LJI32*01	IGLJ2-S2*01	CQVWDISSDRPLF	12
		20373	IGHV4-NL_17*01_S0936	IGHD3-41*01	IGHJ5-1*01	CAKNGGITVFGLVVFGEIDEKNRFDVW	25	9	IGLV1-ACR*01	IGLJ3-S3*01	CSTWDSSLSTVLF	8
			IGHV4-NL_17*01_S0936	IGHD3-41*01	IGHJ5-1*01	CARDDGGITIFGLVDFGELDENNRLDVW	25	6	IGLV1-ACR*01	IGLJ3-S3*01	CSAWDSSLSTVLF	1
			IGHV4-NL_17*01_S0936	IGHD3-41*01	IGHJ5-1*01	CARDDGGITVFGVVDFGELDENNRFDVW	25	12	IGLV1-ACR*01	IGLJ3-S3*01	CSAWDDGLTTVLF	5
			IGHV4-NL_17*01_S0936	IGHD3-41*01	IGHJ5-1*01	CAREGGITIFGVVAFGELDEDNRLDVW	25	9	IGLV1-ACR*01	IGLJ3-S3*01	CSAWDSSLSIVLF	8
			IGHV4-NL_17*01_S0936	IGHD3-41*01	IGHJ5-1*01	CARDDGGITIYGVVDFGELDENNRFDVW	25	8	IGLV1-ACR*01	IGLJ3-S3*01	CSTWDSSLNTLLF	1
		20596	IGHV3-172*01_S2175	IGHD3-41*01	IGHJ5-1*01	CTREIRGIFGLVVFSEWEYYGFDVW	23	7	IGKV1-ABM*01	IGKJ3-I3*01	CQHYYTTPFTF	5
			IGHV3-172*01_S2175	IGHD3-41*01	IGHJ5-1*01	CARKGRGIFGLVTFSEWEYYGFDVW	23	8	IGKV1-ABM*01	IGKJ3-I3*01	CQHYYNTPFTF	6
			IGHV3-ABY*01_S4607	IGHD3-41*01	IGHJ5-1*01	CTREGRGLFGLVIFSEWEDNGFDVW	23	12	IGKV1-ABM*01	IGKJ3-I3*01	CQHYYSTPFTF	5
			IGHV3-172*01_S2175	IGHD3-41*01	IGHJ5-1*01	CTRAGRGIFGLVIFSEWEDIGFDVW	23	7	IGKV1-ABM*01	IGKJ3-I3*01	CQHYYSTPFTF	3
			IGHV3-ABY*01_S4607	IGHD3-41*01	IGHJ5-1*01	CTREGRGLFGLVVFSEWEDNGFDVW	23	12	IGKV1-ABM*01	IGKJ3-I3*01	CQHYYSTPFTF	5

Supplementary Table 3. *IGHD3-41* genotypes

Group	Animal ID	IGHD3-41 Genotype
G1	RHu20	*01/*01
	RQh20	S8240/S8240
	RQR20	S8240/S8240
	RRt20	S8240/*01
	RTo20	S8240/*01
	RUl20	S8240/S8240
G2	NA93	S8240/S8240
	NB18	*01/*01
	NF14	S8240/*01
	RCk19	S8240/*01
	RTo19	S8240/*01
	RWc20	*01/*01
G3	RCj20	S8240/*01
	RFk20	S8240/*01
	RGi20	S8240/S8240
	RKn20	S8240/S8240
	RPf20	S8240/S8240
	RSo20	S8240/S8240
G4	RIe20	S8240/*01
	RQp20	*01/*01
	RTm20	S8240/S8240
	RVt20	S8240/S8240
	RVu20	S8240/*01
	RZu20	S8240/*01
G5	RBu20	S8240/S8240
	RHq19	S8240/*01
	RLt18	S8240/*01
	RTk18	S8240/*01
	RVo19	*01/*01
	RWh19	S8240/*01
G6	MR83	S8240/*01
	MT09	S8240/*01
	RCf19	S8240/*01
	RFu20	S8240/*01
	RLN20	S8240/*01
	RYm20	S8240/S8240

*01, frame 3: ITIFGLVII; frame 1: VLQYLDWLLY

*01_S8240, frame 3: ITIFGVVIT; frame 1: VLQFLEWLLH